ADDIS ABABA UNIVERSITY

ADDIS ABABA INSTITUTE OF TECHNOLOGY

AFRICAN RAILWAY CENTER OF EXCELLENCE (ARCE)

HOMOGENIZING TRACK STIFFNESS OF A MIXED RAILWAY LINE TURNOUT CROSSING USING RAIL PADS AND UNDER SLEEPER PADS

By

EDEN AWEKE

A thesis submitted to the School of Graduate Studies of Addis Ababa University in partial fulfillment of the requirements of the Degree of Master of Science in Railway Engineering (Civil Infrastructure)

HOMOGENIZING TRACK STIFFNESS OF A MIXED RAILWAY LINE TURNOUT CROSSING USING RAIL PADS AND UNDER SLEEPER PADS

By

EDEN AWEKE TELILA | GSR/3616/11

Email: Edenaweke2012@gmail.com

Approved by the Board of Examiners

Henok Fikre (PhD)	_____	_____
ADVISOR	SIGNATURE	DATE
Tensay Gebremedhin (PhD)	_____	_____
EXTERNAL EXAMINER	SIGNATURE	DATE
Celestin Nkundineza (PhD)	_____	_____
INTERNAL EXAMINER	SIGNATURE	DATE
Mr. Ayele Tesema	_____	_____
Chair Person	SIGNATURE	DATE

January, 2021

DECLARATION

I certify that this research work entitled "*Homogenizing Track Stiffness of a Mixed Railway Line Turnout Crossing using Rail Pads and Under Sleeper Pads*" is my own work. The work has not been presented elsewhere for assessment. Where material has been used from other sources, it has been properly acknowledged/referred.

_____

EDEN AWEKE TELILA

DATE:

SYNOPSIS

Turnout is among the weakest parts in railway with disadvantages of complexity, short working life, limited speed, low driving safety and high maintenance and operation costs compared to the tangent tracks. These could be due to the fact that turnouts contain several irregularities both in stiffness and inertia. Thus, these variations of mass distribution and geometric irregularities lead to *stiffness variation along the turnout*. Furthermore, the existence of shared baseplates and spacer blocks between different rails makes the variation severe at the crossing.

This research work investigates the stiffness characteristics along a selected railway turnout crossing from Awash-Kombolcha-Hara Gebaya mixed railway line and proposes suitable rail pads and under sleeper pads to improve abrupt stiffness fluctuations throughout.

A 3D numerical model is established using ABAQUS 6.19 to do deterministic analysis on the characteristics of stiffness along the selected turnout. The FEA model consists a rolling wheel, a through root in a right branching turnout, rail pads, sleepers, under sleeper pads, and ballast and it was first verified by using a static analysis comparison with previously validated simulation model.

The parameters used in the model are extracted from Ethiopian Railway Corporation design files; In the case of data which is not stated there, well recognized literatures are referred. The analysis results for the initial parameters (the as built) shows stiffness increment of about 54 % and reduction of 23% at the approach and crossing panels compared to the crossing nose. The homogenization results a maximum of 19 % stiffness variation between consecutive points altering the stiffness of rail pads and under sleeper pads together. It is also recommended to incorporate other design optimization outputs including rail shape and sleeper spacings in addition to decreasing the density of the ballast under the crossing panel to get the maximum out of this research.

Key Words: Tur*nout; Vertical stiffness; Stiffness variation; Geometric irregularities; Deterministic analysis; Rail pads; USPs;*

ACKNOWLEDGEMENT

My upper most gratitude goes to the Almighty God who let this come true and His Hoy Mother who has always been there revealing the power of her prayers in my life.

I would like to express my sincere thankfulness to all my instructors at African railway center of excellence for their kind assistance throughout the past year. In particular, the guidance provided by my advisor, Henok Fikre (PhD) was priceless in producing such a quality research. Moreover, I truly appreciate Celestin Nkundineza (PhD) for his training and support regarding the FE Software, ABAQUS.

I wish to acknowledge the help provided by Ethiopian Railway Corporation (ERC) - design department staffs, Mr. Tibebu Solomon, Anwar, Nigist Hailu whom have helped in providing design and operational parameters of the Railway line.

I would like to recognize the invaluable assistance that my family and friends provided during my study. Finally, I wish to thank all those whose assistance was a milestone in the completion of this study.

ABBREVIATIONS

AA	Addis Ababa
AAU	Addis Ababa University
BC	Boundary Condition
BOEF	Beam on Elastic Foundation
ERC	Ethiopian Railway Corporation
FE	Finite Element
FEA	Finite Element Analysis
GUI	Graphical User Interface
UBMs	Under Ballast Mats
USPs	Under Sleeper Pads
RCF	Rolling Contact Fatigue
SEP	Strain Energy Potential
RSMV	Rolling Stiffness Measurement Vehicle
TLV	Track Loading Vehicle
CARS	China Academy of Railway Sciences
FWD	Falling Weight Deflectometer

TABLE OF CONTENTS

LIST OF FIGURES

LIST OF TABLES

1 INTRODUCTION

Stiffness variation or irregularity on a track can generally be originated from super structure (rails, rail pads, sleepers, ballast) or sub structure (sub-ballast, subgrade soil, etc). Locations on railway track where there are abrupt stiffness changes are Transition from slab track to ballasted track or from embankment to a bridge, Turnouts, Insulation joints and spots where there are hanging sleepers [1].

Different researchers have studied the relationship between track stiffness variation with track geometry and the effect of track stiffness deviations on variations of the wheel/rail contact. Variation of rail profiles along a turnout disturbs normal wheel-rail contact situations when a wheel transfers from stock rail to switch rail in the switch panel or from wing rail to point rail in the crossing panel [2]. These fluctuations enhance the dynamic impact on the rail and thus yields the track structure deterioration. The effect of sudden stiffness changes on track degradation is crucial and fundamental to a better planned maintenance [3]. A lot has been done on homogenizing track stiffness in switches using under rail pads (URP), elastic ribbed baseplates Under Sleeper Pads (USP), Under Ballast Mats (UBM), reinforced subgrade/ballast layers, reinforced wooden (light) sleepers [4]; by following different approaches.

A study by Jingmang Xu [5] revealed the effect of this dynamically changing stiffness along the switch panel on the Wheel-Rail dynamic characteristics of a high-speed turnout. Nicklisch et al. [6] have also worked on geometry and stiffness optimization for switches and crossings, and simulation of material degradation using different software [6]. In this thesis, the stiffness characteristics along a selected turnout crossing for the operation speed and loading of the new Awash-Kombolcha-Hara Gebaya mixed railway route is studied and stiffness material properties of rail pads and under sleeper pads are proposed to homogenize the track stiffness throughout.

1.1 Background

Rail vehicle wheels are guided along the tracks by coning of the wheels, and in some cases, it might rely on the flanges. Turnouts assist the trains to move from one rail track to another through leverage principle to enable the traffic ability of the rail [7]. When the wheels reach the switch, the wheels are guided along the route determined by one of the points aligned with the facing track.

A common turnout structure has rails of varying shapes of different types. Those are stock rails, switch rails, wing rails, point rails, and check rails. An English engineer Charles Fox has invented the first turnout's point mechanism in 1832 using a lever connected to a pull rod, which moves the points from one track to the next, initiates the mechanism [8].

The uneven distribution of track stiffness in the turnout along the longitudinal direction is highly dependent on the different turnout structural components.

1.2 Problem statement

Differences in structural arrangements longitudinally highly contributes to the fluctuation of track stiffness in railway turnouts. The presence of stiffness variation along a turnout has been shown by different researchers to reach up to 40% at the switch panel and extend up to around 70% between the switch tip and the adjacent track structure [9]. Meanwhile the presence of a couple of rails being placed on a single iron base plate, variation in length of sleepers and the existence of spacer blocks for connecting different rails highly affects the characteristics of track stiffness along a high-speed railway ballast turnout. Moreover, the bending stiffness of the stock rail is different from the bending stiffness of the switch rail, the crossing nose (the frog) is stiffer in bending and has larger mass than the rest of the rails. Hence these variations are both in stiffness and inertia of the rail sections along.

Change in track stiffness causes variations in the train/track interaction forces creating transient high frequency vibrations and low frequency random oscillations which in turn give rise to super structure degradation (rolling contact fatigue of rail surface as a general and wear of rails and sleepers) and track support degradation (leading to differential settlement) respectively. Thus, the ***rate of maintenance*** work and ***energy dissipation*** is very high. In addition, limited speed due to these effects would induce high ***operation cost.***

Even though there are various remedies, which can be applied to reduce the high maintenance costs associated to S&Cs; such as:

- Reducing the turnout population in the network,
- Using more durable and advanced materials,
- Adopting a preventative maintenance strategy instead of corrective maintenance,
- Optimizing the turnout geometry,
- Loosening sub-structure compaction around the crossing panel,

Homogenizing support stiffness is the most efficient and regarded by the researcher to be the best option for the mixed railway route.

Therefore, the stiffness characteristics along a turnout crossing of a mixed railway line under ERC for the train operational speed and loading is investigated. Moreover, there shall be suitable rail pads and under sleeper pads which improves abrupt stiffness changes so that the speed of the through root can be kept and the speed of the diverging root can be increased up to the curved geometry allows.

1.3 Research objective

1.3.1 General objectives

The primary objective of this research is studying stiffness responses along a selected mixed railway line turnout and to propose material properties of rail pads and under sleeper pads that can homogenize stiffness throughout.

1.3.2 Specific objectives

The specific objectives of this thesis are:

→ To investigate the stiffness response along the turnout crossing for the operational speed and loading.

→ To consider hyperelastic non-linear material model of the rubber pads.

→ To further incorporate non - linear material models for other turnout components.

→ To propose material properties of rail pads and under sleeper pads to smoothen the stiffness throughout the crossing panel of the turnout.

1.4 Research questions

The research questions, which the thesis aims to address, includes:

→ What is the stiffness response of the turnout under study, for the expected operational speed and loading?

→ What is the result of considering hyperelastic non-linear material model for the rubber pads?

→ What is the result of incorporating other non-linear material properties for other turnout components?

→ What are the material properties of rail pads and under sleeper pads that can be used to smoothen the stiffness throughout the crossing panel?

1.5 Significance of the research

1.5.1 Contributions:

The output of this research can play a significant role in transforming the conventional approach of turnout design which is barely flexible in considering stiffness variation at different sections of the turnout to an advanced approach. The outputs of this research which considers use of varying stiffness of rail pads and USPs aligning with other research outputs will have an impact in devising consistent track stiffness at every section of the turnout.

1.5.2 Expected outcomes of the research and its beneficiaries

This research is basically expected to have the following outcomes;

→ Clearly show the effect of the operational speed and loading on stiffness characteristics of a mixed line railway crossing structure.

→ Propose suitable stiffness material properties for rail pads and USPs which helps to devise consistent track stiffness.

The output of this research work will be used by;

→ Different researchers,

→ Students and

→ Turnout designers as a reference

1.6 Scope and limitations

This research is limited to one selected turnout along the existing Awash-Kombolcha-Hara Gebaya mixed railway route. Furthermore, the stiffness along the lateral direction of railway turnouts are not taken in to account, thus vertical track stiffness will only be considered under this research.

1.7 Research outline

Brief description of the chapters is presented below to get an overview of the general composition of the thesis.

Chapter 1 - Introduction:	A general overview of the topic, background information, motivation and significance are presented.
Chapter 2 - Literature Review:	The theoretical background required to implement the research methodology and interpret the results is presented.
Chapter 3 - Research Methodology:	The research instruments and methodologies that need to be implemented to answer the questions raised in the statement of the problem are reviewed and presented.
Chapter 4 - Model Information and Verification:	Here a numerical model description on a selected turnout crossing from Awash-Kombolcha-Hara Gebaya railway line - a station around Kombolcha is presented. In addition, model verification is discussed under this section.
Chapter 5 – Results and discussion	The outputs of the FE model are analyzed and discussed and then compared with the initial model outputs.
Chapter 6 - Conclusions and Recommendations:	Findings of the study are summarized under this section with possible courses of actions for the future, as well as possible avenues for further research.

2 LITERATURE REVIEW

Observing the operation hitches on railway line turnouts and reviewing different literatures initiated the study of homogenizing track stiffness of a mixed railway line turnout crossing using rail pads and under sleeper pads in the selected line. This literature review section will present the theoretical background necessary to address the research questions by implementing the research instruments. The literature review will address the following core areas of knowledge:

- *Train Trafficability:* will give information about means of train flexibility, types of turnouts, structural components and design considerations of a turnout;

- *Track stiffness and Track stiffness variation:* will deal with track modules, track stiffness, and different types of track stiffness measuring tools. On top of that track stiffness variation and causes will be presented;

- *Mechanisms to homogenize track stiffness around joints:* will address the different options to homogenize track stiffness. There are various techniques that are being used to homogenize stiffness around turnouts, which offer different materials and methodology. This section only discusses some of them that are related to the main idea of this study.

- *Different types of Hyperelastic material models* are briefly discussed under this section. Moreover, a 3rd degree reduced polynomial function -Yeoh is explicitly presented in detail.

2.1 Train trafficability

At certain points during its journey, a train needs to switch tracks in order to accommodate other trains on the network, and to reach its destination. This process requires the use of turnout, which is alternatively known as a railroad switch. The use of turnouts is

particularly common near major train stations where multiple trains need to be guided to various platforms throughout the station. The picture below of the Frankfurt am Main Central Station shows how complicated turnouts become as the number of trains services increases.

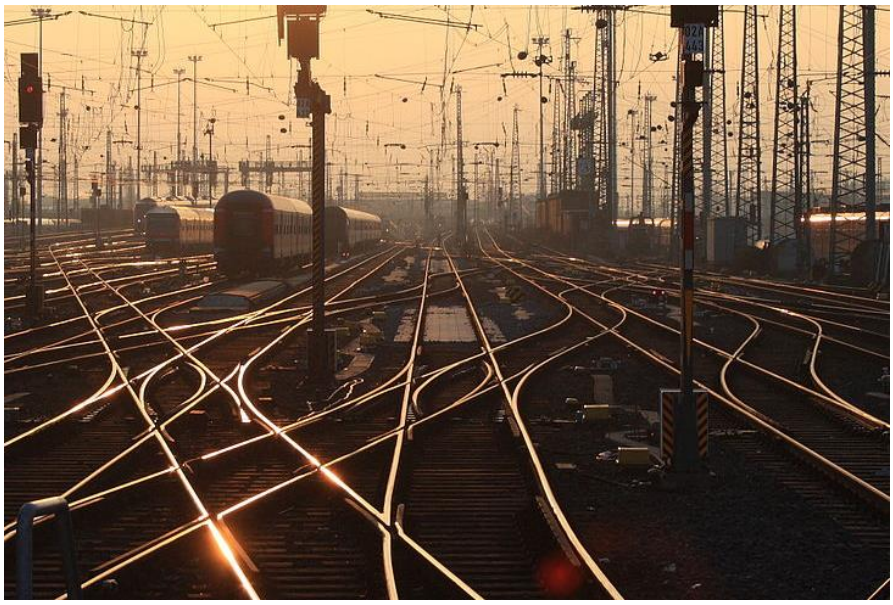

Figure 2-1: Turnouts at Frankfurt main central train station in Germany (Source: Wikipedia Commons)

The appropriate use of switches is critical to the safe operation of trains in the network due to the number of risks associated with switches such as incorrectly set points which can lead to head on collisions by placing trains on the same track or points becoming misaligned due to the forces exerted by the trains, which can lead to derailments. Therefore, trains generally travel at low speeds while switching tracks at turnouts.

There are several components to a railway turnout which will be discussed in this sub-section such as the design of turnouts, structural elements of turnouts and operational considerations.

2.1.1 Turnouts

Railway turnout is a mechanical device that is used to guide the trains from one rail track to another. It is an essential component of railway infrastructure, providing flexibility in traffic operations. English Engineer Charles Fox first invented railway points in 1832 [8].

It allows for train vehicles to cross over or switch between various tracks and in turn maximizing the utility of tracks and assets [7]. Through leverage principle, the railroad switch rod shifts the two movable rails to let the trains drive into the appointed route. It is comprised of a switch panel, a movable point crossing panel, and a closure panel as depicted in Figure 2.2.

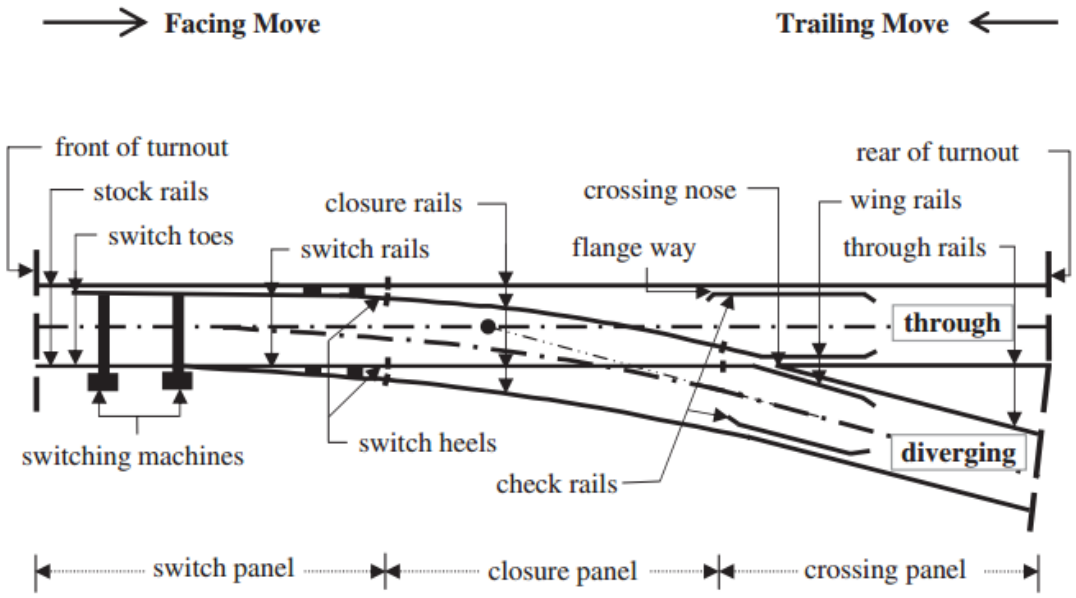

Figure 2-2: Typical turnout structure, Source: [10]

Switch panel: is the part of the turnout through which the direction of movement of a train can be changed. It comprises of two movable switch rails, switching machines (point machines), stretcher bars and two stock rails [11].

- ***The switch rails (switch blades)*** are the movable rails which guide the wheels towards either the straight or the diverging track. The two movable switch rails are held in the correct position by ***stretcher bars*** and move together to one side or the other on flat slide plates, by means of the operating rod/drive rod.

- **A switch motor (switch machine)** is an electric or hydraulic or pneumatic mechanism that aligns the points with one of the possible routes. The motor is usually controlled remotely and has electrical contacts to ensure that the set has completely been set and locked, otherwise, the signal is kept at red to prevent getting into an accident.

Closure panel: is the part of the turnout between the switch panel and the crossing panel, consisting of constant cross-section closure rails [11].

Crossing panel: is part of the turnout which allows for two tracks to intersect at the same level. It comprises of through rails forming the "V" shape at the crossing nose, wing rails (wings) at each side of the crossing nose, check rails (guard rails) and stock rails [11].

- The ***frog***, also known as the ***common crossing***, refers to the crossing point of two rails. This can be assembled out of several pieces of rail or can be a single casting of manganese steel.

- On lines with heavy and/or high-speed traffic, a swing nose crossing (moveable point frog) may be used. To allow for a wheel flange to pass the intersecting rails, the continuous rails are interrupted at the crossing point. The ***wing rails*** are installed for bridging this gap so that, ideally, a wheel can perform a smooth transition across the rail discontinuity.

The switch and point rail profiles are designed to vary in switch and crossing panels. Tongue rails are one of the rail types found in a turnout system which are machined to a very thin section to obtain a well fit with the stock rail. The sharp end of the tongue rail is called the toe and the heavier end is called the heel [5].

2.1.2 Turnout varieties

Turnouts come in a wide range of options, allowing engineers to choose a configuration that best fits their project's needs. The two basic forms of turnouts are [12]:

→ Simple or multiple turnouts: allowing a track to be split in to two (three), depending on the intended change of route.

→ Crossings: where two tracks meet at grade with no change of course

In a simple turnout, one track is split into two. Either the main track can remain straight or both the main track and the turnout track can divert symmetrically from the common route.

→ Equilateral turnout is a type of simple turnout, which is Y-shaped, and the two connected tracks are diverged to two separate rail tracks.

→ Three-way turnout is Ψ shaped and links three rail tracks. It operates by using two switch machines to control two sets of point rail.

→ Multiple slip switch is X-shaped. It looks like the combination of four sets of single turnouts and a diamond crossing.

→ Diamond crossing is a combination of two acute frogs and two obtuse frogs. Which Without switch machines, it is not possible to change routes.

→ Double cross over is formed by joining the upper two points with the lower two points of multiple slip switch. It is flexible for more directions but occupies less area [13].

2.1.3 Structural components of a turnout

A railway turnout provides a way for train vehicles to cross over or switch between various tracks and at the same time maximizing the mobility of tracks. The main structural components of a typical turnout include different shaped rails, switches, crossings, steel plates, bearers, ballast, sub-ballast (optional) and subgrade [7]. These components are divided in to super structure and substructure like the rest of the track.

SUBSTRUCTURE:

The substructure portion is the support for the superstructure part of the turnout and it mainly consists of the ballast, sub-ballast and sub-grade (Figure 2-3) which rests on the natural ground.

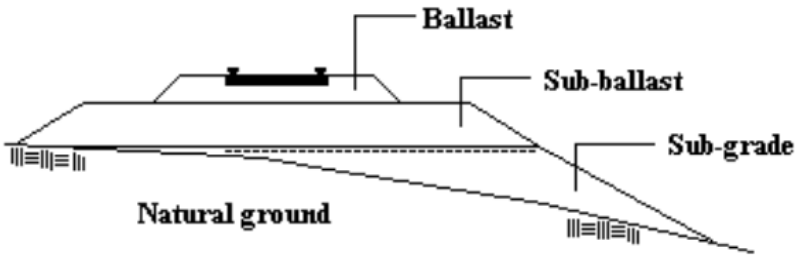

Figure 2-3: Substructure components of a ballasted railway track; source [14]

Ballast: the primary purpose of the ballast is to distribute load to the sub-ballast and maintain track stability in all directions. It also limits movement of sleepers and dissipates

the high static and dynamic loads in addition to its high capacity to drain water on the track [12].

Sub-ballast: Its main purpose is to support the layers above it and disperses the load coming from the traffic further down to the substructure components. It also has good drainage capacity and acts as a filter for small units (fine soil particles of the subgrade) from entering to the ballast [12].

Sub-grade: This component is the foundation for all the layers above creating smooth and uniform base for the sub-ballast to rest on. The fill material mainly used in this section is moraine or blasted stones [14].

SUPERSTRUCTURE:

The superstructure of a railway turnout structure as the rest of the tangent track comprises rails of different shapes, rail pad, fastening system, sleeper and USP (optional) see Figure 2-4. All these parts act together with unique role for each in the structure.

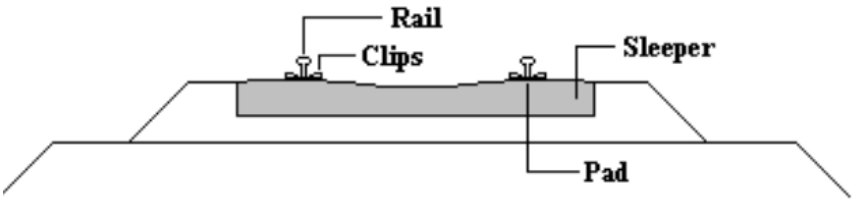

Figure 2-4: Typical track superstructure

Rail: the major role of the rails is to create a strong level surface for the movement of the train wheels with minimum possible friction in between them. It also has to have a capacity to resist thermal growth due to the wheel – rail interaction [12].

Despite the type of structures, either ballasted or ballast less; turnout rails have always had different shapes than the others on the line. At the switch panel, there is a continuously changing rail shape as illustrated in Figure 2-5 (a) & (b).

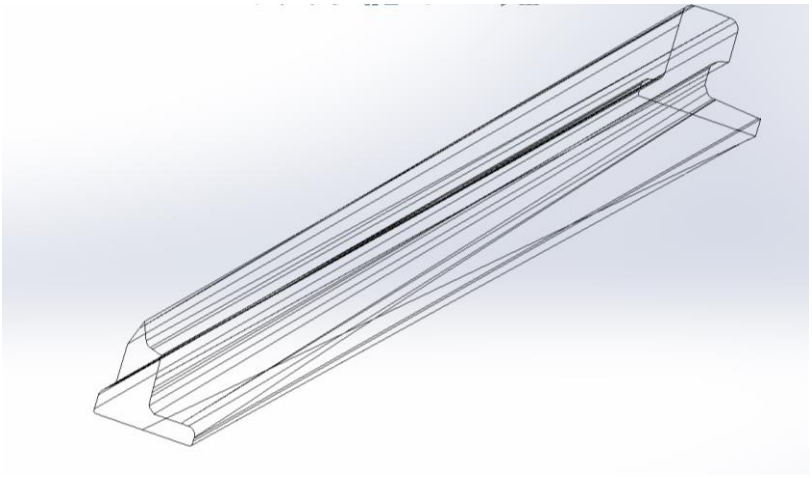

(a)

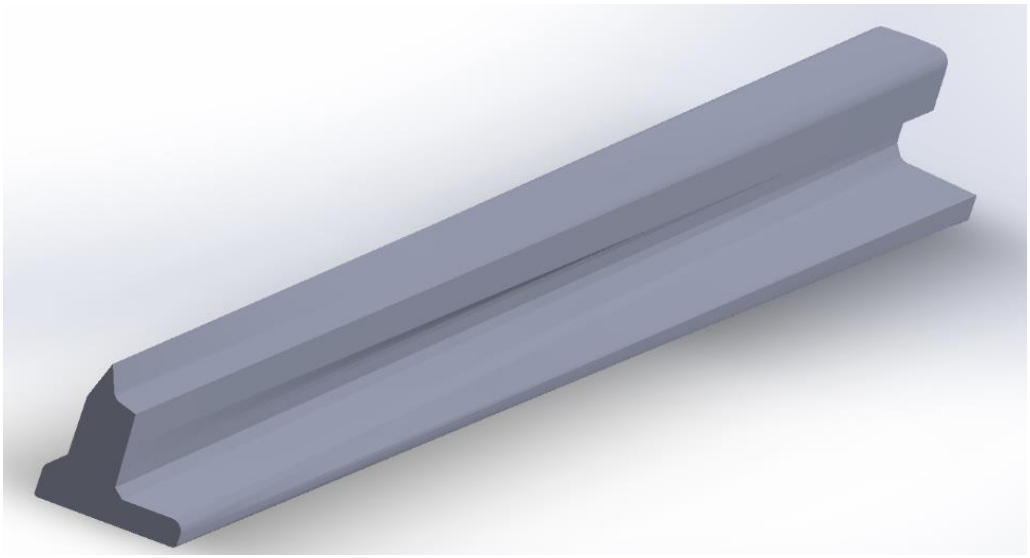

(b)

Figure 2-5: Different shapes of rails in the switch panel

The crossing nose, which is either moving or fixed depending on the design requirements also had a sophisticated shape with continuously changing cross-sections.

Sleeper: The primary purpose of a sleeper is to transfer the load coming from the rails to the support ballast. It also helps maintain the track gauge, keep inclination of the rails and overall stability of the track [14].

Rail pads: These are rubbers or chemical compounds (polymers) which are located in between sleepers and rails. Their main purpose is to absorb shock and vibrations due to dynamic and impact loads as well as irregularities on the rail. Moreover, it insulates transmission of electricity from the rail [14]. These components also has the ability to reduce wear of rail base and the sleeper in contact.

Fastener system: Its key function is maintaining position of the rail by means of different techniques regarding the type chosen. It also dissipates shock and vibrations initiated by the dynamic and impact loads [15].

In General, each component of a railway turnout is highly subjected to wear, rolling contact fatigue, and plastic deformations because of the reasons explained under section 1.2 of this paper.

2.1.4 Turnout design considerations

Turnouts need to be designed in straight track sections. Underneath special conditions, special turnouts could also be designed in curved form. Generally, turnouts are classified by the sort of rail used, by the curve radius and by the turnout angle (the angle between the 2 track centerlines). As an example, UIC60-760-1:15 turnout are from a 60 kg UIC rail profile with 760 m curve radius and turnout angle 1 by 15 [9].

Turnout geometrical classification:

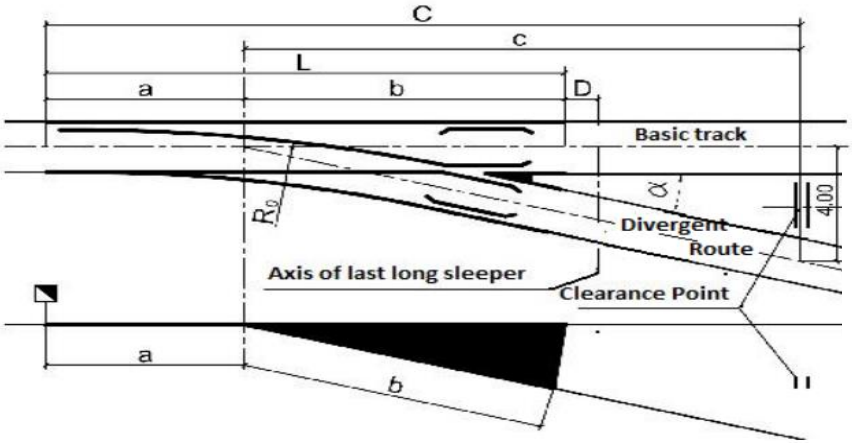

Figure 2-6: Turnout geometrical classification [16]

where:

a - Front tangent (from begin of turnout to its geometric center)

b - Posterior tangent, as well as antenna (from geometric center to end of turnout)

c - Distance between center of turnout (geometric center) and clearance purpose

C - Distance between begin of turnout and clearance purpose

D - Distance between finish of turnout and axis of last long sleeper

The conventional method to increase turnout speeds is to extend the length of the turnout and use a shallower turnout angle. A swing nose crossing (movable purpose frog) are commonly used in high-speed turnouts. High speed turnouts want several purpose machines to maneuver the long switch rail.

Distance between turnouts: Whenever connecting 2 turnouts, some distance should be maintained between them. The suggested distance is therefore = $\mathbf{0.2 \cdot \mathit{V max.}}$

The minimum distance between 2 opposing direction turnouts (LHS and RHS) is six meters [16].

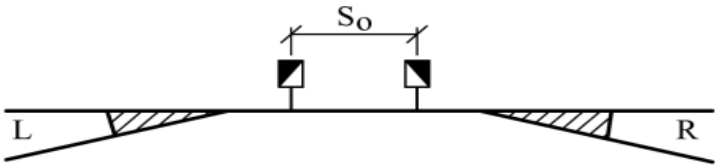

Figure 2-7: minimum distance between two opposing direction turnouts

The minimum distance between the start of turnouts of the same direction (LHS and RHS) S_o is also six meters.

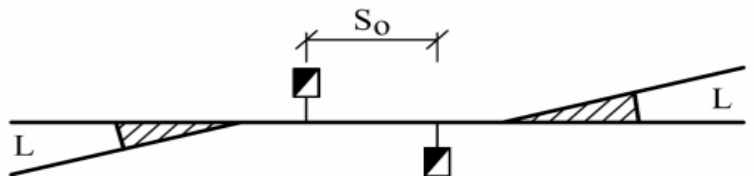

Figure 2-8: Minimum distance between the start of turnouts of the same direction

Turnout running speed calculation: Turnouts have neither cant nor transition curves. Most running speed on turnout depends on the non-compensated lateral acceleration and also the radius of curvature. For reasons of damage and ride comfort, the most lateral acceleration is restricted within 0.6-0.7 m/s^2 [16].

$$\frac{v^2}{R} - g * \frac{h}{s} = a_{y,max} \quad \text{Eq. 2-1}$$

$$h_{min} = \frac{s}{g} * (\frac{v^2}{R} - a_{y,max})$$

N.B: cant at turnout is zero i.e., $h_{min}=0$

Running speed on turnouts:

Some railways calculate running speed on the turnout in regard to cant deficiency $h_{d;}$

$$\frac{s}{g}\left(\frac{v^2}{R} - a_{y,max}\right) = 0 \rightarrow v_{max}\,(\frac{km}{h}) = 3.6 * \sqrt{(a_{y,max}) * R}$$

$$v_{max} = \sqrt{\frac{g}{s}(h_{d,max}) * R}$$

$$v_{max}\,(\frac{km}{h}) = 0.29 * \sqrt{h_d(mm) * R(m)} \quad \text{Eq. 2-2}$$

Distance between turnouts: The minimum distance between the tip of one turnout and also the starting of the consequent therefore shall be determined supported on the kind of turnout in question [16].

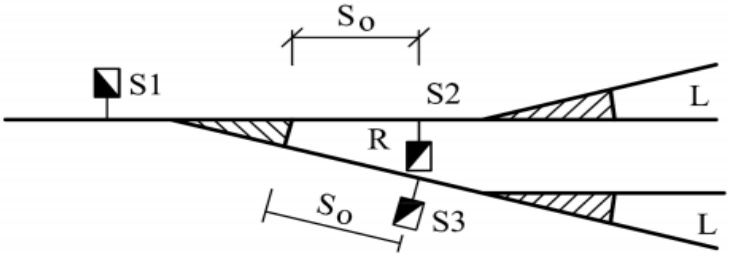

Turnout type	S_o, m
1/8	6
1/9	7
1/12	9
1/20	13

Figure 2-9: Distance between turnouts

Determination of start of turnout: The distance between the start of turnouts, which are planned opposite each other on parallel lines (Turnouts S5 and S6), shall be no less than 2 meters long [16].

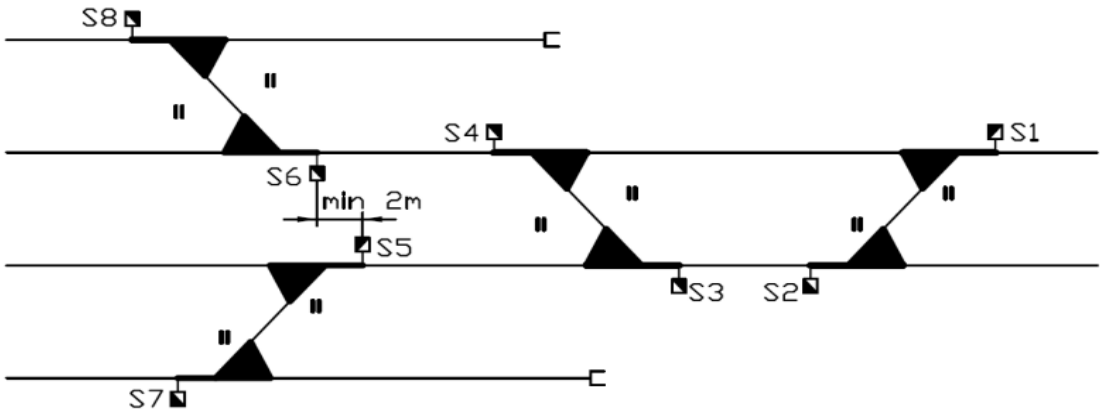

Figure 2-10: Start of turnout

Distance between a turnout and curve: When turnouts are located near horizontal curves, a minimum distance of S_O must be maintained between them. The Recommended distance;

$Sor = 0.2 \cdot V\ max$

The minimum distance between the end of a curve and beginning turnout S_O is 6.0 meters [16].

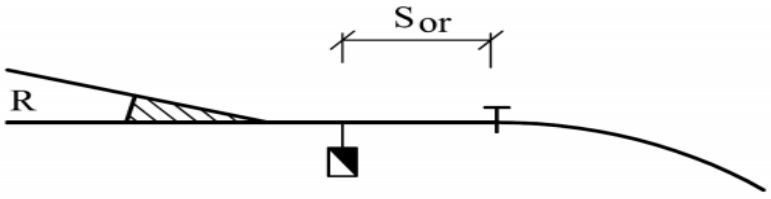

Turnout type	S_{or}, m
1/8	6
1/9	7
1/12	9
1/20	13

Figure 2-11: Distance between a turnout and a curve

The minimum distance between the end of one turnout and the start of a straight line or curve S_{or} shall be determined based on the type of turnout in question.

The wheel-rail interaction at the transition from the closure panel to the crossing, i.e. at the turnouts crossing (frog), induces very large impact forces and also had dynamic effect. Studies showed that it's very likely that railroad turnout bearers or crossties are subjected to severe impact loads, leading to frequent damage which in turn affects structural integrity and durability and settlement. It also had an adverse effect on ride comfort. Conventional built turnouts often transfer high impact forces to the structural members due to the gaps between mechanical connections between closure rails and switch rails (i.e., heel-block joints) [7].

2.2 Track stiffness

Track stiffness may well be a basic parameter of track style that influences the bearing capability of track, the dynamic behavior of passing vehicles and, above all, the quality of track and therefore the lifetime of track components.

Track stiffness is drawn from the relationship of the load applied on the rail to the corresponding rail vertical deflection. On the other hand, track foundation modulus (track modulus) is the measure of vertical stiffness of the track stiffness except the rail itself. The difference between track stiffness and track modulus is that track stiffness includes the rail bending stiffness EI, whereas track modulus comprises only the rest of the superstructure and the substructure as a whole [17]. Track modulus provides a measure of the structural condition of the track and regarded to be a very important parameter, though it's rarely measured and its magnitudes are unknown (or at the best roughly known) for many sections of railway track [18].

Vertical track stiffness or track modulus has for associate degree extended time been thought to be a significant parameter of the structural condition of the track. A typical railway track includes layers of different components with various material characteristics leading to differences in track stiffness. The total track stiffness is mostly driven from the contributions of stiffness of each component [19].

2.2.1 Mathematical models

I. Beam on elastic foundation (BOEF) model by Winkler

Winkler (1867) was the pioneer individual to do innovative researches on the study of mechanical behavior of railway tracks. He first modeled a continuous beam on elastic foundation that represents all track elements to come up with pure bending beam theory. His first trial was established for a track structure comprising of longitudinally placed sleepers [20]. Even though this model uses quite clear simple physical interpretation; it has a drawback of not incorporating shear deformation in the rails; only continuously welded rails are presumed with the springs acting independently [21].

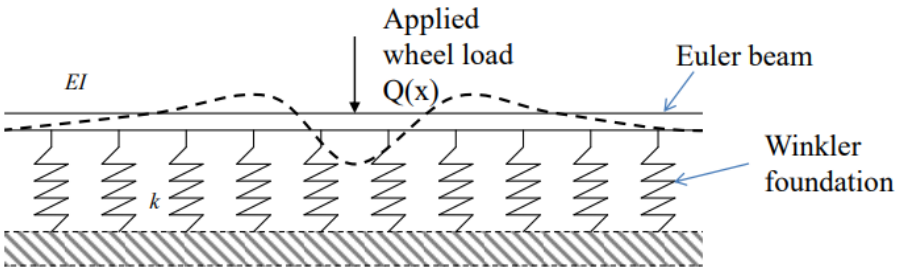

Figure 2-12: Elastic Beam on Winkler's Foundation

According to Winkler support reaction at x_i is;

$$q(x_i) = K * y(x_i) \quad \text{Eq. 2-3}$$

$$EI\frac{d^4y}{dx^4} + ky = Q \quad \text{Eq. 2-4}$$

where; EI – beam bending stiffness

k – the foundation coefficient (track modulus)

Taking equilibrium condition of the beam, deflection under a static load of Q; is calculated as;

$$y = \frac{Q}{2kL} e^{-\frac{x}{L}} \left[\sin\left(\frac{x}{L}\right) + \cos\left(\frac{x}{L}\right)\right]$$

$$y = \frac{Q}{2kL}\eta\left(\frac{x}{L}\right) \quad \text{Eq. 2-5}$$

where; $L = \sqrt[4]{\frac{4EI}{k}}$; is the characteristic length

The maximum deflection is encountered when the load is right above the point where to get the deflection i.e, x=0. Substituting this in to Eq. 2-5;

$$y_{max} = \frac{Q}{2kL}$$

$$y_{max} = \frac{Q}{2kL}\sqrt[4]{\frac{4EI}{k}} \quad \text{Eq. 2-6}$$

II. Tensionless BOEF model according to Kjell Arne Skoglund

This model is an improvement from the traditional the traditional BOEF model in such a way that equal but opposite loads are considered around areas where there exists an uplift. This uplift occurs to the nearby rail and sleeper because of the vertical downwards force at the rail-wheel contact point which is highly dependent on the total load and train speed [21].

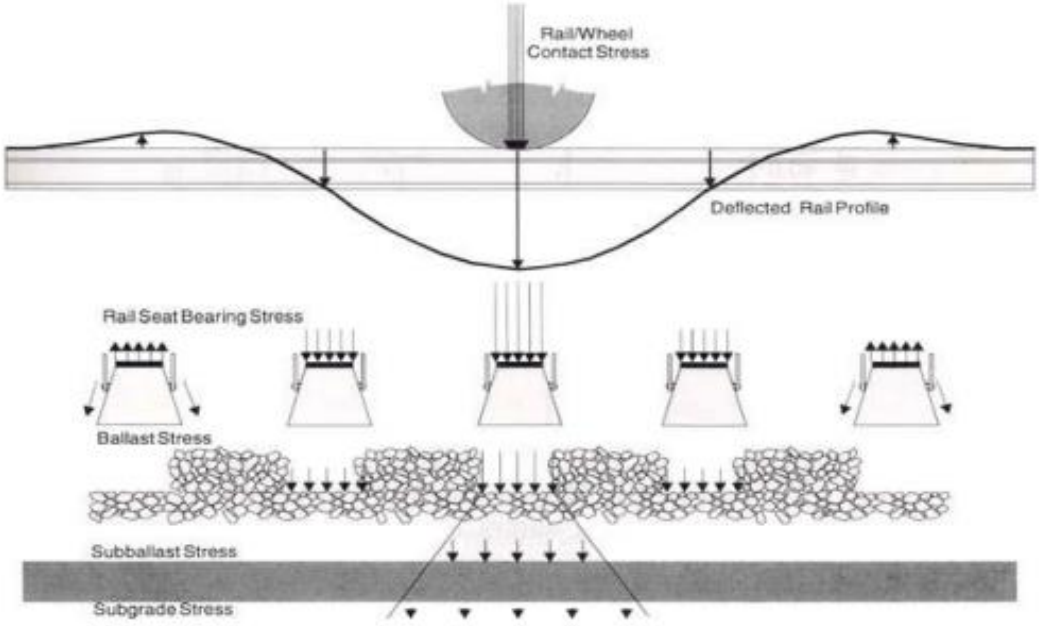

Figure 2-13: Tensionless BOEF by Kiell Arne Akoglund

This specific model yields higher uplift and greater length of uplift zone than predicted by the BOEF model. however, it still suffers from other BOEF limitations

III. Pasternak foundation

This is a two-parameter mechanical model where the reaction of the foundation is determined by a vertical spring stiffness constant and shear interaction is effected by a pure-shear element joining Winkler's springs [21]. This is done by joining the ends of the springs (see Figure 2-14) to the beam having incompressible vertical elements that can only deform by transverse shear. The two parameters involved are KP and GP. Thus, the section force on each face is a shear force only [22].

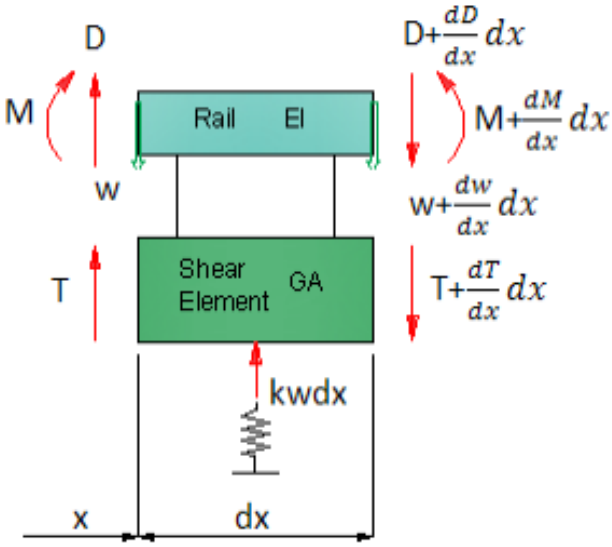

Figure 2-14: Pasternak's two parameter mechanical model

$$p = k_P w - \frac{dV}{dx} \qquad \text{Eq. 2-7}$$

Track dynamic behavior models are categorized in to two depending on the assumptions they put for the support underneath. The first category is when the rail beam is supported by endless track and the second one is when the rail beam is supported discretely.

Continuously supported models of infinite length are based on the beam on elastic foundation theory. The BOEF model is mostly considered the foremost acceptable technique for the analysis of rail foot stress and rail deflections. This model could also be used just for static loading of a track on a soft support (i.e., track with picket sleepers). Dynamic effects can't be analyzed using this model because it contains no mass [20].

In general, relatively high track stiffness provides good track resistance to the load applied and this in return minimizes track deflection. High track resistance with small deflection reduces the track deterioration. However, very high track stiffness might increase dynamic forces at different components of the railway track and this ultimately causes wear and fatigue of track components [17].

2.2.2 Types of track stiffness

Static vertical stiffness:

Static vertical stiffness is the measure of resistance to deformation of a structure when a static load is applied to it. Most researchers prefer it instead of the conventional mechanical analysis of the wheel–rail system. Theoretical analysis and dynamic measurement of track stiffness has become crucial now that there is a huge demand of high-speed and heavy-loaded train transportations.

The discovery of static vertical stiffness is taken as a mile stone in searching for reasonable modelling of the track.

Static vertical track stiffness (k) is computed by dividing the concentrated loads applied on the rail (Q) to the maximum deflection of the track structure (δ_m) beneath the wheel as shown on Figure 2-15. It can be calculated easily since the only requirements are measurement of maximum deflection for the specific load applied [23].

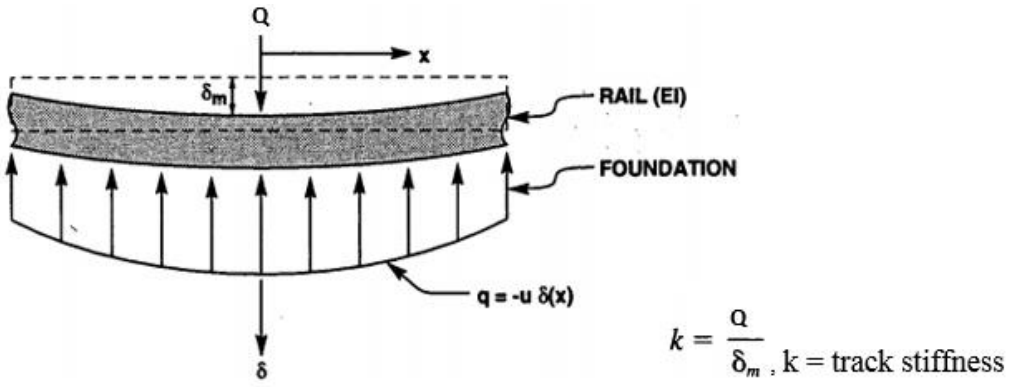

Figure 2-15: Schematic illustration of vertical track stiffness

Dynamic vertical stiffness:

The track structure experiences dynamic load right the moment the train wheel starts to roll over the rail [24]. Thus, dynamic vertical stiffness is the measure of resistance of the track structure when subjected to dynamic loads from the rolling stock on the rail. It is computed as a ratio of the load to the corresponding maximum vertical deformation which are both varying with time (t). i.e,

$$k(t) = \frac{Q(t)}{\delta(t)} \qquad \text{Eq. 2-8}$$

If the computation is in the frequency domain (*f)*, the formula used for the time domain will be readjusted as shown below. Moreover, if the frequency domain is going to be used, it is better to use the inverse of dynamic track stiffness which is termed as the dynamic vertical flexibility (track receptance).

$$\alpha(f) = \frac{Q(f)}{\delta(f)} \qquad \text{Eq. 2-9}$$

2.2.3 Total track stiffness

In general, the rolling stock is supported by the stiffness contributed from the rail through the pads to the sleeper, ballast, sub ballast and subgrade. Thus, there shall be a way to add up each stiffness coming from the track components. Different approaches have been induced to get the total stiffness from the contributions of all these parts and one in every of the best models of the system is as shown in Figure 2-16 [17].

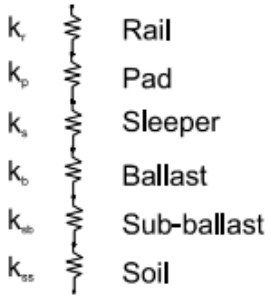

$$\frac{1}{K_{total}} = \frac{1}{K_r} + \frac{1}{K_p} + \frac{1}{K_s} + \frac{1}{K_b} + \frac{1}{K_{sb}} + \frac{1}{K_{ss}}$$

Figure 2-16:Total track stiffness-simplified system

2.2.4 Track stiffness measurement methods

Track stiffness measurement is vital for the design of new railway lines and also for upgrade and maintenance of existing railway lines. Universally there are two types of static and dynamic track stiffness measurement methods namely standstill and continuous [25].

2.2.4.1 Standstill measurement

The total track stiffness acquired from standstill measurements is performed using a quasi-static or dynamic axial load with an output of load-deflection diagram that is then used for stiffness assessment. This type of measurement is often used for research purposes. In general track stiffness, could be measured by four techniques [19].

a. Traditional hydraulic jack-loading methodology
b. Impact hammer methodology
c. FWD methodology
d. TLV methodology

Traditional hydraulic jack-loading methodology: In this method a displacement meter or a dial indicator is mounted on the track to measure the deflection from a certain applied force. Hence, a force–displacement curve is obtained (see Fig. 2-13). Overall track stiffness will then be computed as per the load-deflection relationships [24].

Figure 2-17: Jack-loading diagram and vertical rail deflection measurement

This methodology has been used since the start of the twentieth century and the Talbot committee of the USA has implemented this method to measure track stiffness in 1918 [25].

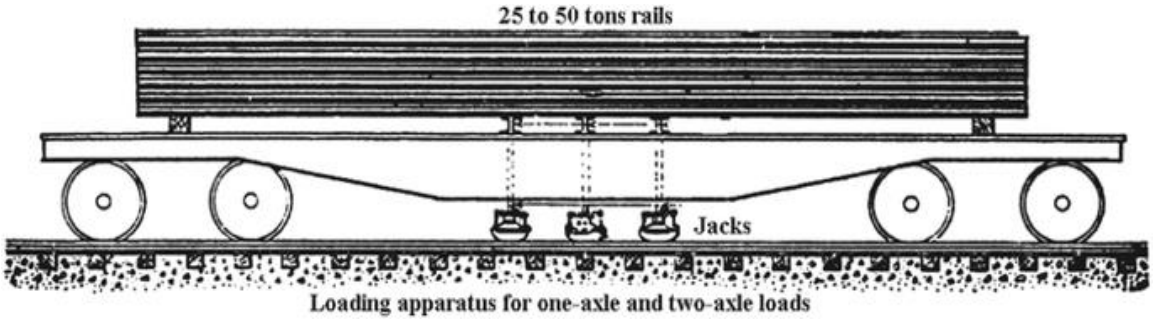

Figure 2-18: Track stiffness measurement - by the Talbot committee of the USA (1918)

Impact hammer methodology: This method measures track vibration by using acceleration transducers mounted on rail or sleepers. It also involves a hummer with a force

transducer attached on it to exert an impulse on the rail head. Once associate impulse load is exerted on the track by the hammer, the transfer function of the track will be obtained. Finally, stiffness of each components and also the total stiffness will be calculated through the track element stiffness and also the overall track stiffness may be calculated through parameter identification. This type of methodology covers a range of frequencies from 50–1,500 Hz, depending on the material type of the hammer head. A softer rubber hammer head is preferable for lower frequencies than the one with a hard-metal head [25].

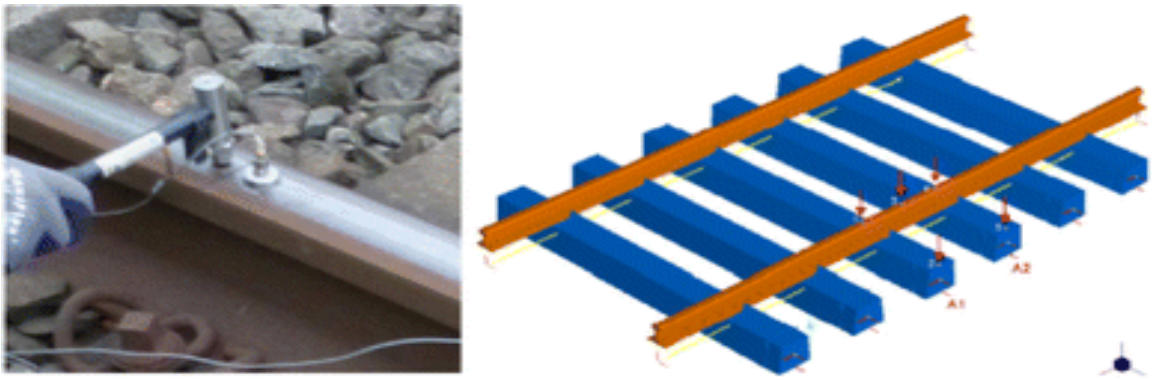

Figure 2-19: Track stiffness measurement using the impact hammer method

FWD (falling weight deflectometer) methodology: In this method a load is used to impact a track and then vibration response is measured for that specific instant. The stiffness can then be computed using transfer functions or different approaches [25].

The FWD methodology, to a precise extent, will show the impact result on a track if a train is running at a high speed. A free-falling mass of 125 kN is used to exert impact for the standard FWD method. Speed geophones are used to measure the vibration response of track system subjected to the loading.

The principle for the track loading vehicle (TLV) methodology: This methodology is somewhat similar to that of the traditional hydraulic jack loading methodology. Except this method is simpler and might yield higher vertical force [19].

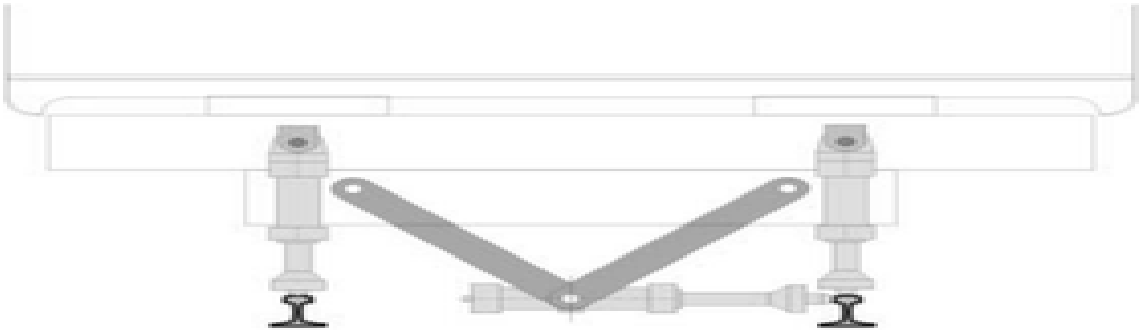

Figure 2-20: Track loading vehicle

2.2.4.2 Continuous measurements

This type of track stiffness measurement is used for measurements on the level of railway network which is mainly for maintenance purposes. In 1997, China Academy of Railway Sciences (CARS) implemented a vehicle for measuring track's elasticity. The vehicle used for this purpose comprises heavy and light rolling stocks at the front and rear respectively. Concrete blocks of weight 150–250 kN are used to increase the axle load of the front locomotive. Finally, the influence of various train axle loads on the measured results are obtained [19].

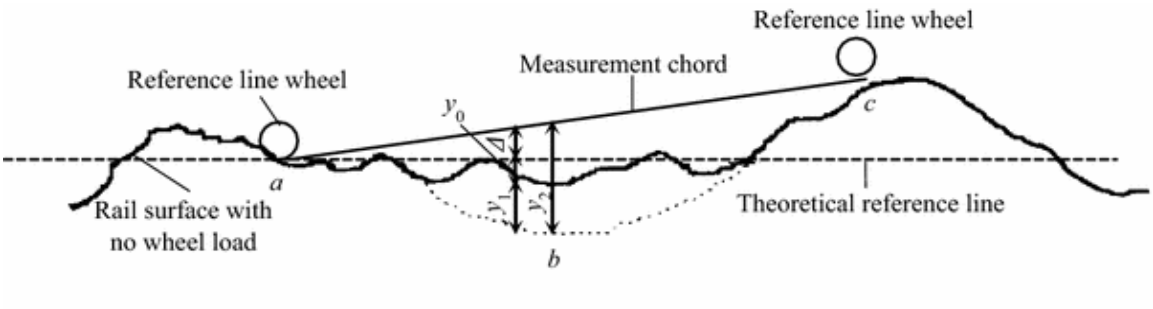

Figure 2-21: Track elasticity measurement with no wheel load on the track - CARS

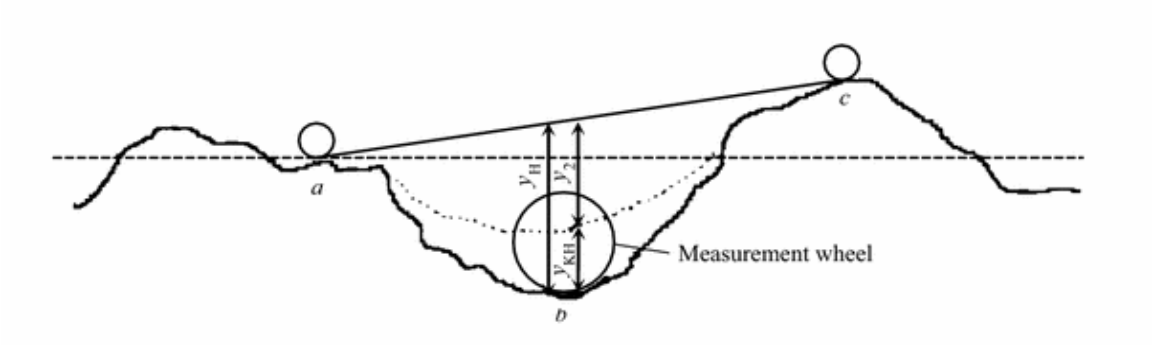

Figure 2-22: Track elasticity measurement with the wheel load of heavy car on track - CARS

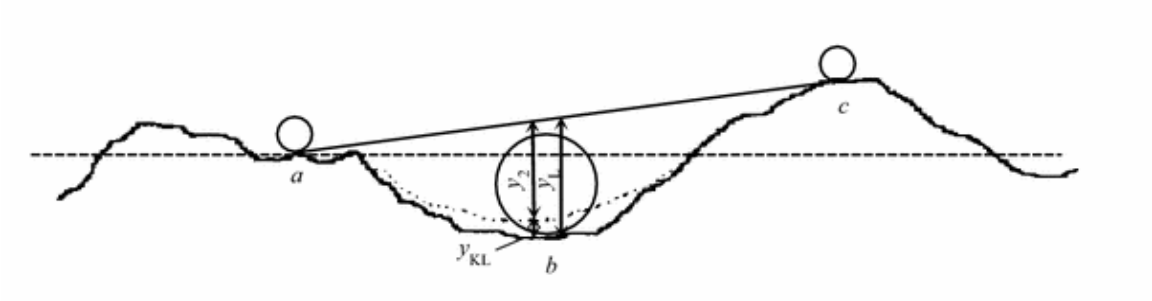

Figure 2-23: Track elasticity measurement with the wheel load of light car on track - CARS

Transportation Technology Center, Inc. in Pueblo, Colorado (USA), conjointly developed a stiffness measure vehicle, with similar measure principle to CARS]. This vehicle includes an important automotive, a lightweight automotive, and a towing locomotive. The displacement measurement is done for the whole track including the subgrade while for the load of 44 kN, it only comprises the rail, sleeper, and ballast with a speed measured to reach up to 60 km/h [19].

Figure 2-24: Track stiffness measurement vehicle of TTCI

In addition, the measurement principle for the stiffness measurement vehicle developed by Swiss Federal Railways is also similar to the above-mentioned ones. This vehicle includes a light car and a heavy car (see Figure below). The weight of the light car can be neglected. The weight of the heavy car is 20 tons. The vehicle speed is 10–15 km/h. The accuracy of displacement measurement can reach up to 0.2 mm [19].

Figure 2-25: Track stiffness measurement vehicle of SBB

2.3 Track stiffness variation and causes

The track stiffness experienced by the rolling stock varies along the track. This stiffness variation is very large within a short distance at some locations. Among the common cases where this variation in stiffness existed, one is when there happens to be a hanging sleeper on the rail which is unsupported from below. The stiffness at this local point will be very low. Another case is around insulated joints, due to that discontinuity on the rail, the bending stiffness of the rail will also have discontinuity leading to a break on the track

stiffness. Transition from an embankment to a bridge can be considered as an additional example where this stiffness variation prevails. Around railway turnouts, there is a rapid change of both inertia and stiffness giving rise to variations of track stiffness which ultimately leads to wheel/rail contact force fluctuation. Hence, the moment track geometry starts to deteriorate, the variations of the wheel/rail interaction forces will increase, and the rate of track deterioration escalates as well. Meanwhile, these variations in stiffness creates permanent deformation of the ballast and the substructure which then aggravates track degradation (high wear, fatigue, track differential settlement) [26].

Fluctuations in track stiffness might originate from the different track superstructure components (rails, rail pads, sleeper, and ballast) or from the substructure components (sub-ballast, subgrade soil, etc).

In the superstructure this variation might happen because of the difference in shape, inertia and spacing of rails or sleepers as discussed previously. However, it could also be caused by a non-uniformly compacted ballast lying or a ballast with varying material properties along the track. Local settlement of the subgrade soil due to the presence of inappropriate soil types leads to huge localized deflection to be an additive factor in the stiffness variation of the track structure [24].

In railway turnouts it is common to have non uniform wheel-rail contact due to variation in rail profile, and moreover the combination of switch rail and stock rail at the transition point to bear wheel loads together creates multiple contact points. Normal wheel-rail contact is altered in the switch panel, when a wheel transfers from stock rail to switch rail and in the crossing panel when a wheel transfers from wing rail to point rail. Furthermore, to ensure the structural integrity and stability of railway turnouts, the shared iron plate of different lengths or the spacer block connects such turnout rails [27].

Woodward et al, discovered that the application of 3D polyurethane ballast reinforcement has provided a high degree of track stability and significantly reducing future track maintenance at many locations in the UK. [28].

Different researchers suggest different mechanisms to reduce maintenance frequency of turnouts and thus enhance railway line efficiency. Which includes reducing turnout

population in the network; using more durable and advanced materials; following preventative maintenance strategy instead of corrective maintenance.

Optimizing the vertical track stiffness at these locations can also be taken as one remedial measure to minimizing the abrupt stiffness changes at the switch panel and crossing panel. Kassa [9] has followed simple numerical procedure based on varying the measured track data parameters of the vertical track stiffness to optimize the stiffness adjusting rail pads and under sleeper pads stiffness along the turnout [9].

2.4 Track stiffness variation and causes along a railway turnout

The fluctuating track stiffness in a railway turnout along the longitudinal direction is mainly caused by the turnout structure. Meanwhile the effect sharing a single iron base plate by two rails, use of different length sleepers and spacer blocks for connecting different rails can influence the characteristics of track stiffness throughout a high-speed railway ballast turnout [2].

Sudden variations of track stiffness result in high dynamic loads that lead to track degradation development of Rolling Contact Fatigue (RCF) defects, differential track settlement, etc). The track deterioration is intensified once it starts because the magnitude of wheel/rail interaction forces increases with it.

Stiffer sections exist around turnouts compared to tangent track due to the existence of increased number of rails, closely spaced longer and heavier sleepers, etc. [4]. Furthermore, bending stiffness of the switch rail is different from the stock rail and other stiffening components, such as the frog, the check rails or the wing rails. These facts will ultimately lead to maximum track stiffness variations of 70% within the switch and crossing panel [6].

The first change of track stiffness happens when the wheel transfers from stock rail sleepers to the switch panel turnout sleepers which are heavier. The sleepers at the beginning of the switch panel contains hollow steel sleepers, to allocate ancillary systems, and the inclusion of the switch rails, which also have a different inertia from the switch toes to the switch heels, that leads also to a stiffness fluctuation [5].

Sleeper length which is continuously increasing in the closure panel adversely affects the uniform track stiffness [4].

Track stiffness variation and causes along a railway crossing

In the crossing panel, the existing of the crossing nose (frog), wing rails and check rails increase remarkably the inertia along the panel. On top of this, there is a change of long bearers to independent short sleepers, after some point which could be placed eccentrically leading to track torsion [4].

Severe impact loads are exerted on the tip of the crossing nose when wheels travel from wing rail to crossing nose in the crossing panel [9]. Meanwhile another detailed research by James et al. [7] briefly explains sleeper right underneath the crossing panel experience the maximum load effects, resulting in the largest deformation.

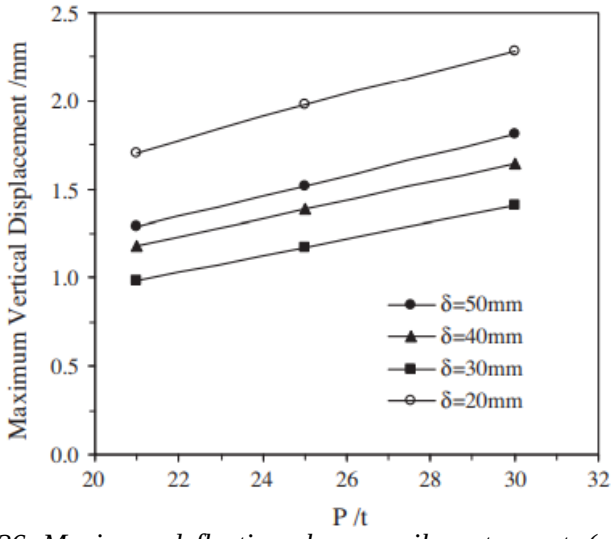

Figure 2-26: Maximum deflection along a railway turnout; (source [24])

As Figure 2-26 illustrates, damage and wear along the crossing panel explicitly at the nose rail frequently occurs at transient zone from 50 mm to 20 mm of crossing rail head section [29].

2.5 Mechanisms to homogenize track stiffness

There are several options available to track designers in order to create homogenous track stiffness. They vary in terms of whether they can be retrofitted to existing track and how effective they are. There are 4 main design options, which are:

- Rail Pads and Bearings;
- Sleeper and Baseplate Pads;
- Floating Track beds and Ballast Mats; and
- Embedded Rails.

Since the design and construction of the rail projects used as part of this research are nearly complete, options such as floating track beds and embedded rails which require early integration aren't discussed in depth.

2.5.1 Use of rail pads

Palsson et al. [30] has carried out a field test to analyze the effect of track stiffness on wheel - rail contact forces using different stiffness rail pads. For their study they used Rolling stiffness measurement vehicle (RSMV) to measure track stiffness and instrumented wheelset mounted on a rolling stock is used to measure the contact forces. The analysis output reveals that soft rail pads were able to reduce contact force, both in the diverging route and through route [30].

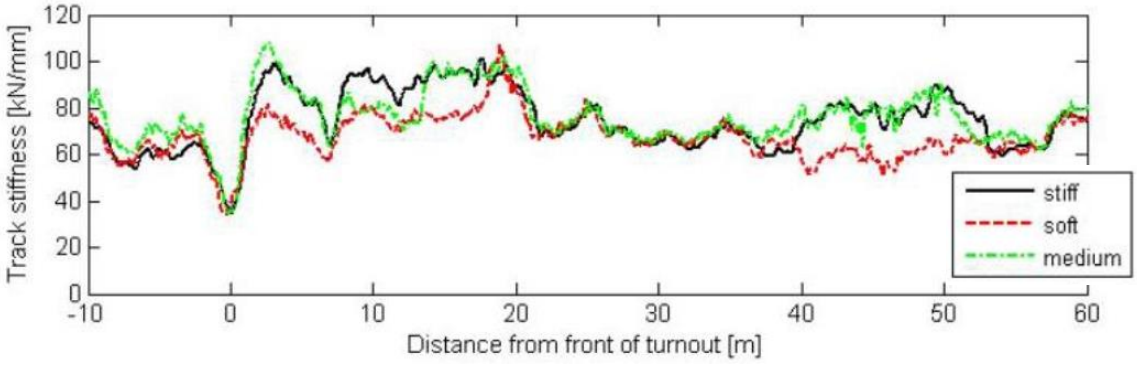

Figure 2-27: Effect of different rail pads in track stiffness along a turnout; [30]

The use of rail pads in shown in the diagram below (shown in blue). It can isolate the vibration forces by absorbing them, and has the benefit of being easily retrofitable on existing train tracks. However, the loads applied due to the need to fasten them to the track has the potential to reduce their effectiveness, and possible influence the track negatively.

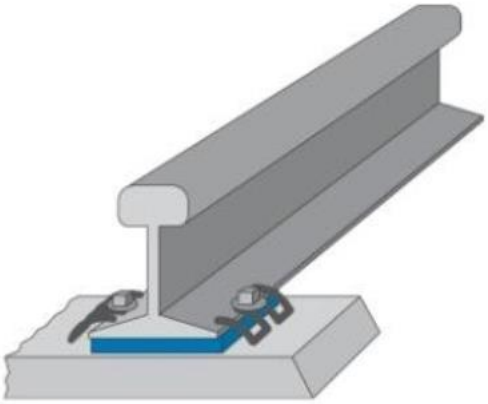

Figure 2-28:Rail Pads

2.5.2 Use of USPs

A finite element model analysis developed by Loy [31] shows the effect on the output using a standard turnout with or without under sleeper pads (USPs). His findings for the rail deflection of a switch without USP, using one type of USP and using different types of USP are shown in the figure below.

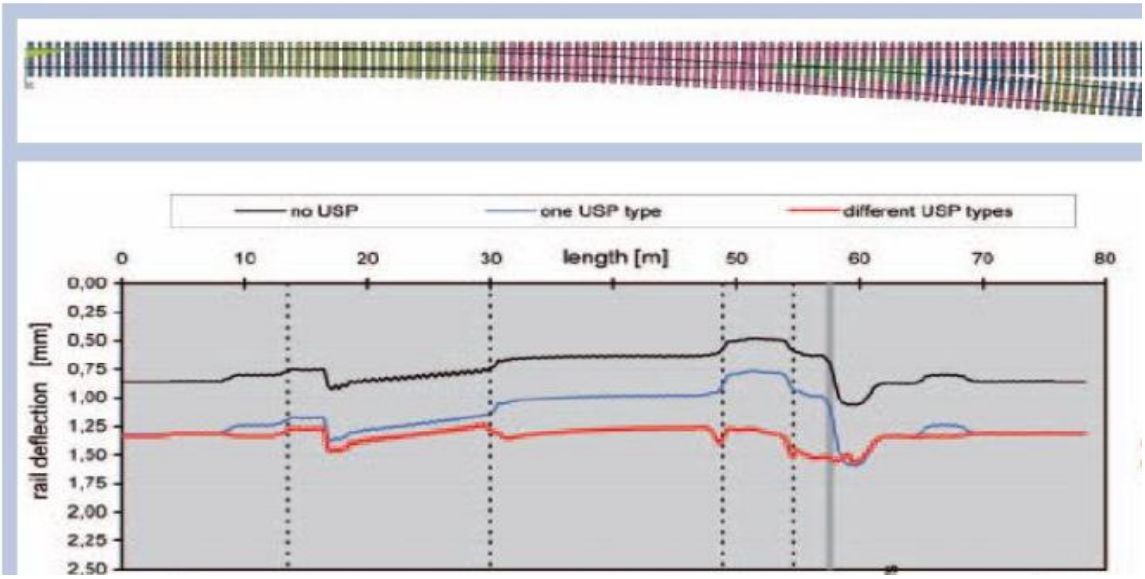

Figure 2-29: Rail deflection comparison with optimized track using different USP [31]

The use of USPs is illustrated in the diagrams below (shown in blue), with the pads placed below the sleepers. Such components can also be retrofitted to existing train tracks, and are considered more effective compared to rail pads. However, the retrofitting process is more complicated for this option [31].

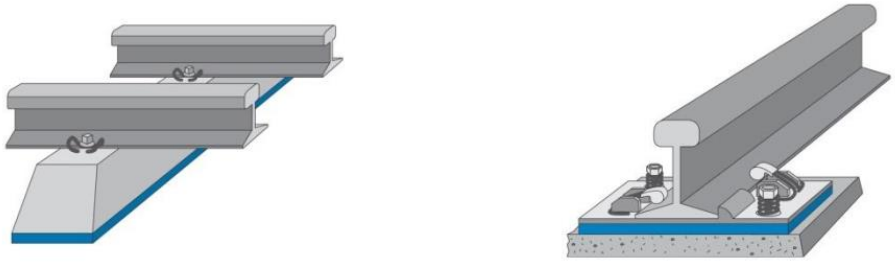

Figure 2-30: Under Sleeper Pads

A Study by Kassa et al. [10] on geometry and stiffness optimization for switches and crossings, and simulation of material degradation has exploited both rail pads and under sleeper pads to get the max effect from the two. Increasing the stiffness value at a location 4.5m from the front of the S&C and reducing it at locations 9.1m and 21.85m from the front of the S&C respectively, has given an interesting output of lower stiffness variation at the three locations. i.e., 409.64MN/m, 441.64MN/m, and 454.4MN/m [6].

2.5.3 Use of UBMs

Under Ballast Mats (UBM) are also employed to provide a higher elasticity to the track, it can be also regarded as a system to homogenize track stiffness such as softer rail pads or USP.

The effect of UBM on dynamic wheel/rail forces acting in the crossing nose and pointed out there is almost no effect. However, even if UBM may not be efficient to reduce impact load and wear on the crossing nose, they are used also as a mechanism to reduce vibration.

2.5.4 Use of pads underneath iron base plates

The choice of turnout rails does not have a significant effect in optimizing the turnout stiffness because the service life limit and production technology. The dimensions and layout of the spacer block's purpose is solely to make sure the turnout is geometrically

stable and that the longitudinal forces are transmitted effectively. Hence, use of pads underneath baseplates is not appropriate for optimizing the turnout stiffness through redesign.

The pads underneath the iron base plates contribute the major elasticity for the fastening system and also the stiffness will be tuned among a large range. The support stiffness is can be modified by altering the structure of the pads underneath the iron base plates. For instance, a grooved or perforated pad underneath the iron base plates can be used. The stiffness optimization of high-speed railway turnout ought to satisfy some basic constraints.

The longitudinal stiffness fluctuation of in a railway turnout ought to be among low control; and there should be a category limit of pads whose stiffness is redesigned to ensure the assembly and replacement handily.

A normal track has a fastening stiffness of about 50 kN/mm and around the turnout section, the elasticity of the fastening system is derived from the pads underneath the rails and iron base plates, wherever the stiffness of the pads underneath the rails is 200 kN/mm. The stiffness of the fastener system within the turnout zone is appreciated from that of the normal track.

2.6 Hyperelastic material model for Rail pads and USPs

Hyperelastic material simulations are vastly used in the modeling of rubber and rubber like materials to consider the material's non linearity. This type of material model accommodates large strains and the relationship with stress is usually not strait [32].

Hyper elastic material models are generally used for ideally elastic materials for which stress – strain relationship is derived from a strain energy potential function. Strain energy on the other hand is defined as the elastic potential energy stored in the material when it is subjected to elongation or compression by an external force [33].

In ABAQUS, Hyperelastic materials are described in terms of "Strain Energy Potential (SEP)" which defines the strain energy kept in the material per unit of reference volume (volume in the initial configuration) as a function of the strain at that point in the material

[34]. The behavior to be defined is provided as either instantaneous (at t=0, before the material relaxes) or long-term properties (at t=infinite, after the material is fully relaxed).

There exist different types of strain energy potential functions (Table 2-1) in ABAQUS to model approximately incompressible isotropic elastomers and the choice of which depends on the data available [32].

Table 2-1: Available SEPs available in ABAQUS

Strain energy function	**Number of Coefficients**	
	Deviatoric	**Volumetric**
Arruda-Boyce	2	1
Marlow	-	
Mooney-Rivlin	2	1
Neo-Hookean	1	1
Ogden	2 per order	1 per order
Polynomial	$N + \sum_{i=0}^{N} i \quad with\, N = order$	1 per order
Reduced polynomial	1 per order	1 per order
Van der Waals	4	1
Yeoh	3	3

In General, when several experimental tests data is available (uniaxial and equibiaxial test data), the Ogden and Van der Waals functions are more accurate in fitting experimental results. But if there is only limited test data available, the Arruda-Boyce, Van der Waals, Yeoh, or reduced polynomial forms provide reasonable behavior.

2.6.1 Types of experimental tests adequate for ABAQUS hyperelastic material model

For homogeneous materials, homogeneous deformation modes are enough for ABAQUS to compute the material model coefficients. For the case that there is limited data provided, ABAQUS establishes strain energy potential that will reproduce the test data to have reasonable behavior in other deformation modes [35].

The following are different experimental test approaches which ABAQUS can use as an input.

- Uniaxial tension and compression
- Equibiaxial tension and compression
- Planar tension and compression (pure shear)
- Volumetric tension and compression

The most commonly performed experiments are uniaxial tension, uniaxial compression, and planar tension are illustrated schematically on the figure below.

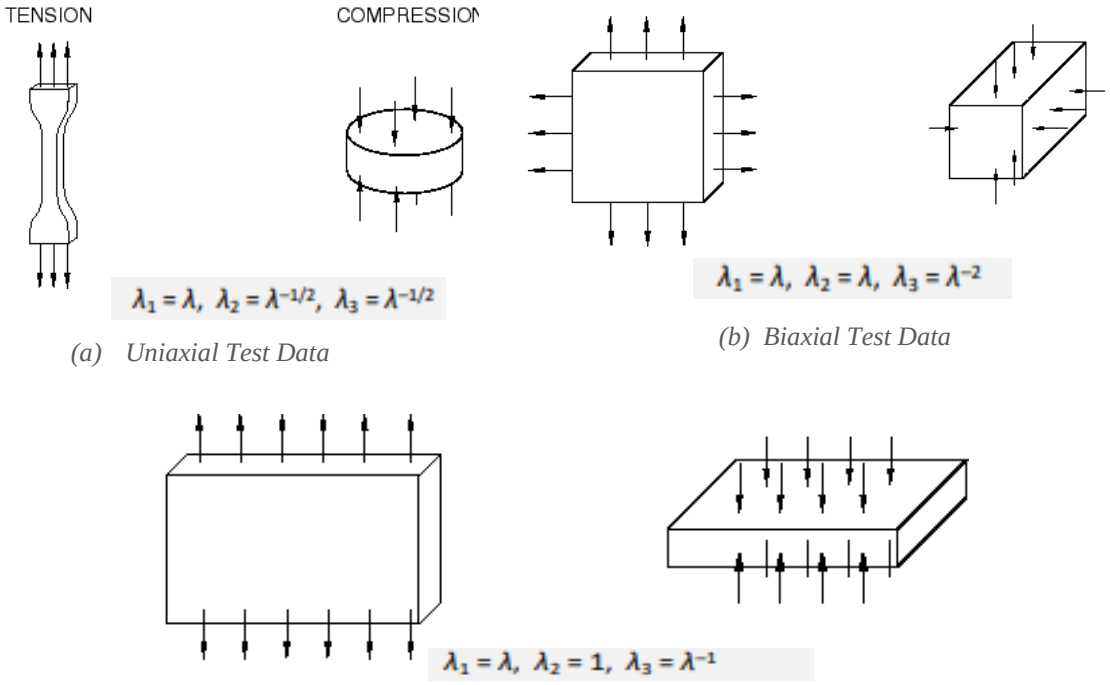

(a) Uniaxial Test Data

(b) Biaxial Test Data

(c) Planar Test Data

Figure 2-31: Schematic illustration of different experimental tests which are accepted by ABAQUS

Finally, when performing material evaluation, ABAQUS provides stability limit information regarding the required standard tests.

2.7 Normal contact forces in the wheel-rail contact

In wheel-rail contact the two bodies generally have a nonconformal contact which is a contact between two dissimilar profiles at a point or a line. The contact area is commonly small compared to the size of the bodies in contact and that is where the stress and deformation is exhibited locally [36].

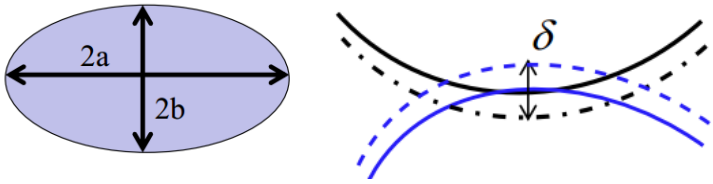

Figure 2-32: Hertz, ellipsoidal normal contact pressure distribution and non-conformal contact

A contact patch develops at the point where there is a contact between the wheel and the rail which is highly dependent on the normal force, geometry and material properties of the bodies under contact. Hertz theory predicts elliptical contact patch and both normal forces and tangential forces (longitudinal and lateral) act on this contact patch [37].

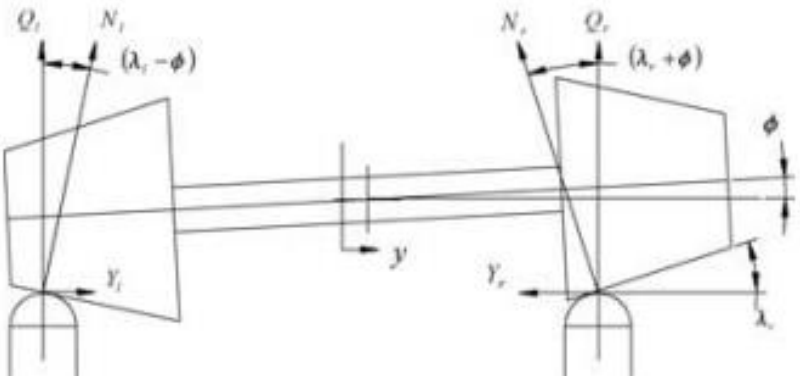

Figure 2-33: Normal and tangential forces on the contact patch

According to Hertz, the normal contact pressure p_z is calculated as [36]:

$$p_z(x,y) = z_0\sqrt{1-\left(\frac{x}{a}\right)^2-\left(\frac{y}{b}\right)^2} \qquad \text{Eq. 2-10}$$

where:

- a & b are long and short lengths of the elipse respectively
- z_0 is the maximum contact pressure at the initial contact point

Integrating the normal pressure distribution to give the total normal force:

$$N = \iint p_z(x,y)dxdy = \int_{-b}^{b}\int_{-a}^{a} z_0\sqrt{1-\left(\frac{x}{a}\right)^2-\left(\frac{y}{b}\right)^2}\,dxdy = \frac{2\pi ab}{3}z_0 \qquad \text{Eq. 2-11}$$

$$z_0 = \frac{3N}{2\pi ab} \quad \text{Eq. 2-12}$$

$$is\ equivalent\ to\ the\ maximum\ contact\ pressure, P_{max}$$

The normal forces developed between the wheel and rail are made up of a force that supports the static and dynamically varying force in response to the vehicle motion caused by irregularities along the track [37].

2.8 Gap analysis

The literature review has identified several issues to resolve for minimizing turnout related operation and maintenance cost of railway line under ERC. The areas, which remain unexplored, are:

- In the previous studies, the pads used for optimizing track stiffness were modeled as a series of springs with Stiffness and Dashpot coefficients given. However, this study uses hyper elastic material models to define the pads.
- Moreover, Non-linear characteristics of ballast materials are taken in to consideration.
- The stiffness characteristics along the selected turnout for the expected train speed and loading needs has not been investigated.
- Suitable rail pads and under sleeper pads shall be used jointly to improve abrupt stiffness changes on the selected railway line so that the speed of the through root of the line under study can be kept and the speed of the diverging root can be increased until the curved geometry allows.

3 RESEARCH METHODOLOGY

This study is an applied quantitative type of research, which will utilize several numerical data and graphs to present the analysis results.

The methodology employed by this thesis will bring together various fields that have been discussed previously in the literature review to answer the research questions that have been posed. Broadly, the methodology section of this thesis employs the following research instruments:

- Data collection;
- Turnout modelling; and
- Stiffness homogenization across the turnout crossing.

The first two instruments are part of the inputs for the ABAQUS Model, which enables to input site-specific design and operation scenario in order to get the homogenizing stiffness of rail pads and under sleeper pads. ***ABAQUS 6.19*** is used to perform the numerical model with some parts being first modeled and imported from ***Solidworks CAD solid modeling software 2020.*** In addition, ***Templot 2*** application software is used to prepare the plan layout of the turnout under study. A well-developed python code (appendix A) [38] is used during the post processing stage to extract maximum deflection at each time increment.

3.1 Data collection

The primary input for the stiffness homogenization is the numerical model, which precisely depicts the actual design and operation condition at the selected site. This information was collected from the design department of Ethiopian Railway Corporation (ERC).

The following data were collected from the ERC:

- Turnout design specifications used in the route;
- Cross sectional information;
- Operation speed and loading of the line;

3.1.1 Site selection

The only railway operator in Ethiopia is Ethiopian Railways Corporation, ERC that is engaged in the huge work towards building an extensive rail network. Among the thirteen routes planned to be built in two phases, the current operating mixed line under ERC is Addis Ababa - Djibouti railway, which is the main means of transportation for passengers, freights and for imported goods from Djibouti, Doharre new port to Ethiopia, Addis Ababa. It provides access of the sea for the landlocked Ethiopia.

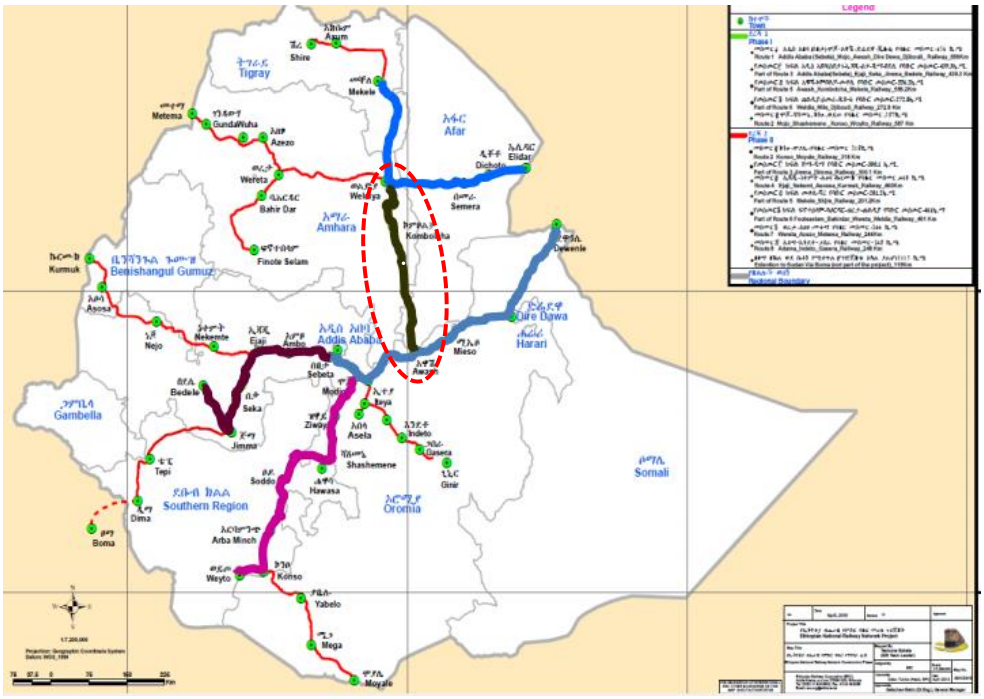

Figure 3-1: Ethiopian National Railway Network

Another root under phase I of the construction is a line initiating from the north east of the city of Awash and arrive to Weldia through the city of Kombolcha. The Awash-Kombolcha-Hara Gebaya Railway Project has a length of 392 kms with an overall progress of 92%. [39]. A turnout from this specific line is selected since the line has not been operational yet and taking field measurements of the turnout is very convenient. The operational speed and loading conditions are assumed to be similar with the Addis Ababa - Djibouti railway line. As the major objective of this research is to investigate the stiffness variation along a selected turnout crossing subjected to the operational loading and speed condition, this line suits well to meet the objective.

Figure 3-2: Turnout photos taken at a shunting area around Kombolcha

3.1.1.1 Turnout Design parameters in the line

In this study of Awash-Kombolcha-Hara Gebaya railway line, the main line and the passenger train route adopt No.12 turnout while other station tracks adopt No.12 or No.9 turnouts; for the depot, post, storage yard, maintenance section and freight yard No.9 turnout are employed. The following table shows parameters of turnouts used in the line:

Table 3-1: Turnout Parameters

Number of Turnout and frog	**Rail Type (kg/m)**	**Dimension of Turnout (mm)**						
		Frog Angle (a)	Radius of lead curve (R)	Total length of Turnout (LQ)	Distance from beginning to center (a)	Distance from center to heel (b)	Distance from heel to last turnout tie L’	Distance from heel to last long turnout tie (L’)
9	50	6°20’25’’	180000	28848	13839	15009	8100	5700
12	50	4°45’49’’	350000	37907	16853	21054	10500	8100

3.1.1.2 Operational data

The design speed for passenger trains equals or is less than 120km/h and that of freight trains equals or is less than 80km/h. but according to the data collected from ERC regarding the current operation data the speed for both passenger and freight trains is 45Km/hr with a tonnage of 24 -29.

3.2 Finite Element (FE) modelling

Considering reasonable computational effort, this paper utilizes a nonlinear 3D FE analysis using ***ABAQUS 6.19*** software. The model consists Rails, Rail pads, Steel plates, USPs, Sleepers, and Ballast. The plan layout of the turnout is prepared using ***Templot 2*** application software.

The material properties, Part dimensions, Wheel/Rail Interface (W-R), Loading and Speed used in the model are presented in detail in **section 4.3 and 4.44.4**. The wheel is set to travel the turnout crossing by a facing move, i.e., it gets to the switch points before it gets to the frog.

3.3 Analysis approach

For the analysis, a train wheel load (half of the axle load) is simulated by a transient load (load varying with time). The finite element model of the railway turnout is applied to calculate the rail displacement, contact forces and maximum stress; then the track stiffness of the turnout crossing is obtained based on a relationship between the load and rail deflection [19]. The maximum vertical deflection for each time step along the 2.8m track is extracted from the software using a customized python code. Each Scenario followed the same procedure to compute the stiffness.

3.4 Work flow

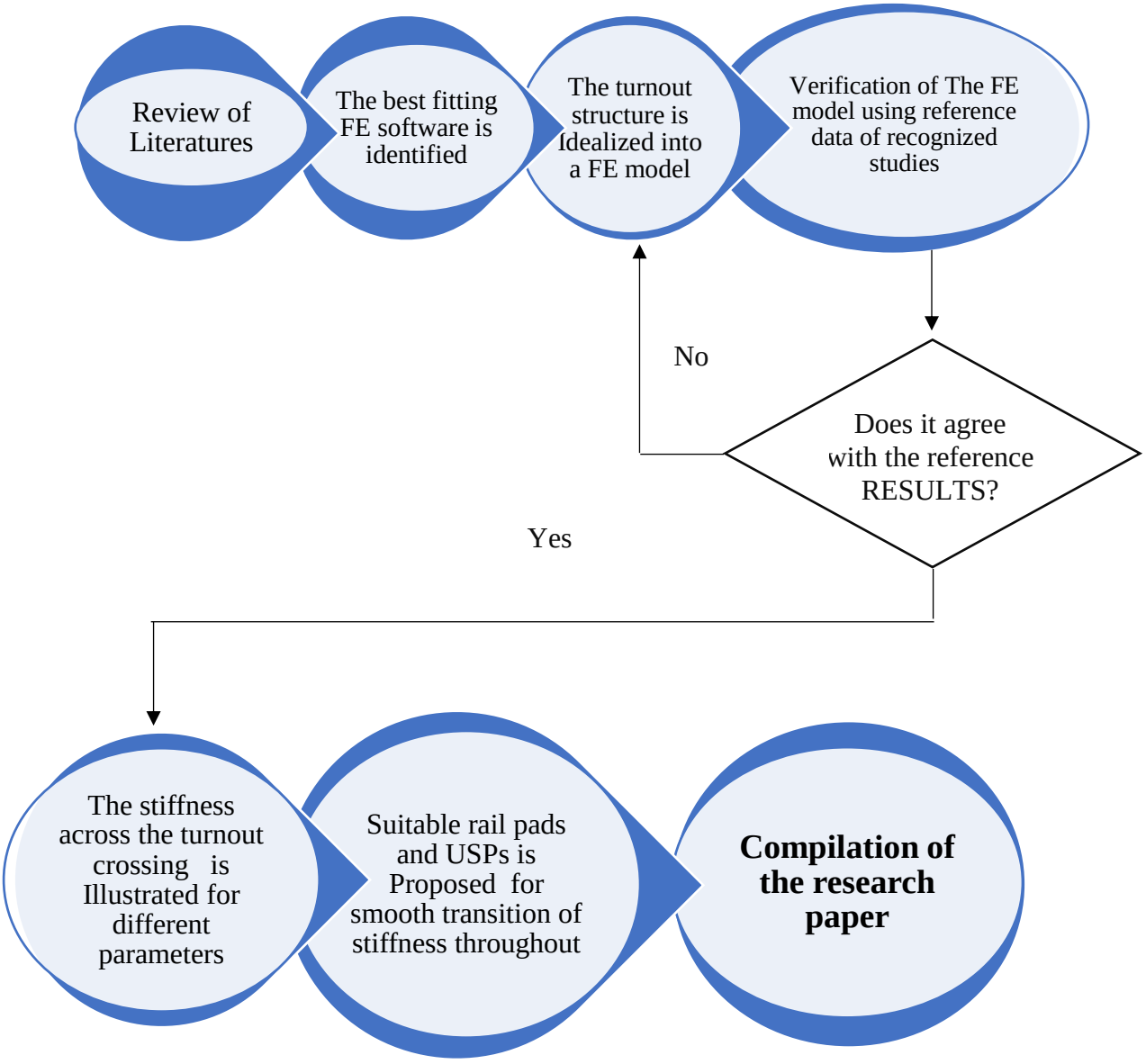
Review of Literatures
The best fitting FE software is identified
The turnout structure is Idealized into a FE model
Verification of The FE model using reference data of recognized studies
No
Does it agree with the reference RESULTS?
Yes
The stiffness across the turnout crossing is Illustrated for different parameters
Suitable rail pads and USPs is Proposed for smooth transition of stiffness throughout
Compilation of the research paper

4 MODEL INFORMATION AND VERIFICATION

4.1 Evaluating the best fitting software

Varies finite element software are assessed to come up with the best fitting software for the modeling and analysis involved in this study.

Table 4-1: Comparison between different FE software

FE software	Pros and Cons	Best applicable
ANSYS [40]	- User friendly environment - Can uniquely simulate electromagnetic performance across component, circuit and system design, and can evaluate temperature, vibration and other critical mechanical effects - ***Requires heavy computational power to give accurate results for complex analysis.*** - ***Faster database is a requirement***	- Energy Industry - Problems involving dynamics, statics, fluids, electromagnetic, thermal, and vibrations
LS DYNA [41]	- Ideal for dynamic analysis - Capable of simulating complex real-world problems - Handles large deformations (for example the crumpling of sheet metal parts) - Can simulate Automotive crash and Explosions - ***Graphical user interface is not interesting compared to other FE software*** - ***Very expensive to purchase*** - ***Not efficient at implicit time integration***	- Used by the automobile, aerospace, construction, military, manufacturing, and bioengineering industries.

PLAXIS 3D [42]	- Primarily used for Geotechnical analysis and simple geometric problems. - Staged-construction modeling and analysis capability is better. - Suite for dynamics for load modeling and PlaxFlow for groundwater analysis. - ***Requires heavy computational power and it is more expensive.*** - ***Less tutorials available.*** - ***Results window is a bit complex to understand.***	- Geotechnical analysis and rock mechanics
NASTRAN [43]	- Used to analyze linear and nonlinear stress, dynamics, and heat transfer characteristics of structures and mechanical components. - Has a Multidisciplinary Structural Analysis version (MSC). - ***The complex GUI coupled with low visual sims isn't great.*** - ***It is not a complete package.*** - ***Thermal resistance calculation is absent.*** - ***The mesh control isn't advanced enough.***	- General-purpose

ABAQUS /CAE, or "Complete ABAQUS Environment" which is a computer code application used for modeling and analysis of parts and assemblies (pre-processing) and visualizing the finite part analysis results [44]. ABAQUS has a wide variety of material models such as elastomeric and hyperelastic material modeling [45].

According to LLC, FEA services [44], the main Advantages using ABAQUS are:

Non-Linear Performance: Even though, FEA models do take time to run. The strength of the ABAQUS code that was originally developed as a nonlinear solver is that it will run any nonlinear simulation quicker and can converge on more true, additional realistic results than different codes.

Contact Modeling: Real applications square measure made from assemblies, not single components. The components of those assemblies operate by returning into contact with one another. ABAQUS is out and away the most effective FEA code at handling all styles of contact. Also, its CAE interface currently makes it elegantly straight forward for a typical user to line up several contacts within the FEM.

Efficient Substructures: ABAQUS supports standard substructure processes like super elements. The ABAQUS sub model method is elegantly straightforward enough. Fixing a functioning sub model from a world model is mostly performed in minutes. In recent years, the ABAQUS sub modeling capability was developed to operate with nonlinear analysis.

Multi-physics: ABAQUS performs nearly all types of multi physics iron analysis, whereas the operations are supported by the ABAQUS /CAE interface. With ABAQUS /CAE, users will seamlessly operate multi-physics and co-simulation techniques between the assorted I/O information sets and between the solvers.

Extreme Deformation: ABAQUS package has been well matched for nearly thirty years to manage extreme deformation simulations because of its intrinsic nonlinear code.

Fracture and Failure: ABAQUS offers a general framework for modeling bulk material damage and failure over a large variety of materials (composites, metals, concrete, etc.) and structures. This framework permits simulation of damage initiation and evolution while not the necessity for specifying any initial state within the structure.

Development and Support: ABAQUS user community contributes documented examples using ABAQUS for unique applications. On top of this, the presence of this documentation, amounting to thousands of articles and papers makes it preferable by designers.

The issue with ABAQUS is that the 3D modeling features are not advanced to accommodate complex shapes. Because of this, a 3D CAD design software, SOLIDWORKS is parallelly used in modeling the turnout in this study to encounter this shortcoming.

Consequently, looking at the above merits this software holds and observing successful researches done using this software in addition to the fact that many tutorials on this specific field of study exist better than the other FE software, ABAQUS is chosen to be used in this study.

4.2 Model verification and validation

4.2.1 Basics

Users of results obtained from the model in this paper are rightly concerned with whether a model and its results are "to be reliable". This concern is addressed through model verification and validation.

Model verification: is frequently defined as "ensuring that the computer program of the computerized model and its implementation are correct" [46]. On the other hand,

Model validation is often defined as "substantiation that a computerized model within its domain of applicability possesses a satisfactory range of accuracy consistent with the intended application of the model" [47].

With this regard, referring to [46], ***Comparison to Other Models*** which is one type of validation technique is used to verify and validate this paper. This type of technique uses comparison of Various results of the simulation model to be validated (e.g., outputs) to results of other (valid) models. The other valid models could either be known results of analytic models, or other simulation models that have been validated before.

Therefore, A previously calibrated paper by James Sae Siew, Olivia Mirza, and Sakdirat Kaewunruen which is published on 2015 has been used to verify the 3D FE model. The paper is entitled "Nonlinear Finite Element Modelling of Railway Turnout System considering Bearer/Sleeper-Ballast Interaction".

a) The Reference FE Model

The model referred comprises of fully 3D deformable solid parts. The track components included in the study are different rails, crossing nose, length wise diverse sleepers, and finally a ballast layer which acts as the track support. The assembled model is shown in Figure 4.1.

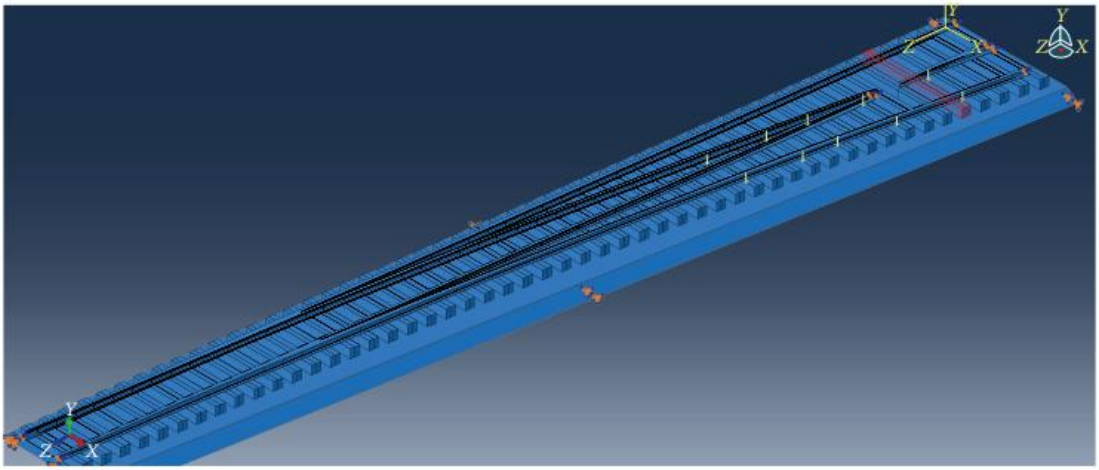

Figure 4-1: Assembly of a Reference 3D Model used for verification

Material properties used in the reference model:

Materials	Elastic Modulus (GPa)	Compressive Strength (MPa)	Tensile Strength (MPa)
Concrete	38	36-55	4.0-6.3
Rails	205	_	_

Constraints and Boundary Conditions:

A Tie Constraint is used in between the rails and the underlying sleepers/bearers and also between the sleepers and the ballast in order to let ABAQUS generate optimized interface mesh and also to reduce the computational effort [7]. The refined interface mesh is required since mesh sizes and the material densities are different between each tied object. The tie constraints are set surface to surface in order to allow uniform distribution between the tied components.

- **As per the reference model, Encastre (fixed boundary condition)** is applied to the bottom surface of the ballast to simulate the structures below, See figure4-2.
- **Symmetrical constraint** is used to the associated planes at the ends of the rail to idealize the rails continuity.

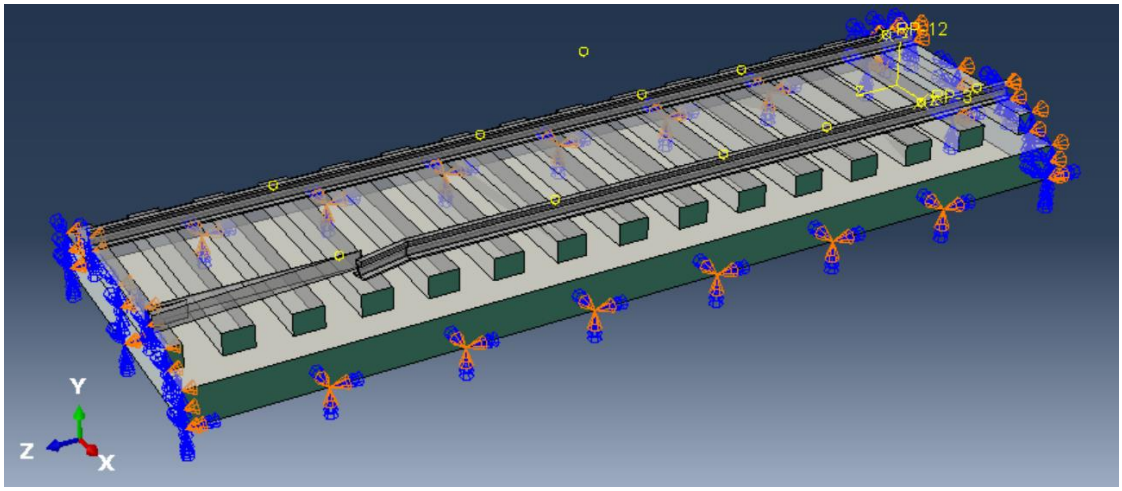

Figure 4-2: Boundary condition - Static model

Load Conditions:

The design loads are set to represent the worst-case load arrangement deployed onto a railway track. The FE model analyzes the turnout's response for a set of concentrated axle loads among which four of them are 300 kN and one is 360 kN axle load found 2 meters ahead of the group.

The effective vertical Unsprung mass per wheel, M	245 kg
The effective vertical rail damping rate per wheel, C	55.4×10^3 N/m
The effective vertical rail stiffness per wheel, K	62×10^6 N/m

To maximize the computing time efficiency, the reference model uses 100mm×100mm mesh [7].

b) The FE Model to be Verified

Similar model parameters (Material properties, Loading, Constraint and Boundary Conditions) are used to verify the FE model; in order to reduce computational effort some parts are simplified by taking the Flexural rigidity (EI) of the parts equivalent as shown in Figure 4-3. An application software ***SkyCiv*** is used to calculate the moment of inertia of the parts.

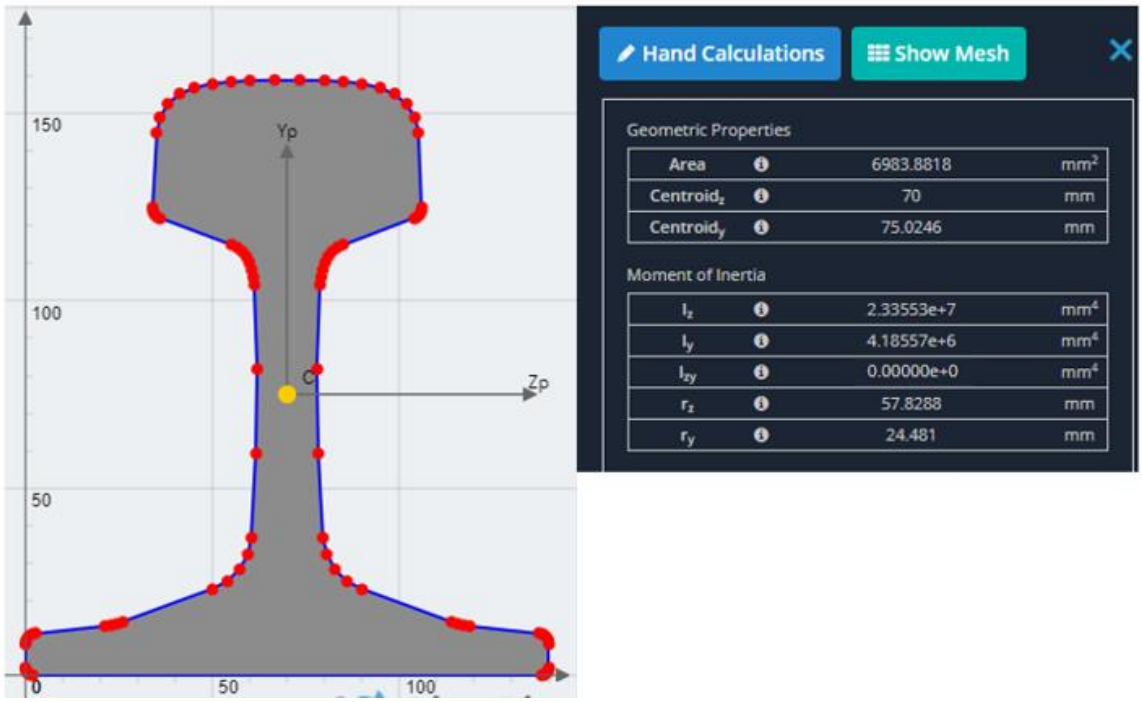

(a)

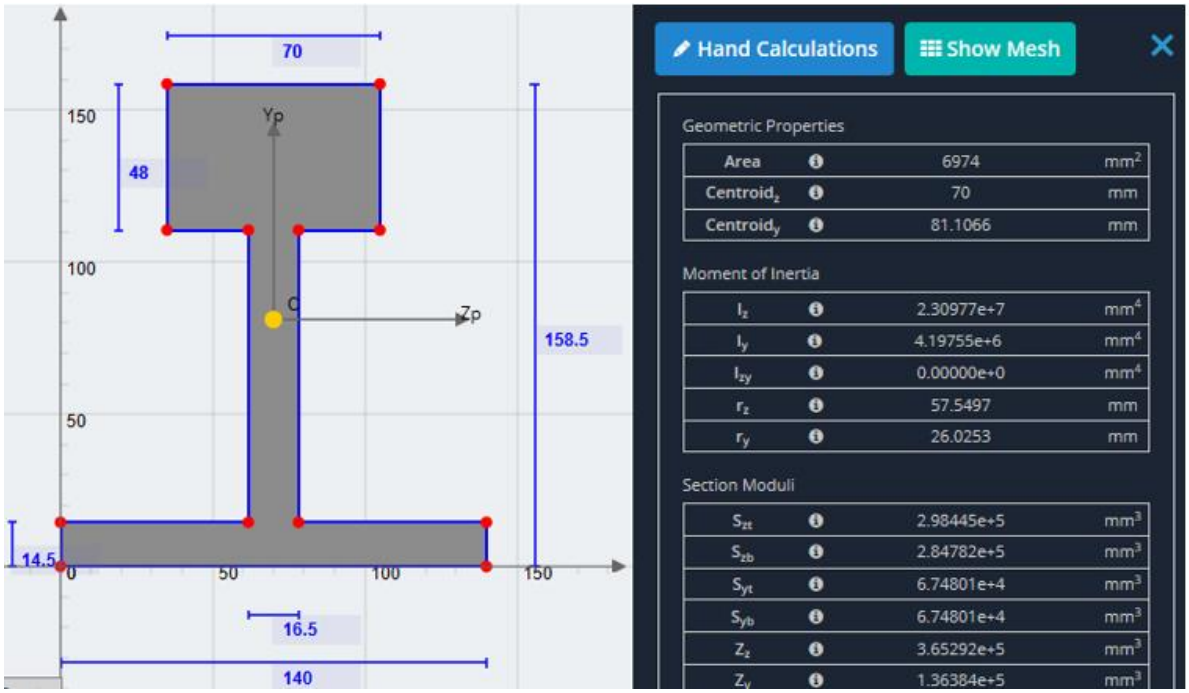

(b)

Figure 4-3: (a) Moment of Inertia of actual UIC 54 Rail; (b) Moment of Inertia of simplified UIC54 Rail

Moreover, Assembly of the Model to be verified and loading arrangements are shown in Figure 4-4.

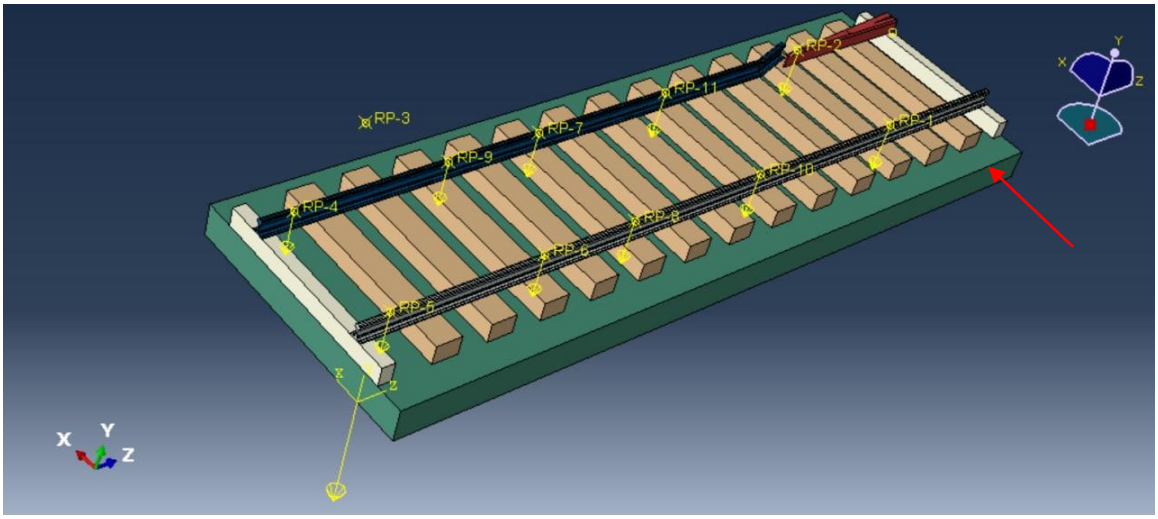

Figure 4-4: Assembly of the 3D Model to be verified

4.2.2 Output analysis and comparison

The Sleeper right underneath the crossing nose (named Sleeper 47 on the reference paper) is chosen for verifying the model. This is because it is the area of maximum deflection and where frequent maintenances are encountered, i.e. the major focus area of this paper.

The outputs of both models; i.e., Model with actual and simplified rail parts get along each other well with regard to stress, deflection and so on as shown in Figure 4-5 (a) & (b). This simplification on the shape of parts also helps on modeling the dynamic 3D model with a reasonable computation effort.

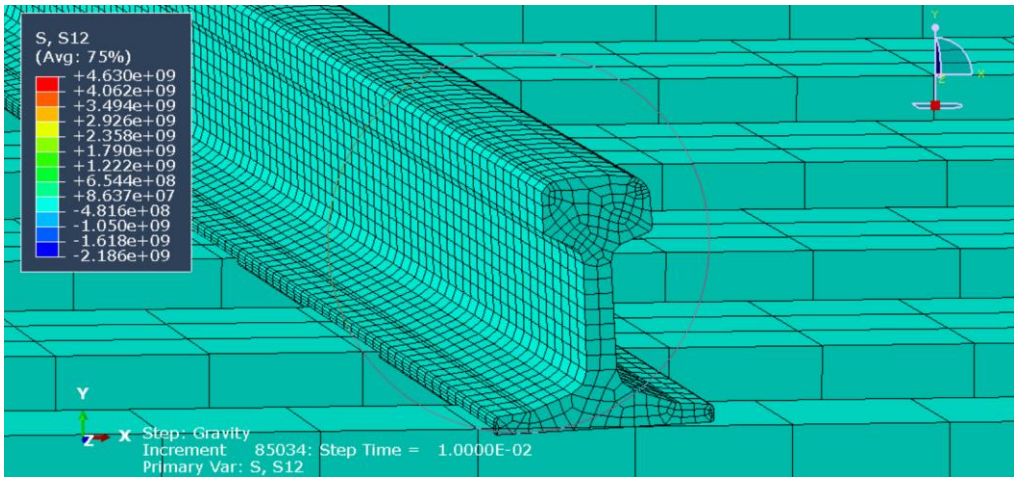

(a)

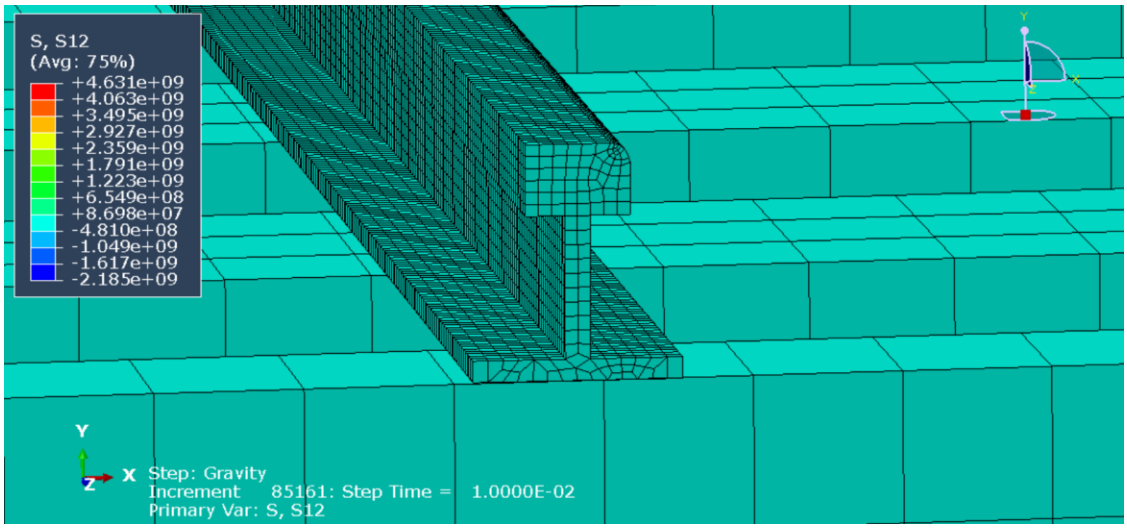

(b)

Figure 4-5: Stress results (S12) - actual model (a); simplified model (b)

a) Deflection of sleeper right underneath the crossing nose: the maximum deflection of a sleeper right underneath the crossing nose of the model to be verified is compared with the corresponding output of the reference model. the graph below best illustrates the deflection.

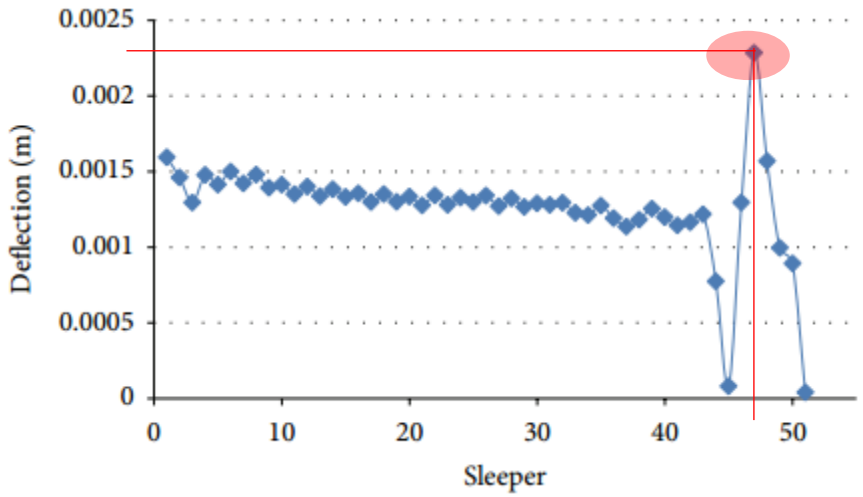

Figure 4-6: Deflection response at the middle of Sleepers 47 of the reference model

The maximum deflection at sleeper 47, (the sleeper right underneath the crossing nose is ≈ 2.4 mm.

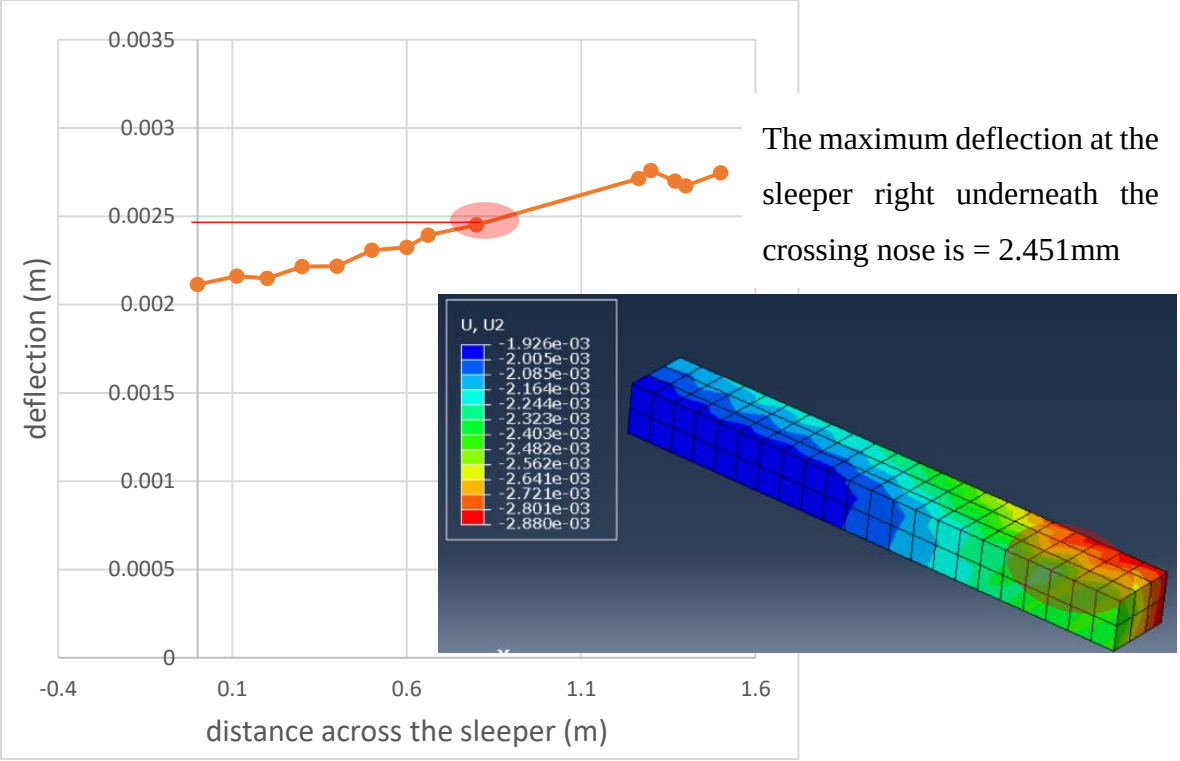

The maximum deflection at the sleeper right underneath the crossing nose is = 2.451mm

Figure 4-7: Deflection of the sleeper underneath the crossing nose of the model to be verified

b) ***Bending stress, S22*** of the sleeper right underneath the crossing nose: The Bending stress of a sleeper right underneath the crossing nose of the model to be verified as shown in Figure 4-8 (a) is compared with the corresponding output of the reference model.

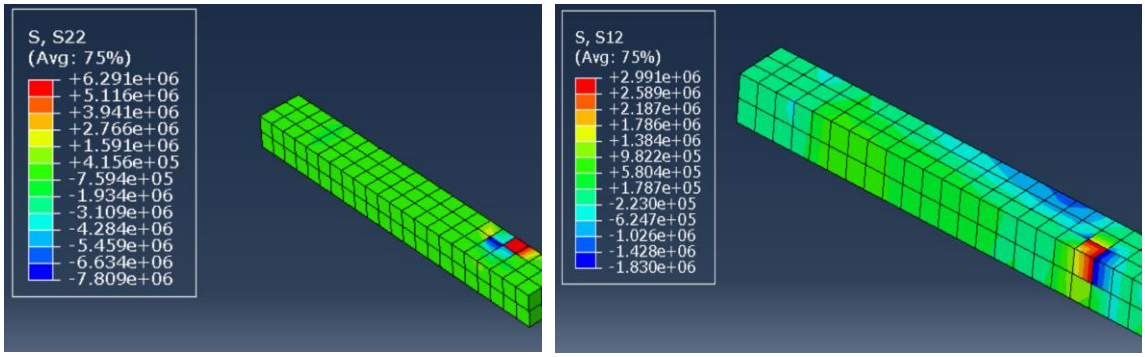

(a) *(b)*

Figure 4-8: Bending stress (a) and Shear stress (b) of sleeper under the crossing nose

c) ***Shear stress, S12*** of the sleeper right underneath the crossing nose: The Shear stress of a sleeper right underneath the crossing nose of the model to be verified is shown in Figure 4-8 (b) is compared with the corresponding output of the reference model.

The maximum analysis error observed on the stress parameters selected is less than 2.5 % and the error observed on the vertical deflection of the sleepers is 2.1%, which is very small and is summarized and presented in table 4-2.

Table 4-2: Verification of Results Summary

	Vertical Deflection (mm)	Bending S, S22 (N/m^2)		Shear S, S12 (N/m^2)	
		Min	Max	Min	Max
Reference Model	2.38	-7850000	6293000	-1835000	3001000
Actual Model	2.451	-7809340	6290530	-1829930	2990810
Error	2.167 %	0.52%	0.04%	0.34%	0.277%

4.3 The dynamic 3D model - background and model information

Turn out no. 9, from a turnout around Shunting area at Kombolcha town; which is shown in Figure 4-9, is selected for all the analysis and sample stiffness homogenization in this study. The turnout dimensions and other parameters are shown in Table 4-3.

Table 4-3: Turnout number 9 Dimension,

Turnout and frog No.	9	Distance from beginning to center (a)	13839
Rail Type (kg/m)	54	Distance from center to heel (b)	5009
Frog Angle (a)	6°20’25’’	Distance from heel to last turnout tie (L’)	8100
Radius of lead curve (R)	180000	Distance from heel to last long turnout tie (L’)	5700
Total length of Turnout LQ	28848		

Figure 4-9: Photo of a turnout around shunting area at Kombolcha town;

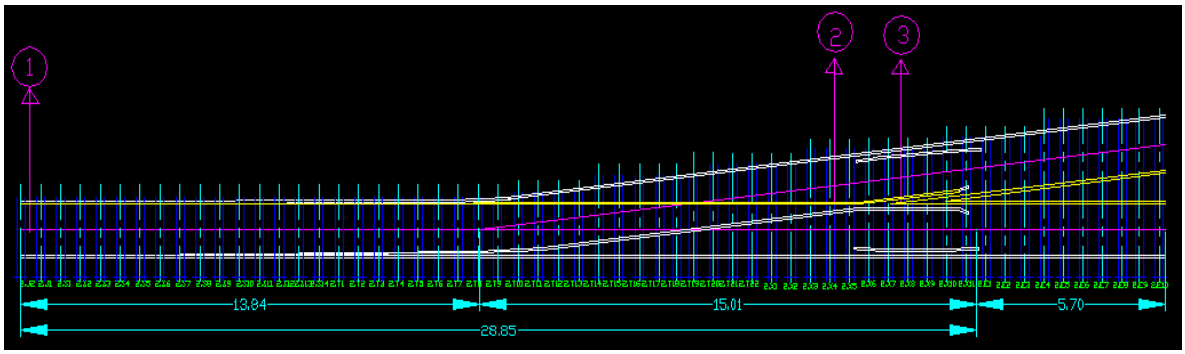

Figure 4-10: Plan layout of the selected turnout No.9 - extracted from Templot 2 software

The lay out of the turnout is modeled using Templot2 desktop application. The yellow-colored lines represent the parts modeled for this study. Many researches are conducted regarding stiffness characteristics of a turnout, from which most of them agreed on the location of the critical section to be specifically at the crossing point while the switch and crossing panels have lesser stiffness compared to the crossing panel [9]. Thus, the ≈28 m actual turnout is modeled in to ≈ 3m length 3D turnout on ABAQUS mainly comprising the crossing panel.

4.4 The finite element modeling details

4.4.1 Model components - parts

All the model parts; wheel, rail, rail pad, different steel pads, sleeper, under sleeper pad and the ballast are modeled as deformable 3D solid parts [48]. Because of shape complexity, the wheel and the rail are first modeled on ***solid works CAD solid modeling software 2020*** and then imported to ABAQUS.

Considering the difficulty of meshing of some parts with subsequent change of curvature and also resource optimization, the shapes are simplified by equivalently stiff parts i.e., equivalent flexural rigidity (EI).

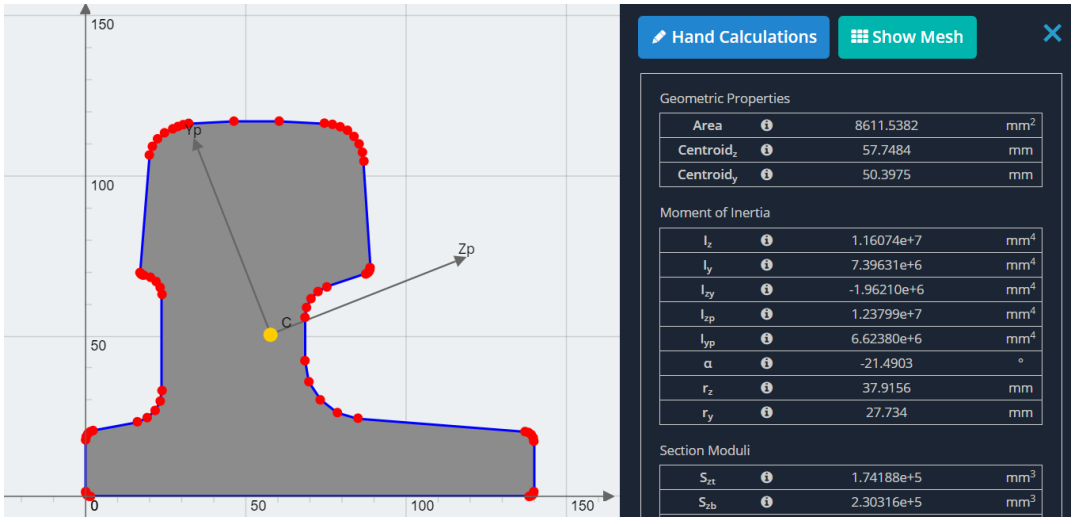

(a)

Area	*8611.5382*	mm^2
I_x	*1.16074e+7*	mm^4
I_y	*7.39631e+6*	mm^4

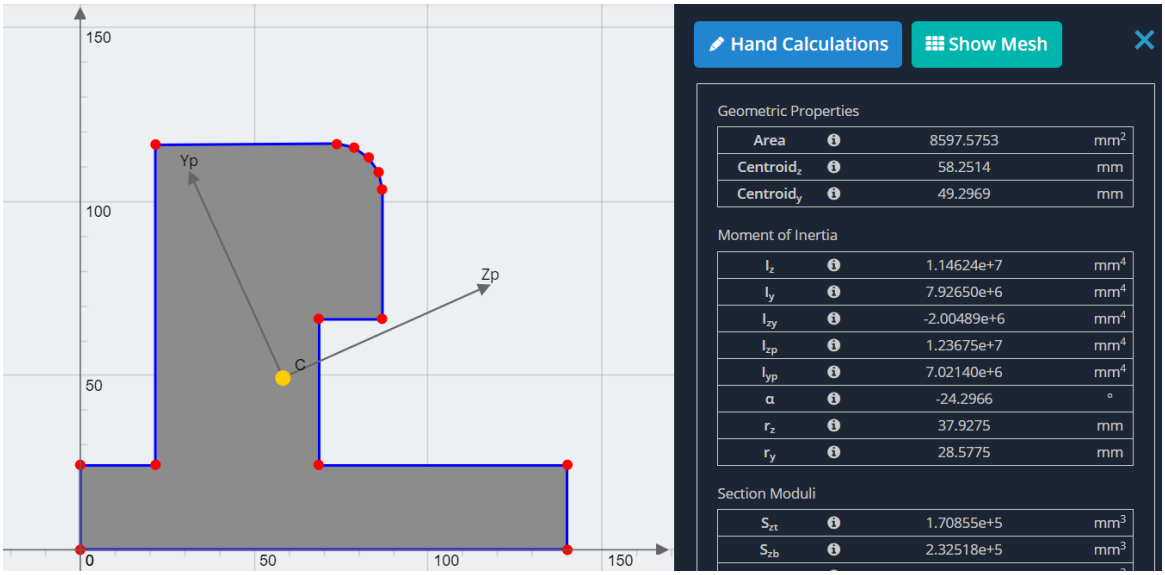

(b)

Area	*8597.5753*	*mm^2*
I_x	*1.14624e+7*	*mm^4*
I_y	*7.92650e+6*	*mm^4*

Figure 4-11: (a) Moment of Inertia of actual Tongue rail;

(b) Moment of Inertia of simplified Tongue rail)

4.4.2 Model components material properties

The FE model developed comprises the wheel, rail, rail pad, different steel pads, and sleeper, under sleeper pad and ballast components.

The component description, dimension, and material type of the track components used in the simulation are as described in Table 4-4.

Table 4-4: Details about the components of the track structure used in the model

Component Description	**Dimension**	**Parameters**	**Value**	**Unit**
Rail (High manganese Steel)	UIC 54	Young's Modulus (E)	190	GPa
		Poison's ratio (ν)	0.23	-
		Density (ρ)	7880	Kg/m3
		Yield Stress	450	MPa

		Strain (%)
Yield Stress (MPa)	450	0.00%
Ultimate Stress (MPa)	1076	21.53%

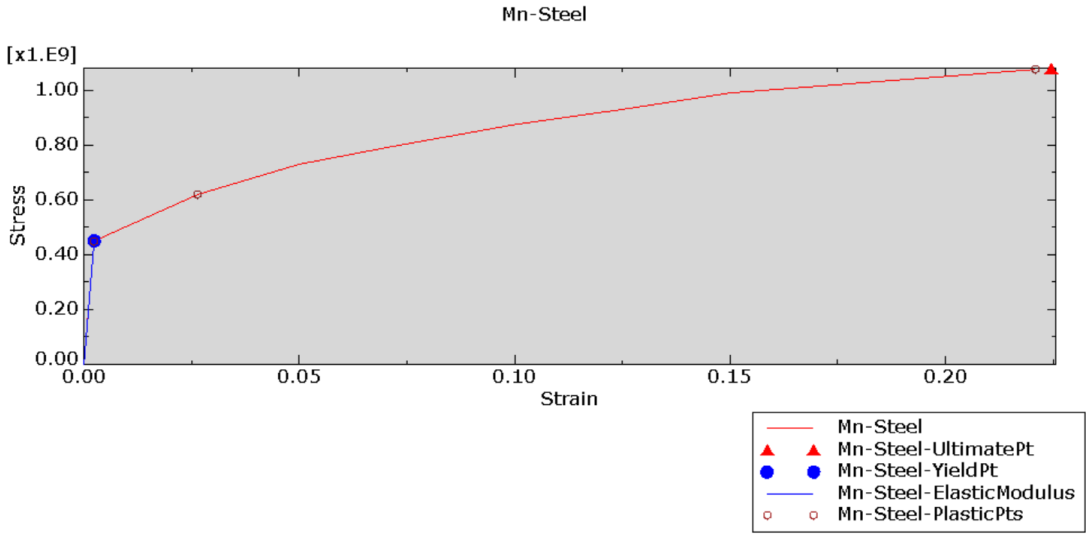

Figure 4-12: Mn steel property - stress - strain curve

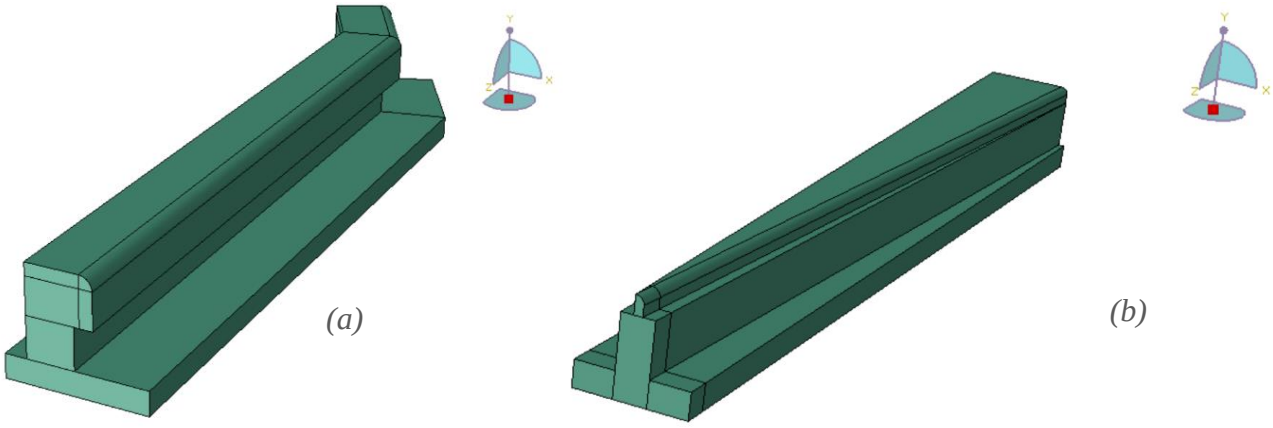

Sleeper	0.28m*0.205m	Young's Modulus (E)	37	GPa
		Poison's ratio (ν)	0.2	-
		Density (ρ)	2750	Kg/m3
Ballast [49], [50]	4.48m*0.2m	Poison's ratio (ν)	0.3	-
		Density (ρ)	2500	Kg/m3
		Young's Modulus (E)	250	MPa
		Friction angle	60	°

Component Description	Dimension	Parameters	Value	Unit
Wheel	Φ=0.76m	Density (ρ)	7800	Kg/m3
		Young's Modulus (E)	210	GPa
		Poison's ratio (*v*)	0.3	-
		Yield stress	627.3	MPa
Pads	Varies	Density (ρ)	1200	Kg/m^3
		Hyper elastic rubber parameters	3^{rd} order SEP function	

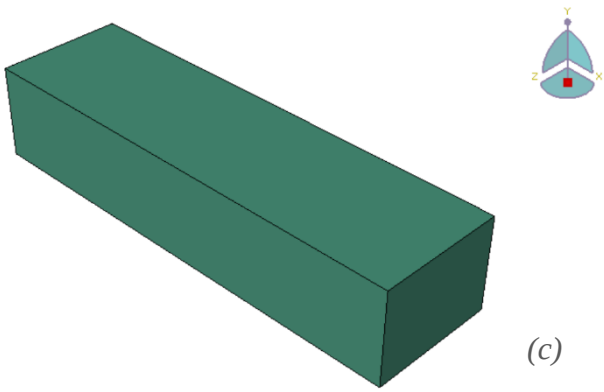

(c)

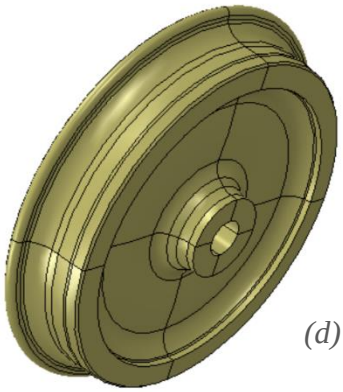

(d)

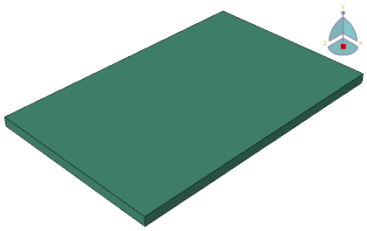

(e)

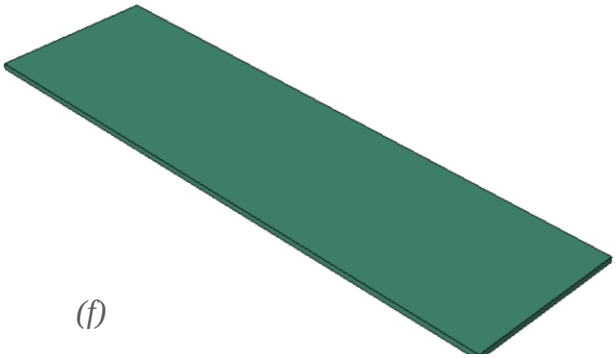

(f)

Figure 4-13: Modeling of Major Parts (a) Tongue rail; (b) Crossing nose; (c) Sleeper (d) P8 Train Wheel; (e) Rail Pad; (f) USP

The global coordinate system XYZ is defined as: The Z-axis is parallel to the longitudinal direction along which the wheel-set travels, the Y -axis is the vertical pointing upwards, and the X-axis is perpendicular to both X and Y directions, which the rotational displacement is set, forming a right-handed Cartesian coordinate system. The 3D model assembly is illustrated in Figure 4-14.

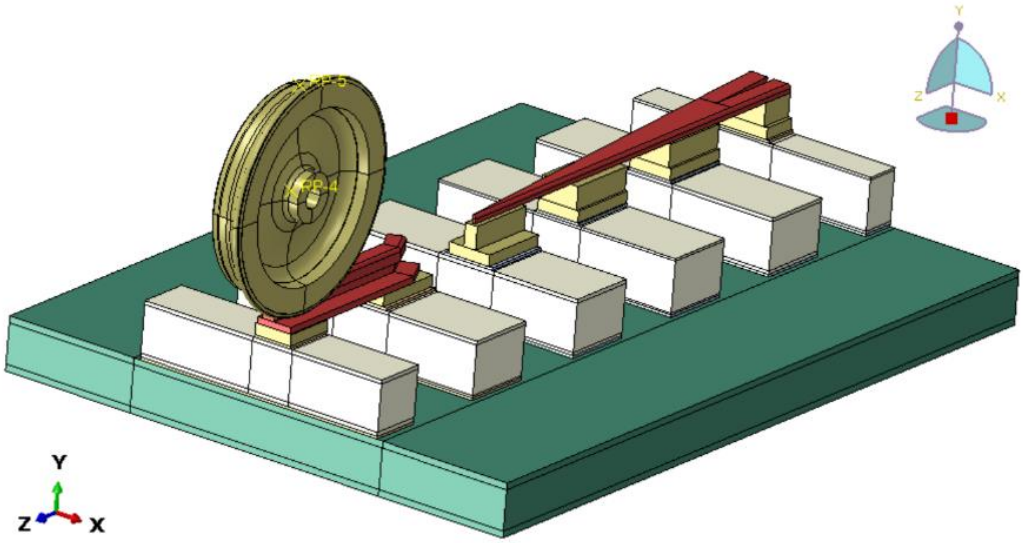

Figure 4-14: 3D Model Assembly

4.4.3 Yeoh hyperelastic model for nonlinear finite element analysis

In 1990, Yeoh noted a significant decrease of shear modulus at low strains of a black-filled rubber during his study and he has also observed the same issues with unfilled rubber. Thus, he proposed to consider an exponentially decaying term in the hyperelastic model by adding to the strain energy density of the model which is known as the Yeoh model function [35].

$$W = \sum_{i=1}^{N} C_{io}(\bar{I}_1 - 3)^i + \sum_{k=1}^{N} \frac{1}{D_k}(J-1)^{2k} \quad \text{Eq. 4-1}$$

where;

W = strain energy function

J = volume ratio after and before deformation, if the material is incompressible, J = 1

$$J = \sqrt{I_3} \quad \text{Eq. 4-2}$$

$\bar{I}_1$ = a function of the volume ratio and first invariant of Cauchy-Green strain tensor

$$\bar{I}_1 = J^{-2/3} * I_1 \quad \text{Eq. 4-3}$$

I_1, I_3 - invariants of Cauchy-Green strain tensor:

$$I_1^c := tr(C) = C_{II} = \lambda_1^2 + \lambda_2^2 + \lambda_3^2 \quad \text{Eq. 4-4}$$

$$I_2^c := det(C) = \lambda_1^2\,\lambda_2^2\,\lambda_3^2$$

N, C_{i0} and D_k: input coefficients

$\lambda_1^2, \lambda_2^2, \lambda_3^2$ - stretches (stretch ratios): the ratio of the length of a deformed line element to the length of the corresponding undeformed line element: i.e.,

$$x_1 = \lambda_1 X_1, x_2 = \lambda_2 X_2,\ x_3 = \lambda_3 X_3 \qquad \text{Eq. 4-5}$$

Yeoh Hyperelastic model is simple and demands only few parameters to get reasonable numerical results. It can also describe a wide range of deformation.

4.4.3.1 Hyper elastic rubber material Properties

A typical uniaxial test result of rail pad rubber material [51] is used as an initial data to extract the suitable coefficients of the Strain Energy Potential function on ABAQUS.

As discussed in detail in section 2.6 of this paper, a 3rd degree reduced polynomial function -Yeoh (Figure 4-16) is selected to suit the intended material model after comparing it with results of other SEP functions (Figure 4-15).

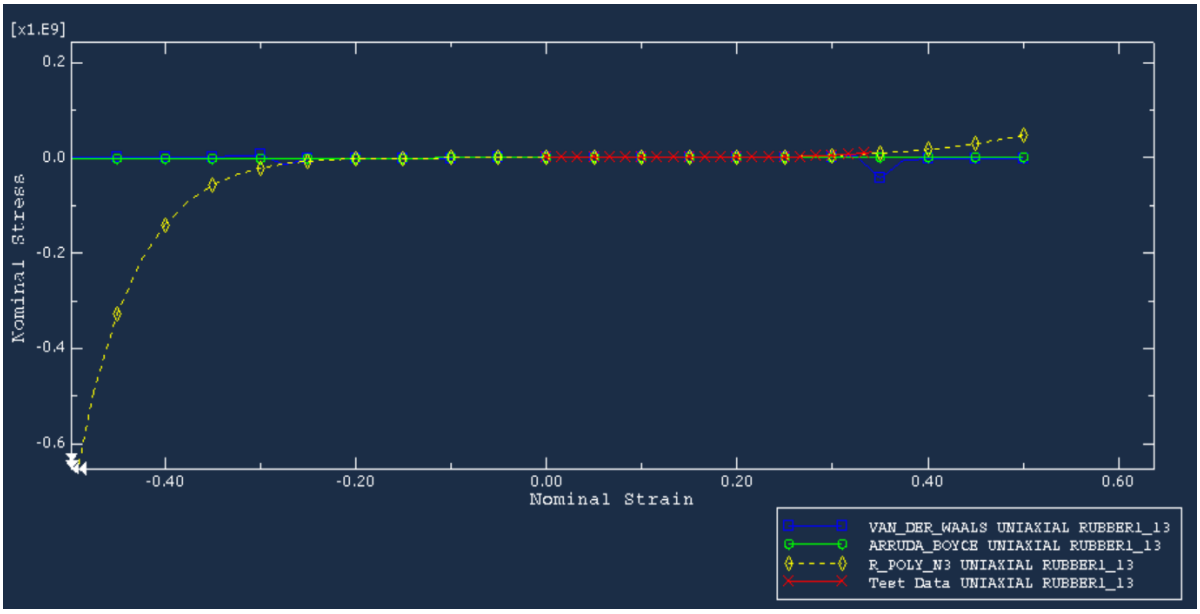

Figure 4-15: Comparison of Results for different SEP functions

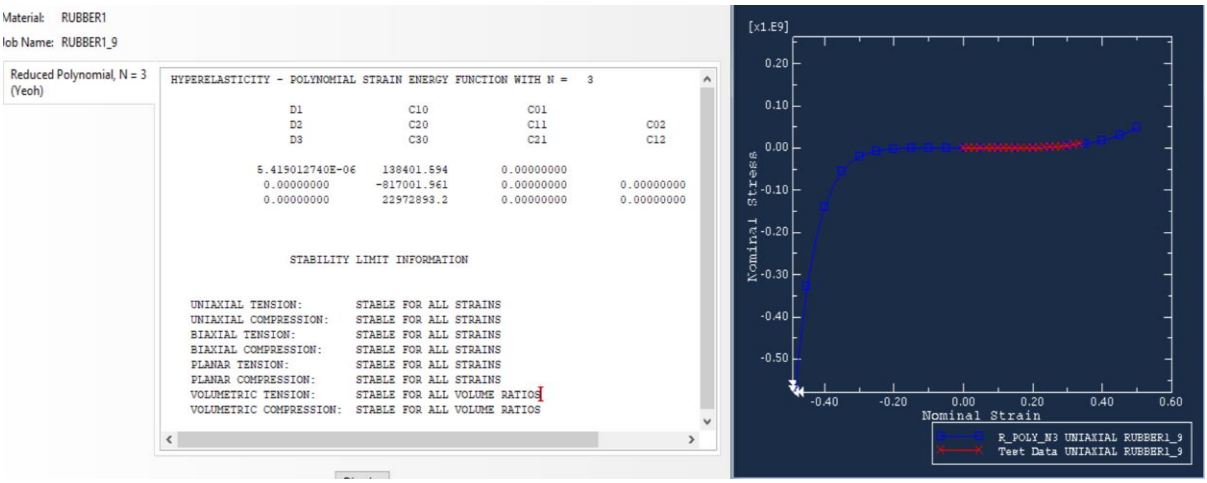

D1	*5.419012740 E-06*
C10	*138401.694*
C20	*-817001.961*
C30	*22972893.2*

Figure 4-16: Results of 3rd degree reduced polynomial function (Yeoh)

The coefficients of the third order reduced polynomial extracted from here are then used to estimate the biaxial and planar (pure shear) characteristics of the rubber material. As illustrated in Figure 4-16, the limits are ***stable for all strains***.

4.4.4 Mohr-Coulomb plastic model

There exist different models to characterize failure behavior of materials when they are subjected to stresses. Some of the theories developed are very complex when defining the constitutive model which makes them hard to deploy in practical situations. This theory is used in FE models as Mohr-coulomb plastic model which allow the materials either harden and/or soften isotopically relating to the stress plane, and a piecewise elliptic shape in the deviatoric stress plane [52].

In Mohr-coulomb model, a linear failure envelope to determine the critical combination of normal stress and shear stress will be considered. In other words, the shear stress and the normal stress produce the friction angle that represents the failure plane. From the relation between shear strength and normal stress, it can be illustrated by plotting Mohr's circle to present a state of stress with the mathematic function of failure envelop as shown in Figure 4-17. The compressive stress and shear strength act on to the tangency points between the

circle and the failure envelop. At the average of principal stress or the difference between the maximum principal stress and minimum principal stress, the maximum shear stress can be defined [53].

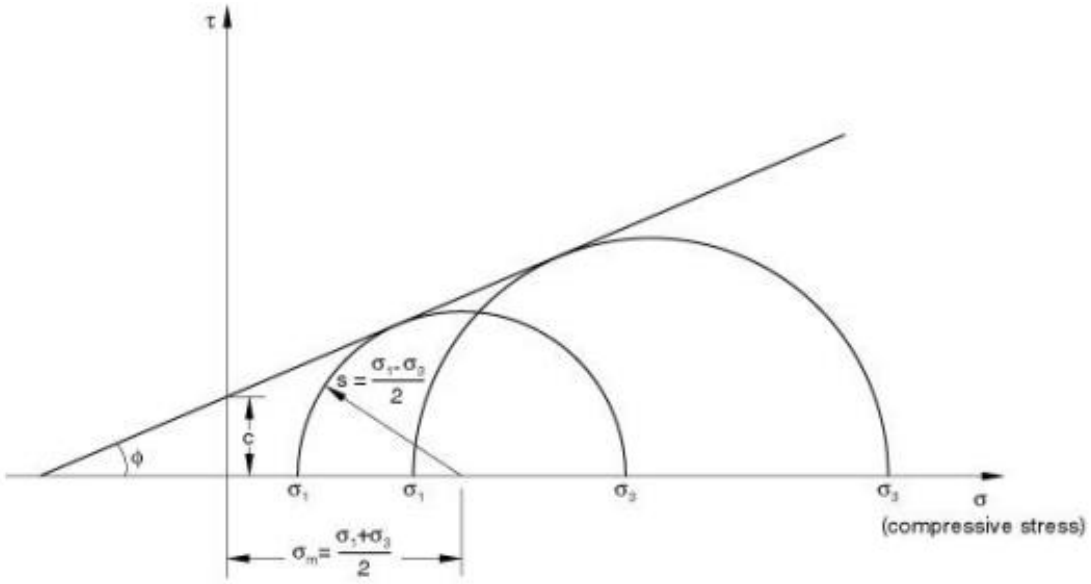

Figure 4-17: Mohr-Coulomb yield model (ABAQUS 6.14, 2014)

Maximum shear stress; $s = \frac{\sigma_1 - \sigma_3}{2}$

and $\sigma_m = \frac{\sigma_1 + \sigma_3}{2}$

$$\tau = c - \sigma \tan \phi \qquad \text{Eq. 4-6}$$

where C is a cohesion of the soil

ϕ is friction angle

τ is a shear strength of the soil; $\tau = s \cos \phi$ Eq. 4-7

σ is a compressive stress; $\sigma = \sigma_m + s \sin \phi$ Eq. 4-8

Substituting Eq. 2-12 and Eq. 2-13 in to Eq. 2-11 and multiplying both sides by cos ϕ;

$$S = \sigma_m \sin \phi - C \cos \phi = 0 \qquad \text{Eq. 4-9}$$

This can be rewritten in a more convenient way for general state of stress as:

$$F = R_{mc} q - p \tan \phi - c = 0 \qquad \text{Eq. 4-10}$$

where; $R_{mc}(\Theta,\phi) = \frac{1}{\sqrt{3}\cos\phi}\sin\left(\Theta+\frac{\pi}{3}\right)+\frac{1}{3}cos\left(\Theta+\frac{\pi}{3}\right)\tan\phi$

Θ is the deviatoric polar angle; $\cos(3\Theta) = \left(\frac{r}{q}\right)^3$

P is the equivalent pressure stress; $p = -\frac{1}{3}\,trace\,(\sigma)$

q is the Misses equivalent stress; $q = \sqrt{\frac{3}{2}(S : S)}$

S is the deviatoric stress; $S = \sigma + P\,I$

r is the third invariant of the deviatoric stress; $r = \frac{9}{2}(S\,.\,S : S)^{1/3}$

The shape of yield surface in the deviatoric plane is as shown in Figure 4-18, which has a friction angle range of 0° to 90°.

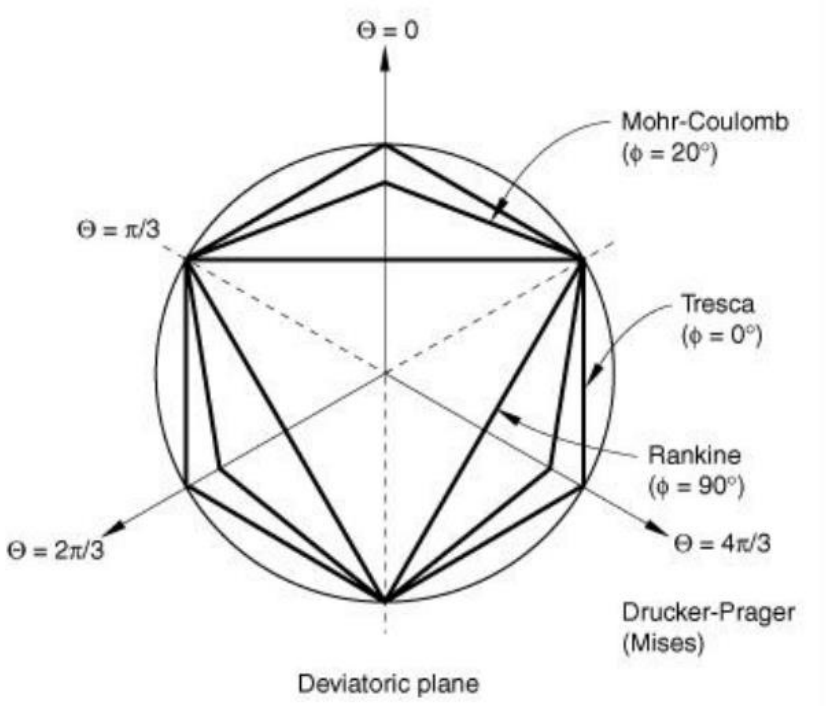

Figure 4-18: Mohr-Coulomb surface in deviatoric plane (ABQUS 6.14, 2014)

The pressure-independent Tresca model is formed a perfectly hexagonal deviatoric section at friction angle equal to 0°. On other hand, at the maximum friction angle at 90°, the tension cutoff Rankine model is reduced and form a triangular deviatoric section.

Mohr-Coulomb plasticity model has been used to define the ballast in this study. A study by Indraratna et al. [50] shows that the friction angle of railway ballast material varies

between 66° to 67° for different gradations. Another study by Zhang Jin et al. [49] uses different groups of ballast materials with angle of internal friction between a range of 58° and 62°.

4.4.5 Interactions and Constraints

The wheel is set to roll along the crossing panel in the presence of Master – Slave Interaction with the rails. The potential contact surfaces are defined wide enough to cover the rolled contact surfaces of both the wheel and the rail as shown in Figure 4-19. In addition, MPC Beam type of constraint is used between the wheel interior surface and the center point.

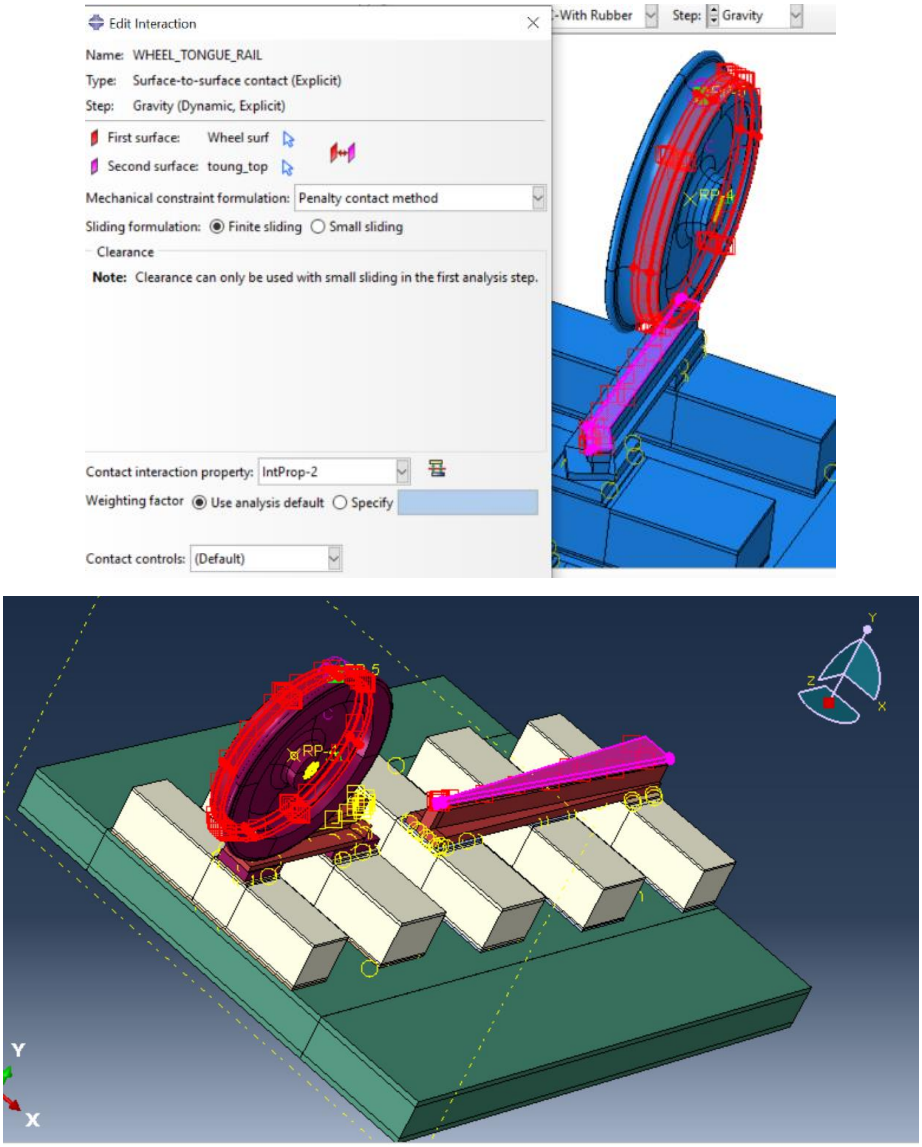

Figure 4-19: Wheel-Rail Interactions

Likewise, Tie Constraint is used in between each part in order to let ABAQUS generate optimized interface mesh [7], and also tie constraint allows rapid transitions in element mesh density within the model. The discretization method of tie constraint being surface-to-surface formulation helps to avoid stress noise at the tied interfaces [54] in addition to reducing the computational effort [55] considering the focus of this study.

To simulate the primary suspension between the vehicle and bougie, a spring -dashpot system is comprised to the model with parameters stated under Table 4-4.

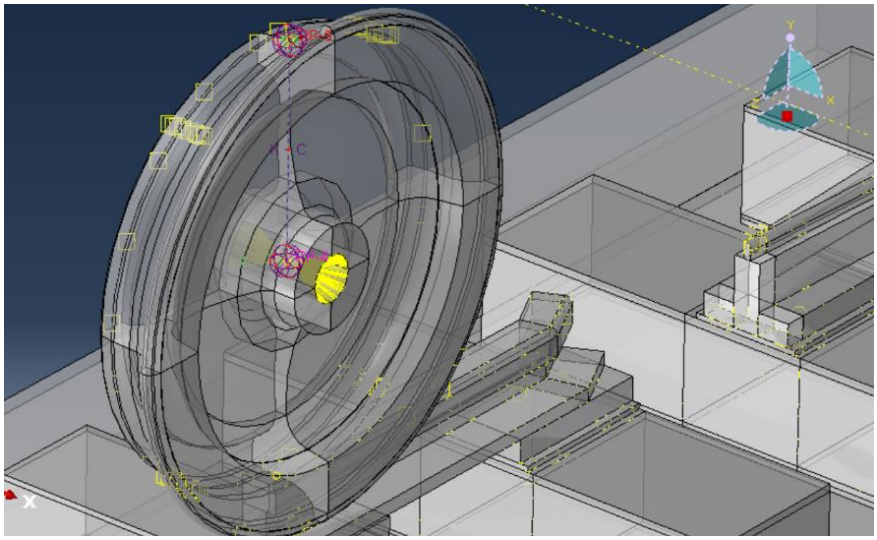

Figure 4-20: Primary Suspension (Spring - Dashpot)

4.4.6 Boundary Conditions

The boundary conditions at both ends of the track are set fixed only on the longitudinal direction (i.e., Z-symmetry) to simulate the continuity of the track. Moreover, the lateral movement of the wheel set is constrained by applying symmetric boundary conditions. The bottom of the Ballast is set Encastre (U1=U2=U3=UR1=UR2=UR3=0) [21] and [55].

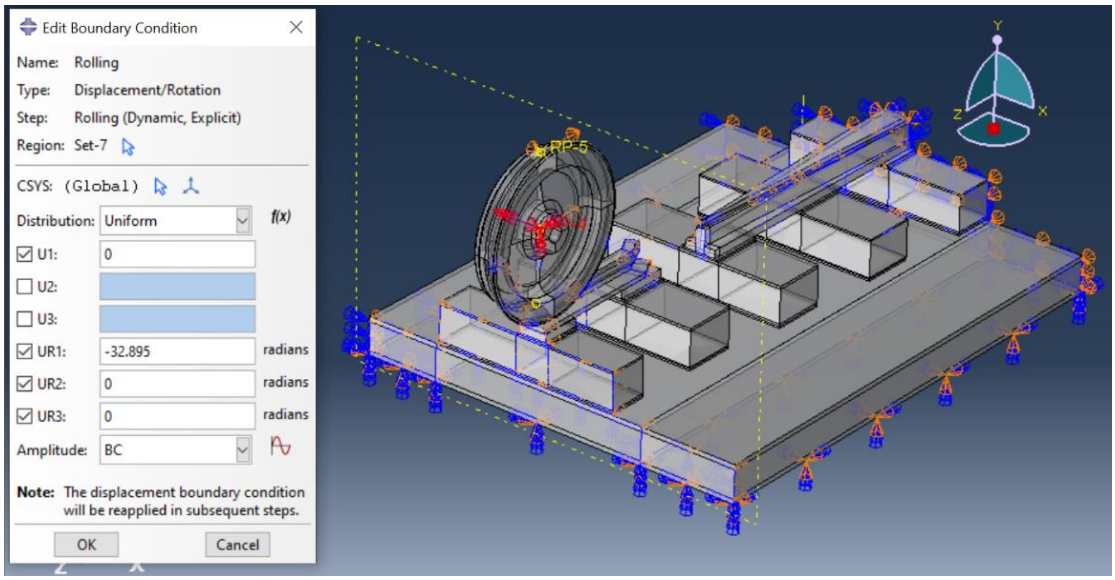

Figure 4-21: Boundary Conditions

4.4.7 Loading Conditions

The portion of the sprung mass from the train set is lumped into Mc, that is connected to the wheel through the primary suspension (Kc and Cc) in addition to the unsprung mass from the wheel set itself which is applied at the center of the wheel. Moreover, the traction effort is considered to be 718.2 Nm assuming there is 50% of wheel slippage. Other operational parameters used in the model are according to the data collected from ERC.

Table 4-5: Loading and suspension parameters

Operation Axle loads	24 tons
Unsprung mass	600 kg
Spring stiffness	62 N/mm
Dashpot coefficient	55.4 N. S/mm
Wheel/Rail Interface (W-R)	Master - Slave penalty interaction

The angular velocity (ω); which shows how fast the wheel is rotating is calculated from the linear velocity as:

$$V = S / t; \qquad S = R \cdot \theta \qquad \text{Eq. 4-11}$$

$$\omega = \theta / t \qquad \text{Eq. 4-12}$$

Thus, from Eq. 4-11 and 4-12;

$$\omega = \frac{V}{R} \qquad \text{Eq. 4-13}$$

where;

R: Wheel Radius = 0.38m;

θ: Curve angle = 360º;

v: Train Speed = 45 Km/hr = 12.5 m/s;

t: time in seconds;

S: Total travel distance = 2.8 m

$$\omega = \frac{12.5\ m/s}{0.38\ m} = 32.895 \text{ rad/s; and}$$

$$t = \frac{S}{V.} = \frac{2.8\ m}{12.5\ m/s} = 0.224 \text{ sec}$$

4.4.8 Element type and meshing

In the FE model, all the track components are meshed with C3D8R type of element which is an 8-noded linear brick, reduced integration element. Selection of mesh size is done based on a reference of similar nature [7] which conducts sensitivity analysis. The referred model uses ABAQUS FE software and proofed that the 60 mm and 100 mm meshes yield similar precision and accuracy of the numerical results as depicted on Table 4-6.

Table 4-6: Sensitivity analysis for mesh size selection

Mesh size (mm)	Deflection (mm)	Computational time (s)
60 × 60	2.54	24,784
70 × 70	2.32	12,638
80 × 80	2.28	10,824
90 × 90	2.59	5,655
100 × 100	2.54	5,547

The finer mesh takes almost 4.5 times the amount of time to compute compared to the coarser one. Thus, to maximize the computing time efficiency, a maximum mesh size of 100 mm × 100 mm is chosen for this study. The total number of nodes and elements in the

simulation model are 161,209 and 223,888 respectively. The mesh is denser around interaction areas and where results are to be extracted. The minimum mesh size used in the model is 5mm x 5mm.

Table 4-7: Model - Mesh Details

Element Type	Element shape	Geometric order	No. of Elements
C3D8R	Hexahedral	linear	161,209

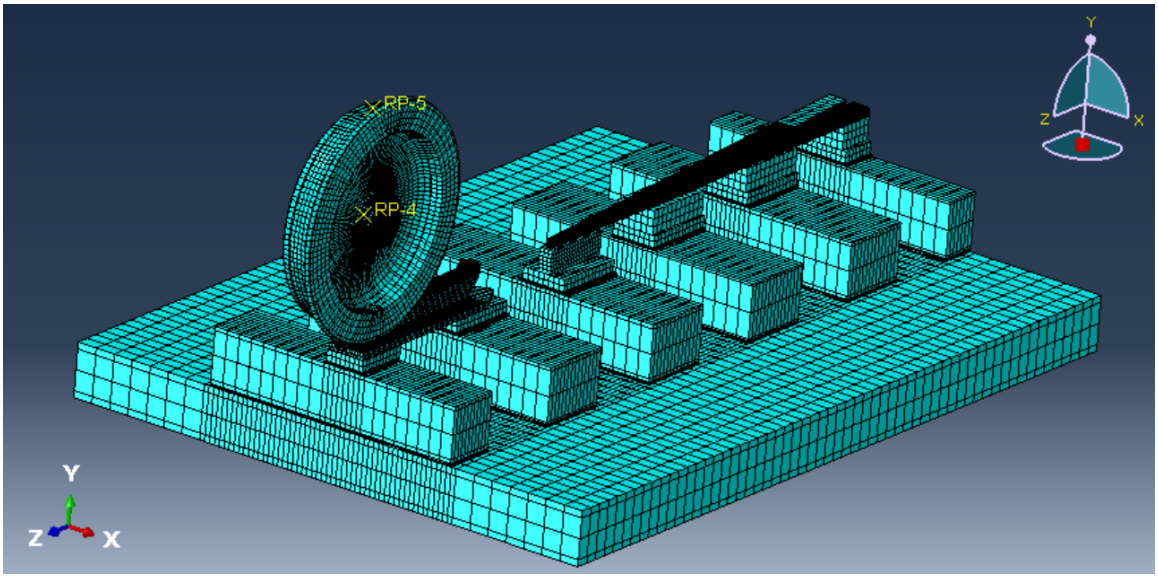

Figure 4-22: 3D Model mesh

5 RESULTS AND DISCUSSION

5.1 Analytical approach

Pasternak's two parameter mechanical model (Figure 5-1) is considered to compute maximum deflection both on the portion of closure rails and crossing which later is used to validate the numerical analysis results.

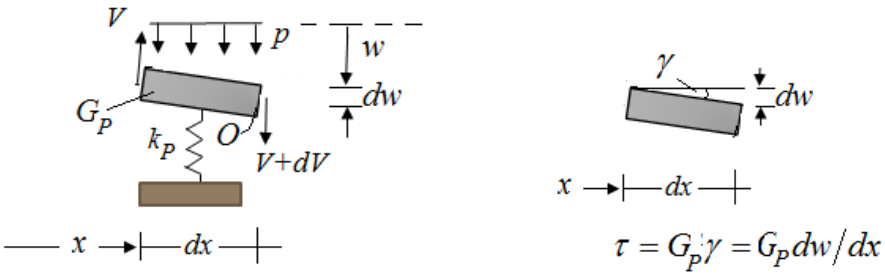

Figure 5-1: Pasternak's mechanical model [22]

$$p = k_P w - \frac{dV}{dx}$$

$$p = k_P w - \frac{d(\tau.1)}{dx}$$

$$p = k_P w - \frac{G_P d^2 x}{dx^2} => p(x) = k_P w(x) - G_P w''(x) \qquad \text{Eq. 5-1}$$

Then the differential equation of the beam becomes

$$EIw^{iv}(x) - G_P Bw''(x) + Bk_s w(x) = Bq(x);\ or$$
$$EIw^{iv}(x) - TBw''(x) + Bk_s w(x) = Bq(x)$$

The homogenous solution has the usual form of

$$w(x) = Ae^{mx}$$

After substitution, rearranging and introducing $\hat{k}_s = k_s B$ and $\hat{T} = TB$, one obtains the characteristic polynomial:

$$m^4 - \frac{\hat{T}}{EI}m^2 + \frac{\hat{k}_s}{EI} = 0$$

The characteristic polynomial has the four separate roots of

$$m_{1,2,3,4} = \pm\sqrt{\frac{\hat{T}}{2EI} \pm i\sqrt{\frac{\hat{k}_s}{EI} - \left(\frac{\hat{T}}{2EI}\right)^2}}$$

Thus, the solution has the form of:

$$w(x) = A_1 e^{m_1 x} + A_2 e^{m_2 x} + A_3 e^{m_3 x} + A_4 e^{m_4 x} \qquad \text{Eq. 5-2}$$

Three cases arise depending on whether the internal square root is positive, zero or negative. However, the case for which $\hat{T} < 2\sqrt{\hat{k}EI}$ is the most common case in practice, as the shear interaction can rarely be larger than double the square root expression, which is the product of the beam rigidity and the soil stiffness. In this case, the internal square root will be positive, and the four roots form two pairs of conjugate complex numbers expressed as:

$m_{1,2,3,4} = \pm(\alpha \pm i\beta)$ where;

$$\alpha = \sqrt{\hat{\lambda}^2 + \frac{\hat{T}}{4EI}}; \beta = \sqrt{\hat{\lambda}^2 - \frac{\hat{T}}{4EI}}; \hat{\lambda} = \sqrt[4]{\frac{\hat{k}_s}{4EI}} \qquad \text{Eq. 5-3}$$

With these roots substituted back, and for an infinite beam, $C_1 = C_3 = 0$, one obtains the solution as:

$$w(x) = e^{-\alpha x}(C_2 \cos\beta x + C_4 \sin\beta x)$$

But if we consider a beam of infinite length subjected to a concentrated force, P and considering two boundary conditions;

$$w'(0) = 0, => C_4 = \frac{\alpha}{\beta}C_2; and\ w(x) = Ce^{-\alpha x}\left(\cos\beta x + \frac{\alpha}{\beta}\sin\beta x\right)$$

$$\int_0^\infty k_s w(x)dx = P/2\,, => C = \frac{P\hat{\lambda}^2}{2\hat{k}_s\alpha}$$

This finally results in a deflection formula of:

$$w(x) = \frac{P}{2\hat{k}_s}\frac{\hat{\lambda}^2}{\alpha\beta}e^{-\alpha x}(\beta\cos\beta x + \alpha\sin\beta x) \qquad \text{Eq. 5-4}$$

Since the current analysis involves dynamic characteristics of the train, the static load in Eq. 5-4 is first amplified by a factor which is a function of the train speed (v) [29].

$$F_d = \mu F_s \quad \text{Eq. 5-5}$$

$$\mu = 1 + \frac{0.4\,v}{100} \quad \text{Eq. 5-6}$$

Where α is load magnification coefficient, and F_d and F_s are dynamic and Static loads respectively.

Therefore, substituting Eq. 5-6 in to Eq. 5-5:

$$F_d = (1 + \frac{0.4*45}{100}) * (12{,}000\ \text{kg} + 600\ \text{kg}) * 9.81\ \text{m/s}$$

$$= 145.86\ \text{kN}$$

Table 5-1: Parameters used for the analytical computations

Young's Modulus (E)	1.90e+11	N/m2
Track Support (K)	6.00e+07	N/m
x/L	0	
αX_1, βX_1	0	
Q	145, 855.08	N

The maximum deflection is calculated analytically using Eq. 5-4 at six locations of the rail; the location points are picked at 32mm, 65mm, 1100mm, 1710mm, 2340mm, and 2500mm distance from the start of the closure rail. These locations are systematically selected along the turnout to represent the geometrical variations.

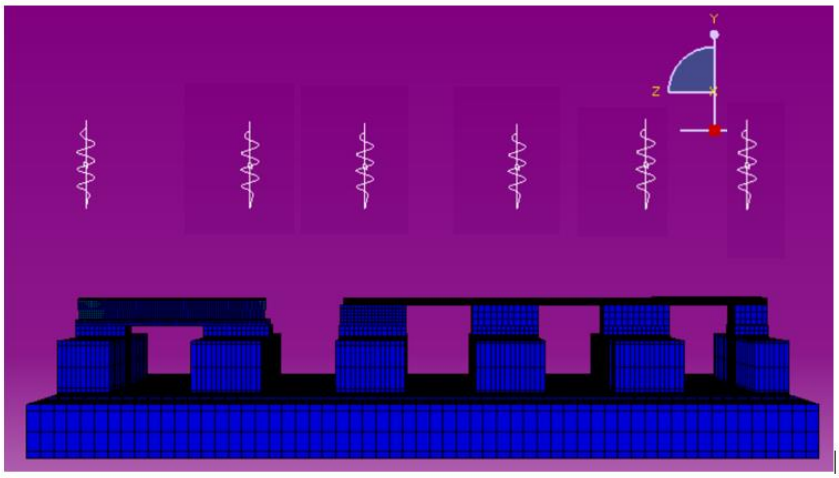

Figure 5-2: Locations to compute maximum deflection

Table 5-2: Maximum deflection at subsequent locations along the crossing- Pasternak's method

Location from closure front (m)	Section	Moment of Inertia (I) (m4)	Flexural Rigidity EI	αβ	$\hat{\lambda}$	Maximum Deflection *w*, (at x=0) (mm)
0.32	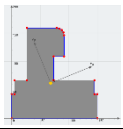	3.075E-05	5.839E+06	0.884129	0.9402954	0.71815
0.65	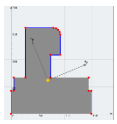	3.075E-05	5.839E+06	0.884129	0.9402954	0.71815
1.1	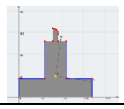	1.828E-05	3.471E+06	1.146722	1.0708788	1.62722
1.71	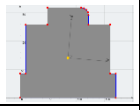	4.143E-05	7.867E+06	0.761716	0.8727731	1.04658
2.34	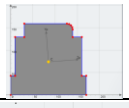	4.706E-05	8.937E+06	0.714680	0.8453961	0.72750
2.5	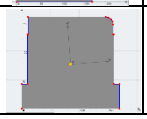	5.265E-05	9.998E+06	0.675708	0.8220217	0.73754

The maximum deflection, 1.62722 mm is observed at 1.1m away from the front of the closure, which is the point right below the crossing nose (Figure 5-3).

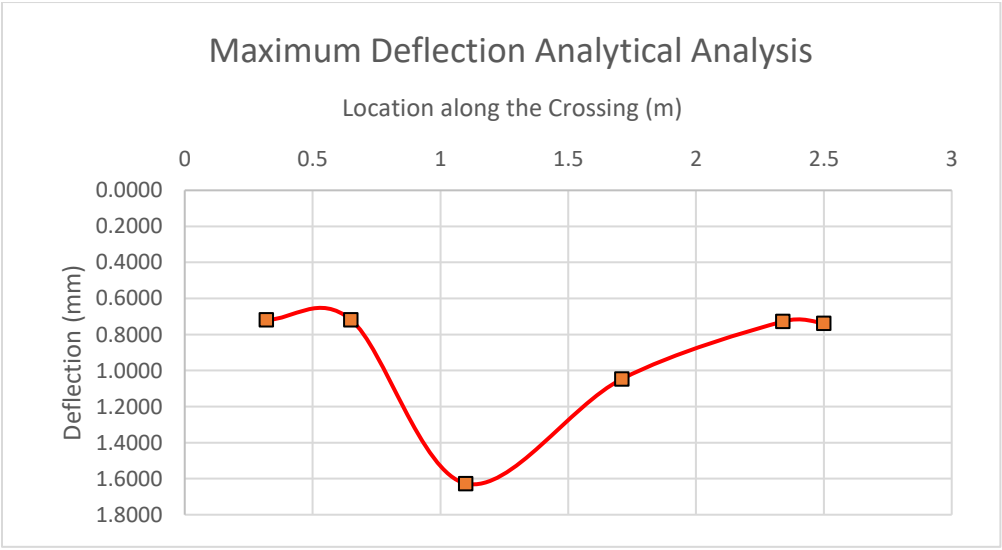

Figure 5-3: Maximum Deflections at the selected points along the rails

5.2 Numerical computations

Several FE model analyses are performed considering different rail and sleeper pad properties to modify the stiffness variation along the crossing panel. Under the initial model, all the rail pads and sleeper pads are simulated with a uniform hyper elastic material property as explained in section 4.4 of this paper. For the later analysis the rubber pads under the rail and sleepers of different locations are given different properties observing the out puts of the initial analysis.

5.2.1 Results from uniform rubber pad properties

This scenario is drawn by using the parameters given on Table 4-4 and using a hyper elastic material for all the rubber pads. The coefficients used in equation (9) for the 3rd degree reduced polynomial function of Yeoh are presented in Table 5-3. The reference material properties are adopted from an experimental study by Sarawade [51].

$$W = \sum_{i=1}^{N} C_{io}(\bar{I}_1 - 3)^i + \sum_{k=1}^{N} \frac{1}{D_k}(J-1)^{2k} \qquad \text{Eq. 5-1}$$

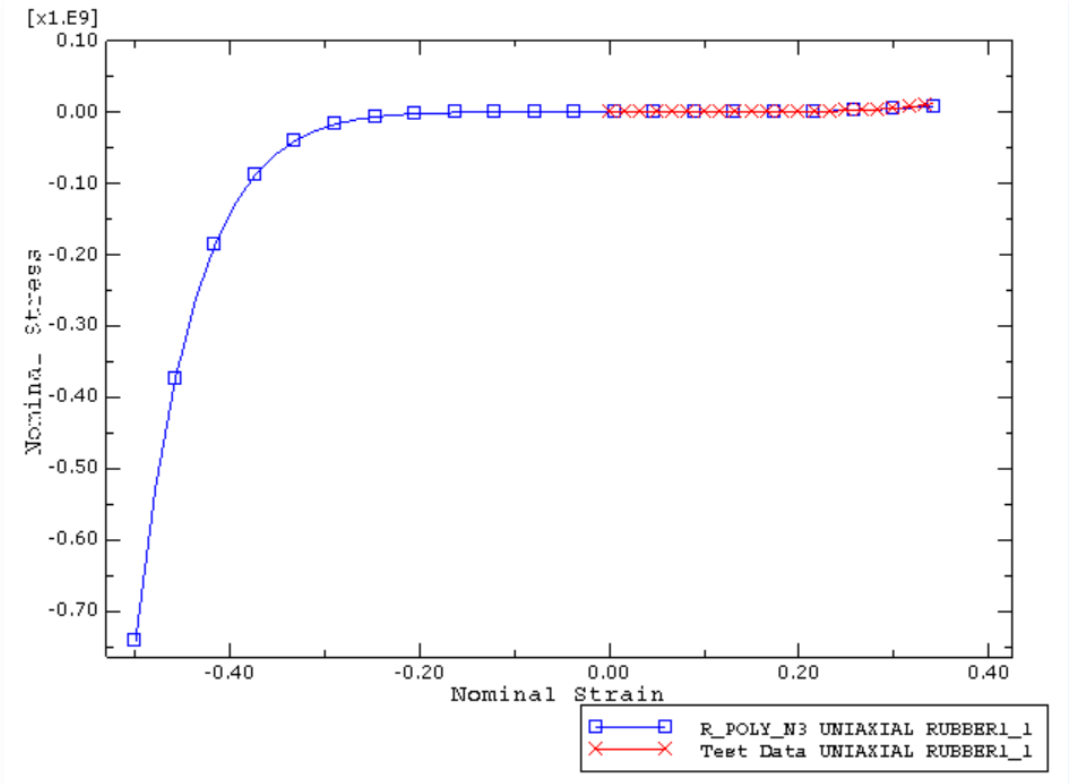

Figure 5-4: Material properties of the initial rubber proposed – Case 1- Uniaxial results

Table 5-3: Coefficients of Yeoh SEP - for the initial scenario

Coefficients	**Pa**
C10	138,738.507
C20	-815,796.495
C30	23,032,497.3
D1	1.0812E-5

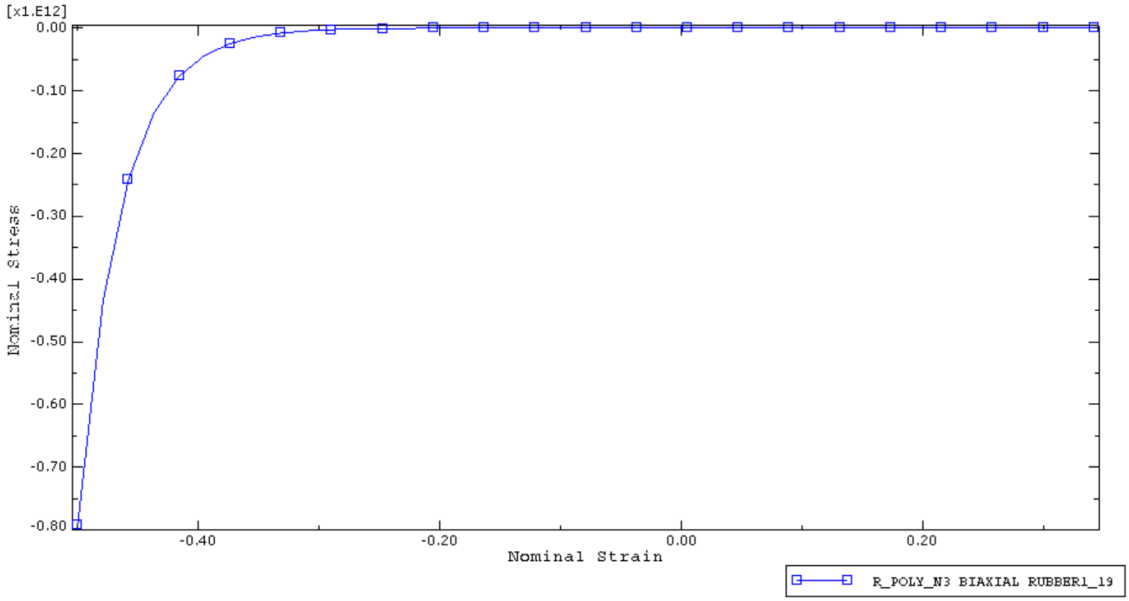

Figure 5-5: – Case 1- Biaxial results

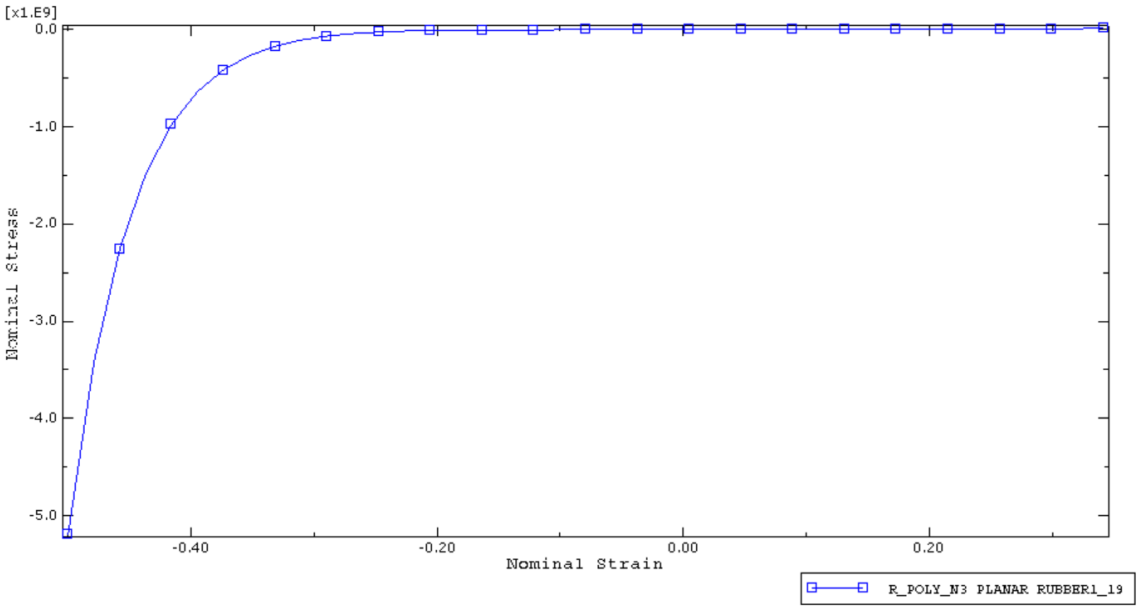

Figure 5-6: – Planar results - Case 1

Then the maximum contact forces and maximum deflections at the wheel rail contact locations in addition to the maximum stresses are extracted from the FE analysis.

I. Maximum contact force

The maximum contact force is also extracted from the history output request for the two rails separately as shown in Figure 5-7 and Figure 5-8. Then the two separate results are combined to then calculate the stiffness at the specific locations of interest.

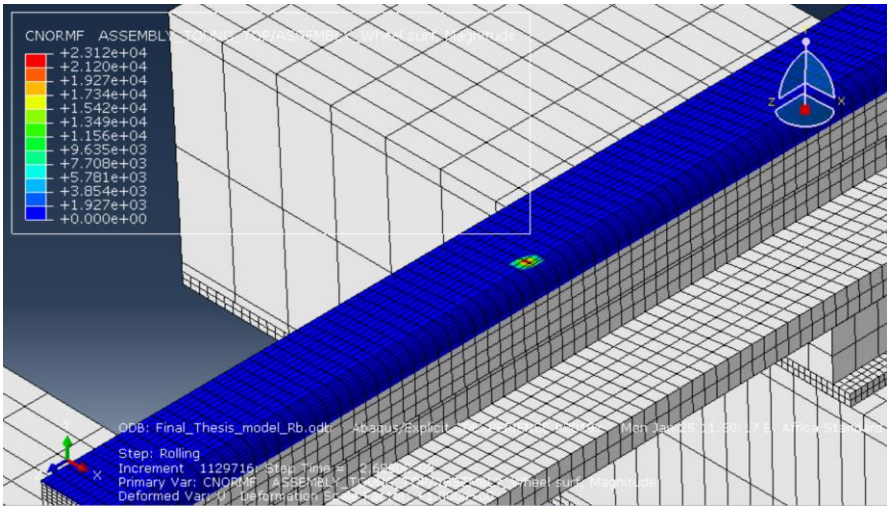

(a)

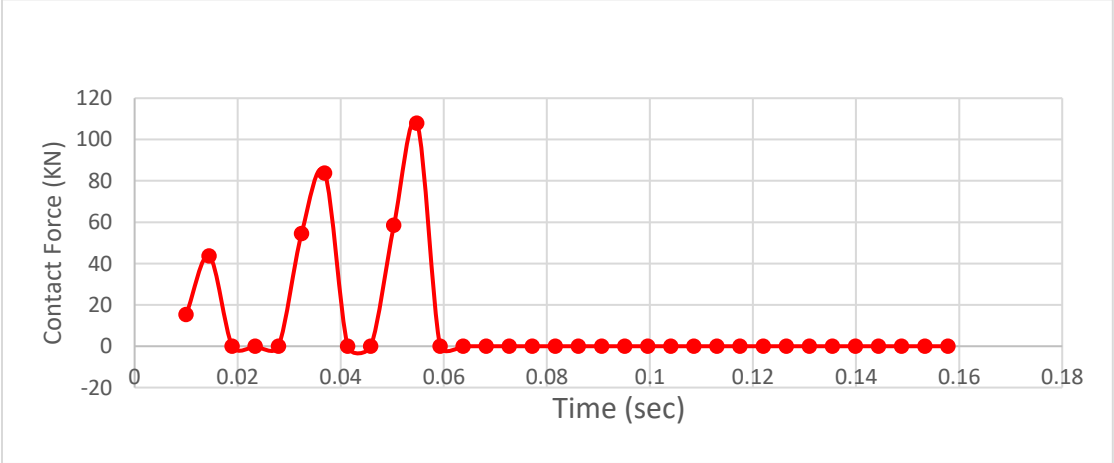

(b)

Figure 5-7: (a), (b) Contact force at the tongue rail before the wheel reaches the nose

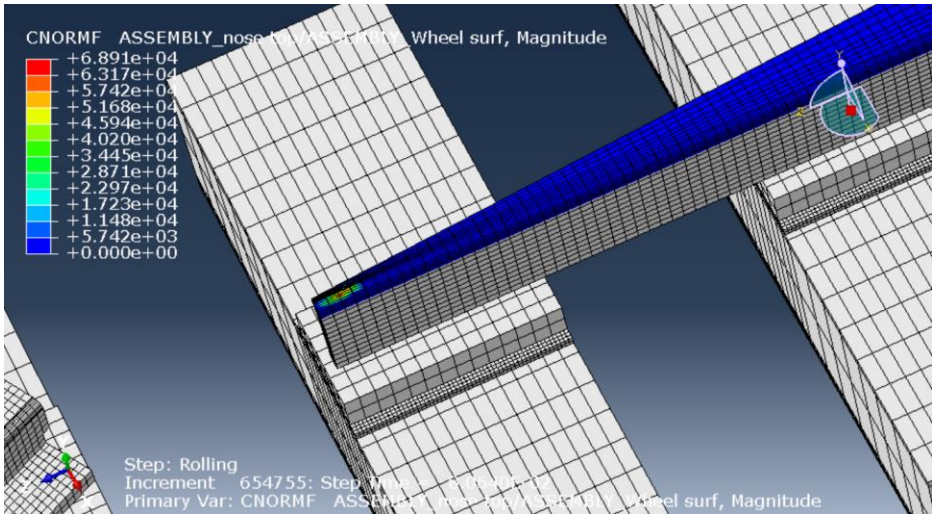

(a)

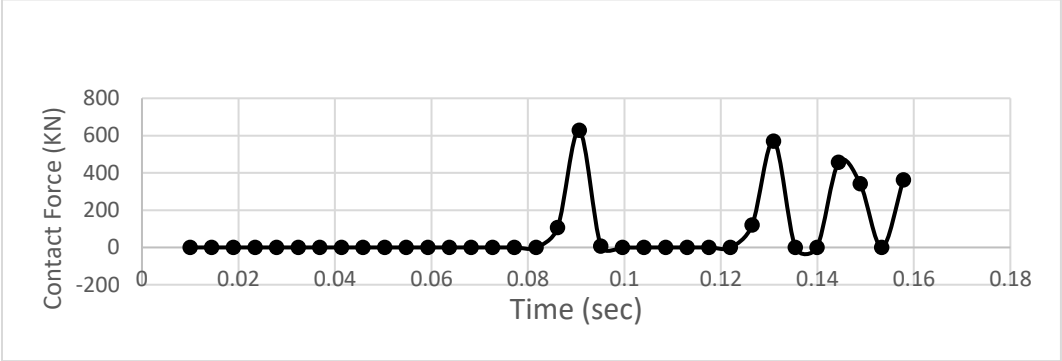

(b)

Figure 5-8: Contact force at the crossing nose

The contact forces extracted from the two separate rails are combined (Figure 5-9) to show the effect in an unceasing manner according to the time which the wheel leaves the first rail and joins the second one.

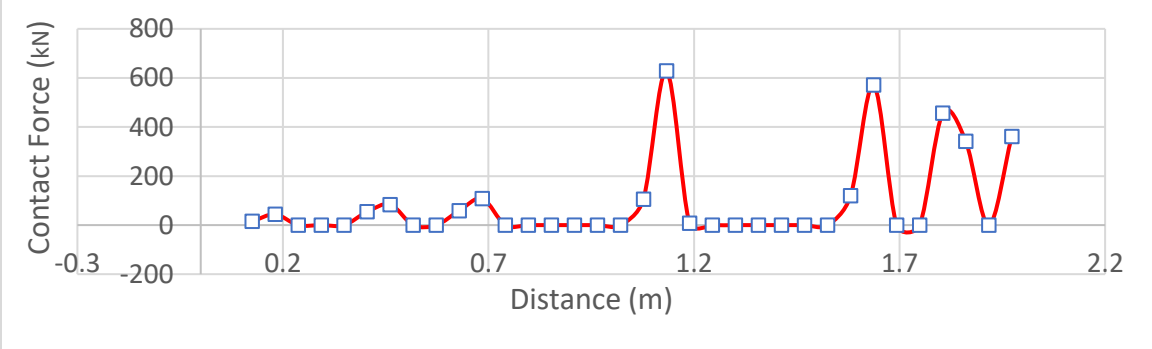

Figure 5-9: Contact forces combined along both rails

II. Maximum deflection

The maximum deflection observed along the turnout crossing at different layers is extracted from the model using a python code (appendix A) and presented in Figure 5-10.

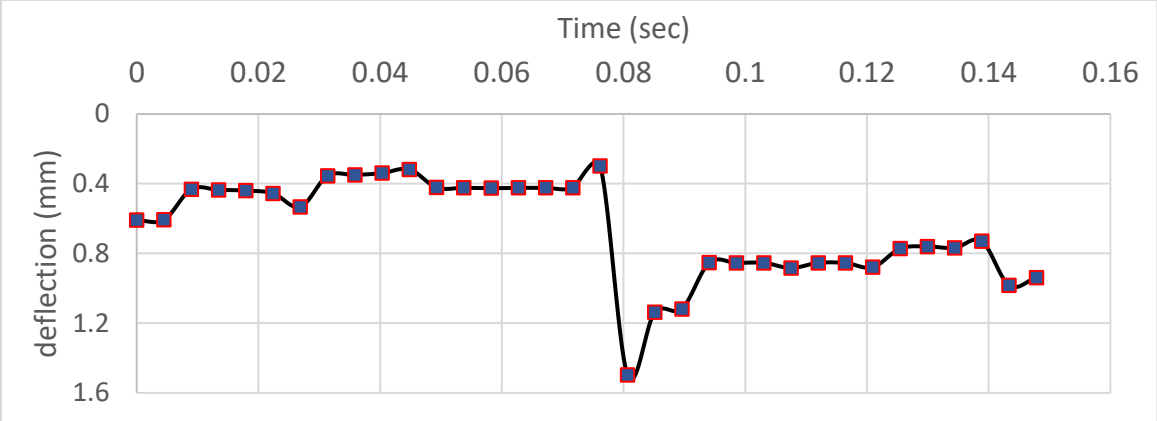

Figure 5-10: Maximum Deflections along the turnout crossing

As it is clearly illustrated (Figure 5-10), the maximum deflection is 1.496 mm which occurs at t = 0.08 sec, this is the time taken for the wheel to reach at the crossing. The reason for encountering such a sharp deflection at that point could be the varying moment of inertia of the crossing nose in addition to the high impact load during the transition.

III. Stiffness

The stiffness is finally computed from the extracted contact forces and deflections along both rails (Figure 5-11). The figure clearly illustrates that the stiffness around the closure panel is less compared to the consecutive sections after. And the stiffness right after the crossing nose is greater than the stiffness right at the crossing point exactly how most studies illustrate. There is almost 54% reduction in stiffness at the closure panel from the crossing nose. On the other hand, the crossing panel has a stiffness increment of about 23% compared to the stiffness right at the crossing nose.

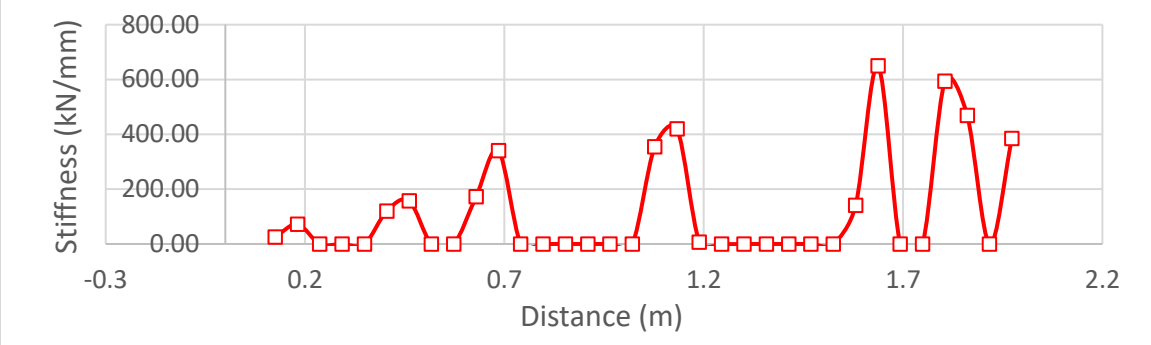

Figure 5-11: Stiffness along both rails

IV. Maximum normal contact stress on the rail

The maximum contact stress is extracted for both closure rails and crossing nose for the initial model parameters. As depicted on Figure 5-12, The maximum stress is observed when the wheel reaches at the crossing nose.

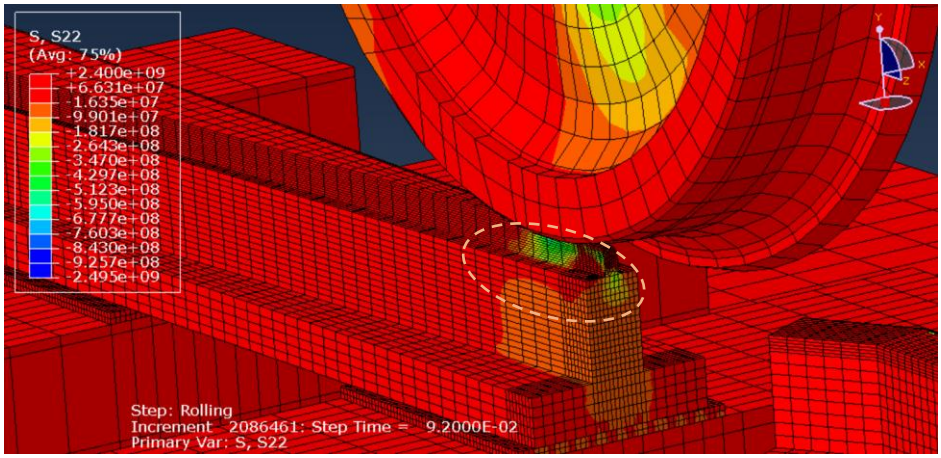

(a)

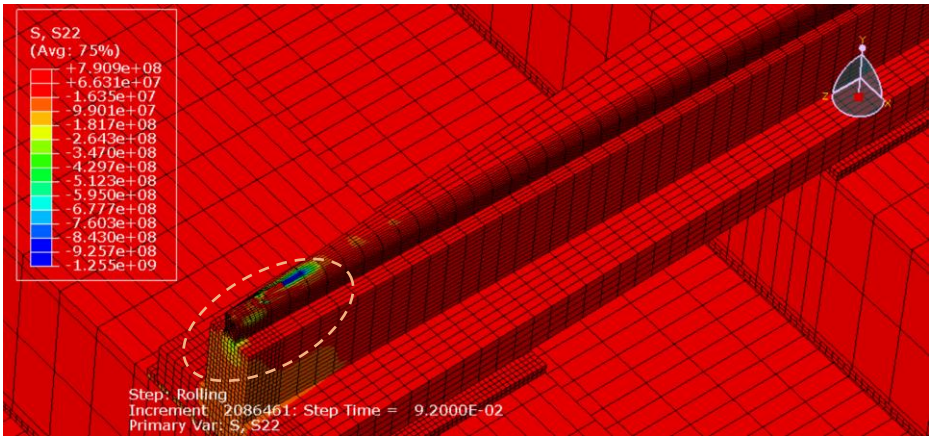

(b)

Figure 5-12: (a), (b): Stress, S22 when the wheel is at the crossing nose

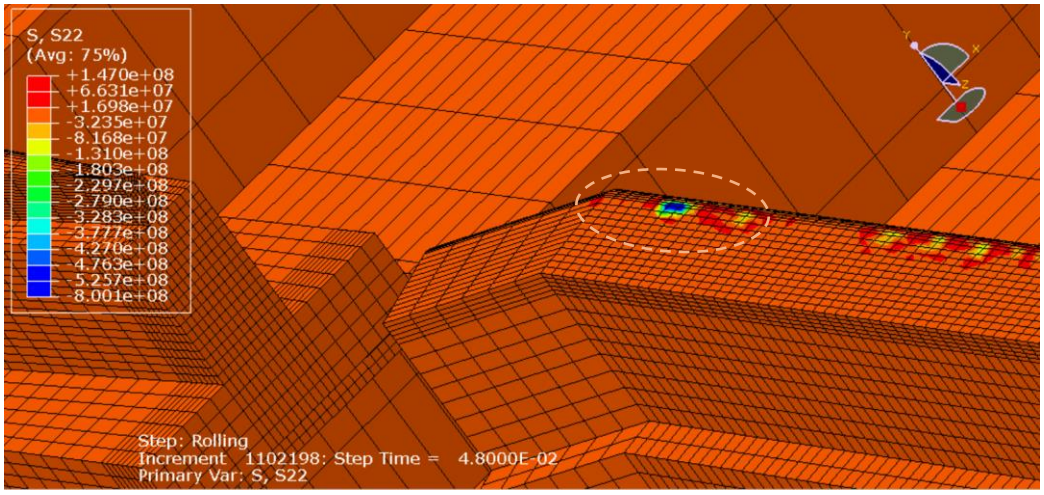

Figure 5-13: Stress, S22 when the wheel is at the closure panel

5.2.2 Comparison with the analytical model results

The maximum deflections at the selected six locations of the rail are computed analytically under section 5.1. Likewise, the numerical results at these specific locations are extracted and compared with the analytical outputs as follows.

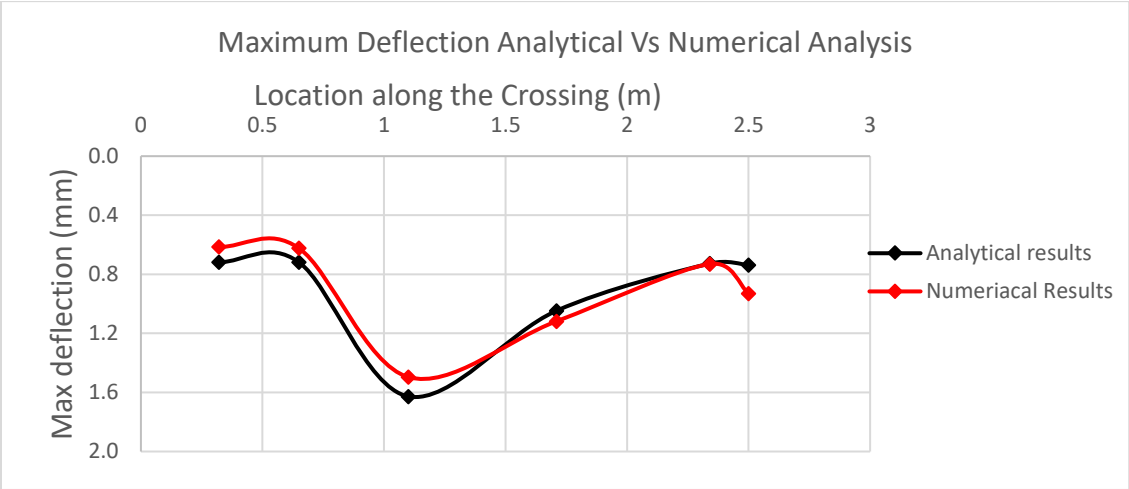

Figure 5-14: Comparison of Maximum deflection (Analytical Vs ABAQUS outputs)

The results from both approaches show good agreement which increases the reliability of the other subsequent numerical computations in addition to the initial model verification done using a static load.

5.2.3 Results from varying rubber pad properties

To illuminate the stiffness variation observed along the panel; rubber pads with varying stiffness properties are proposed. Increasing the stiffness of the rubber pad at the closure panel by 30%, reducing the ones after the crossing nose by 10% and keeping the rubbers at the crossing nose as it is resulting a better stiffness transition throughout. The rubber materials used are modeled as per the Yeoh Hyperelastic material model for nonlinear finite element analysis. The coefficients used for the rubbers under the closure panels and after the crossing nose are presented in the subsequent figures. The other parameters of the material model which the pads are expected to meet are presented under appendix C.

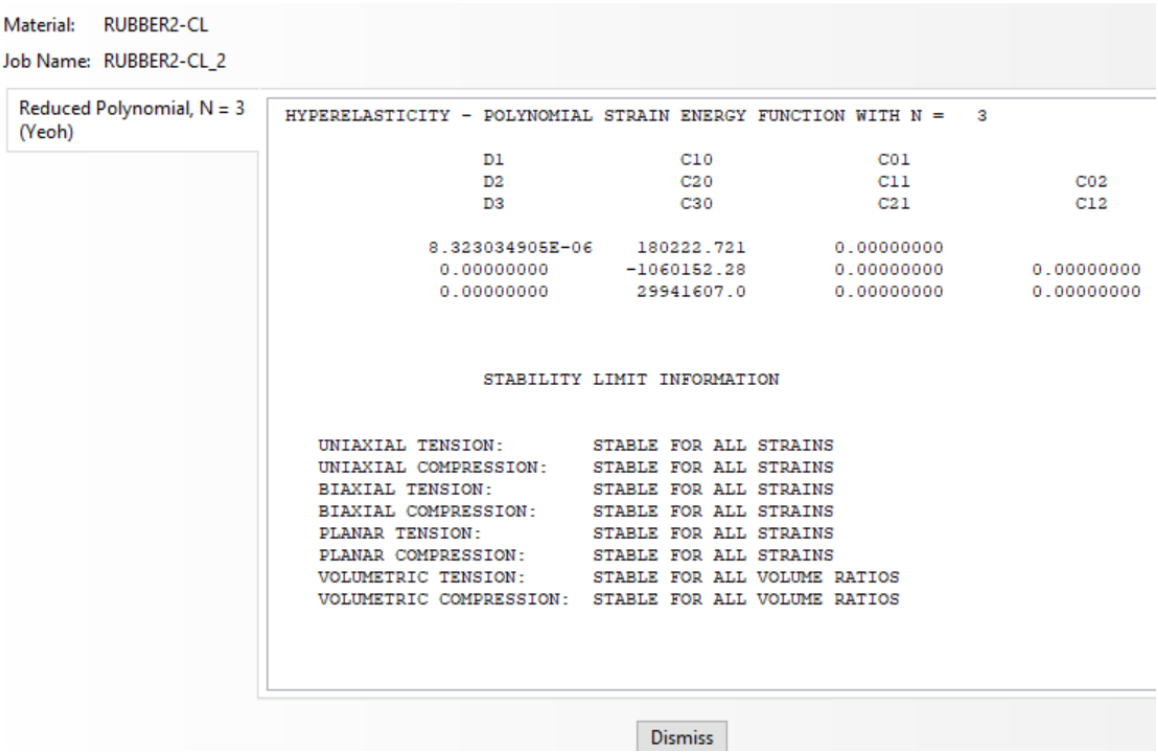

D1	*8.323034906E-06*
C10	*180222.721*
C20	*-1060152.28*
C30	*29941607.0*

Figure 5-15:Yeoh Coefficients for rubber pads at the closure panel

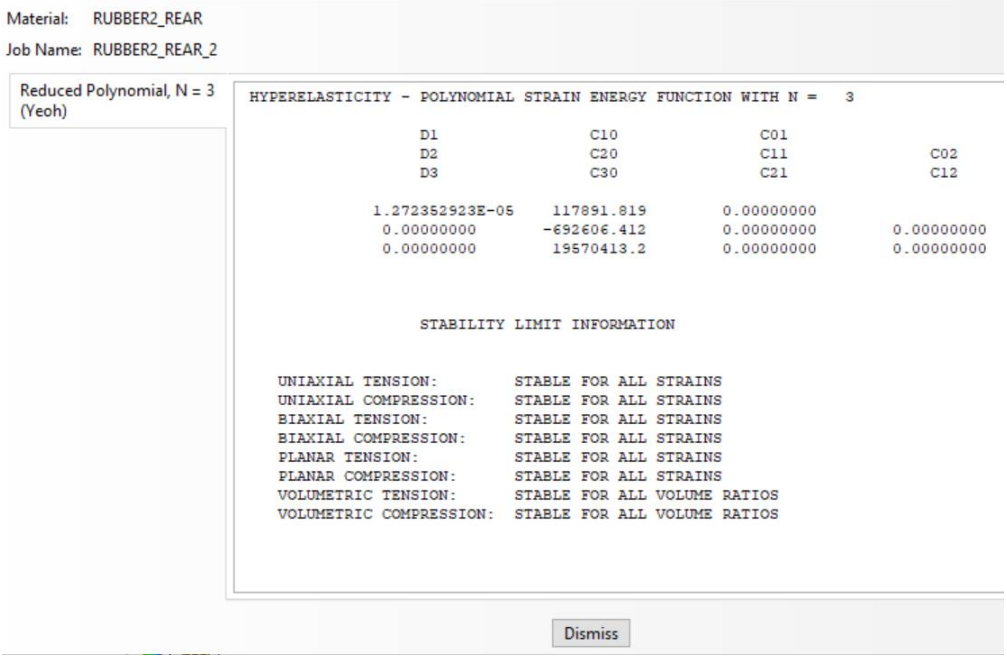

D1	*1.272352923E-05*
C10	*117891.819*
C20	*-692606.412*
C30	*19570413.2*

Figure 5-16: Yeoh Coefficients for rubber pads past the crossing nose

I. Maximum contact force

The contact force is illustrated on Figure 5-17, where the maximum force, which is located at the crossing panel is reduced from 628 kN to 361 kN due to the introduction of non-uniform pads along the turnout. In other words, there is a 37.74% reduction in max Contact force; at the crossing point. It is worth noting that those zero contact force points are there because of larger time increments used for the analysis and coarser mesh sizes set for the aim of reducing computational effort.

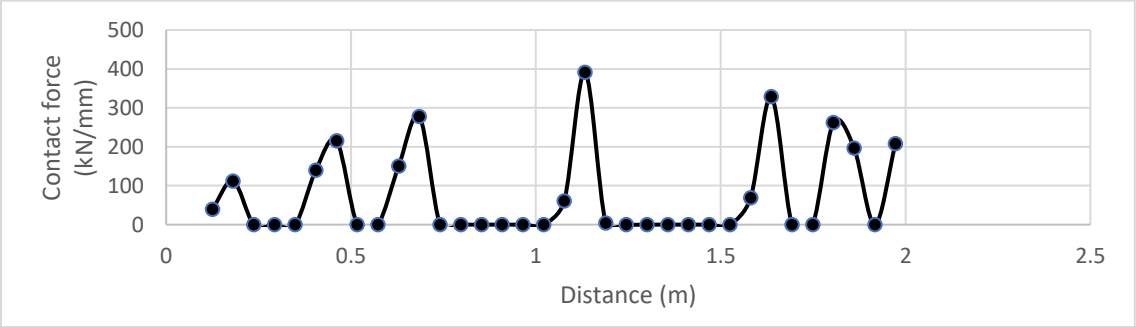

Figure 5-17: Contact Force - Homogenized Model

II. Deflection

The maximum deflection extracted at each step time increment for the homogenized model is quite larger than the original model, However the abrupt deflection changes are lowered and smoothened for the homogenized case as shown in Figure 5-18.

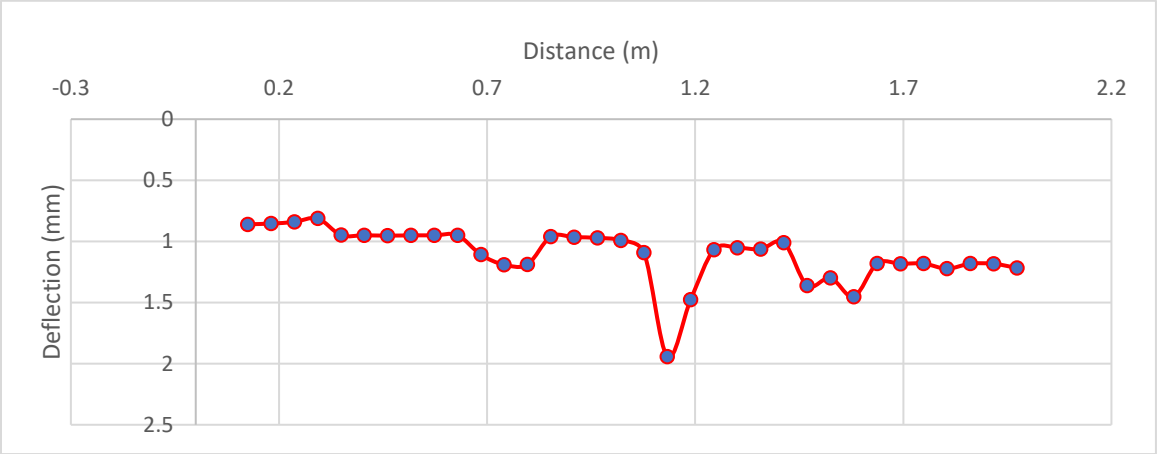

Figure 5-18: Maximum deflection - Homogenized Model

III. Stiffness

The Corresponding stiffness computed from the contact forces and deflections along the line show a very pleasing effect giving a comparable result throughout. The zero stiffness areas are due to the fact that contact forces are zero at those locations which intern is because of the issues regarding mesh size and relatively larger time increments.

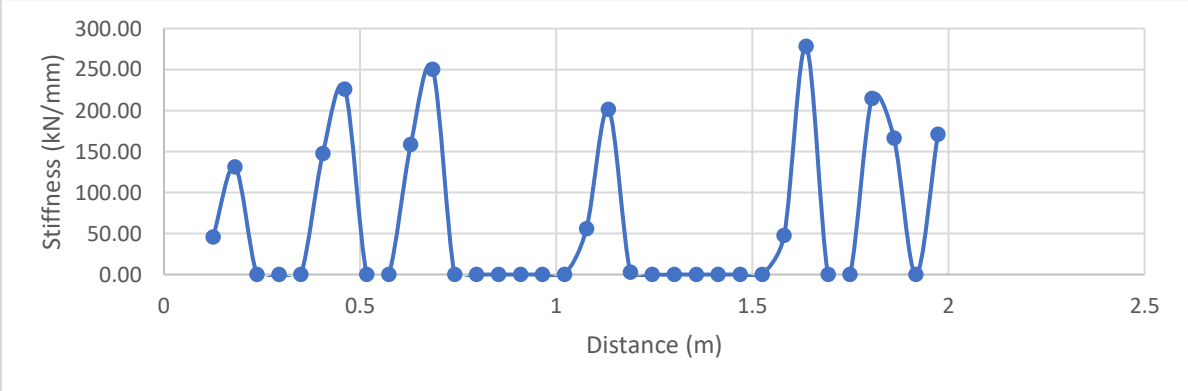

Figure 5-19: Stiffness - Homogenized Model

IV. Maximum normal contact stress on the rail

The maximum normal contact stress is extracted from ABAQUS both on the closure rail and at the crossing nose as depicted on Figure 5-20 and Figure 5-21 to see the effect of provision of rail pads and USPs on the rails.

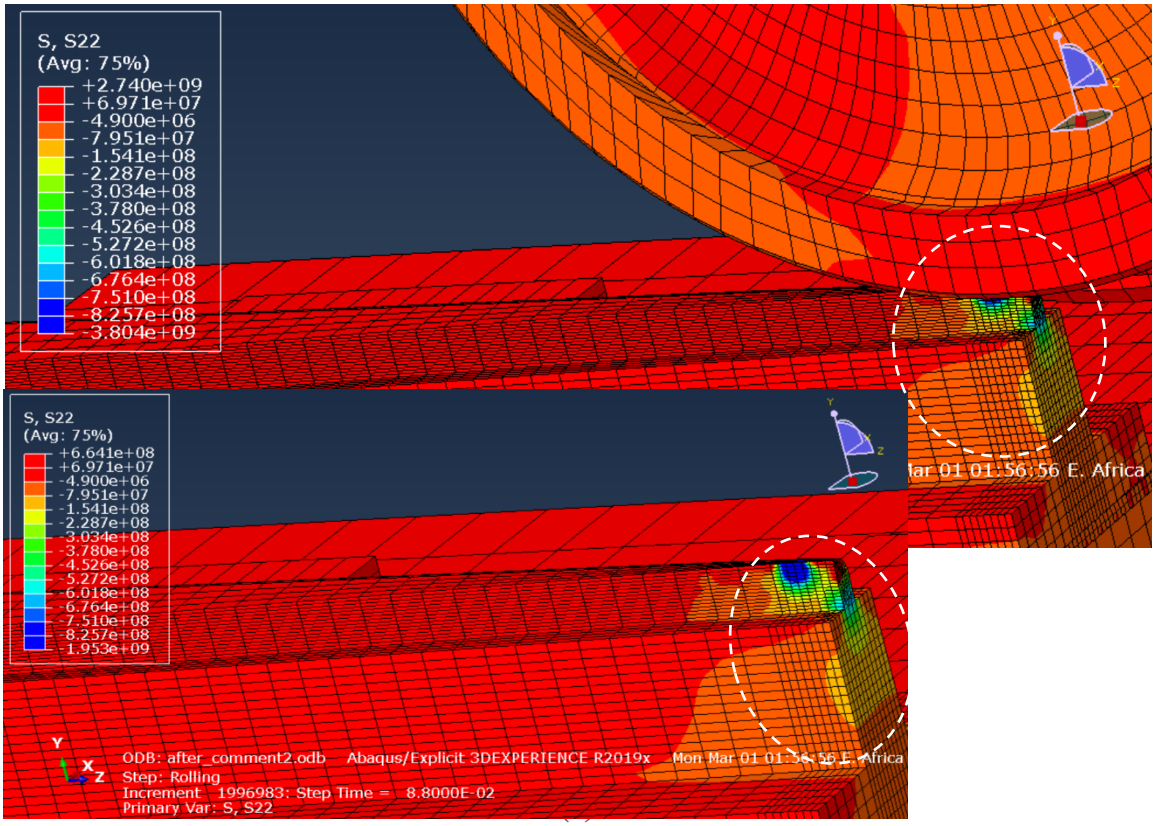

Figure 5-20: Stress, S22 when the wheel is at the crossing nose - Homogenized model

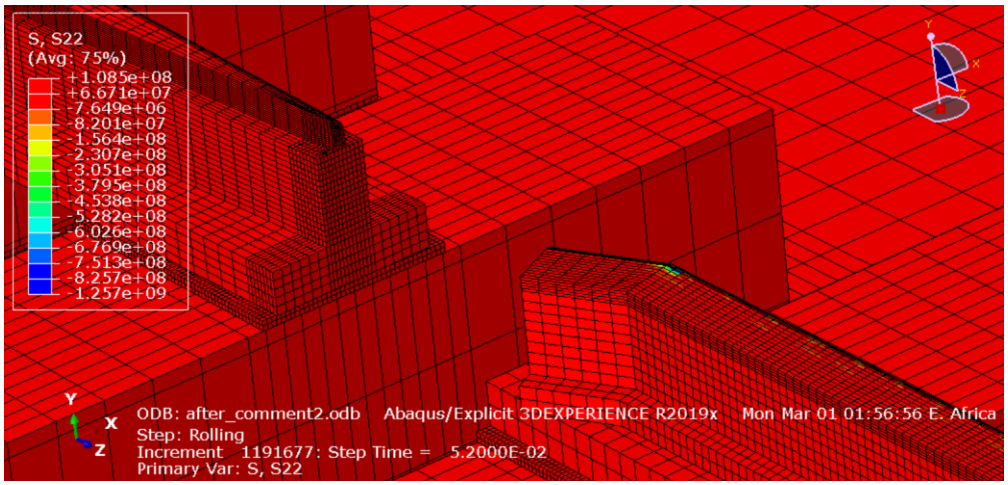

Figure 5-21: Stress, S22 when the wheel is at the closure panel – Homogenized model

5.2.4 Comparision between outputs of initial and homogenized model

As it is clearly shown in Figure 5-22, there is an overall increment in deflection as expected from lowering the support stiffness. The maximum deflection is 1.496mm and 1.943mm for the initial and homogenized models respectively which makes an increment equal to 0.45mm.

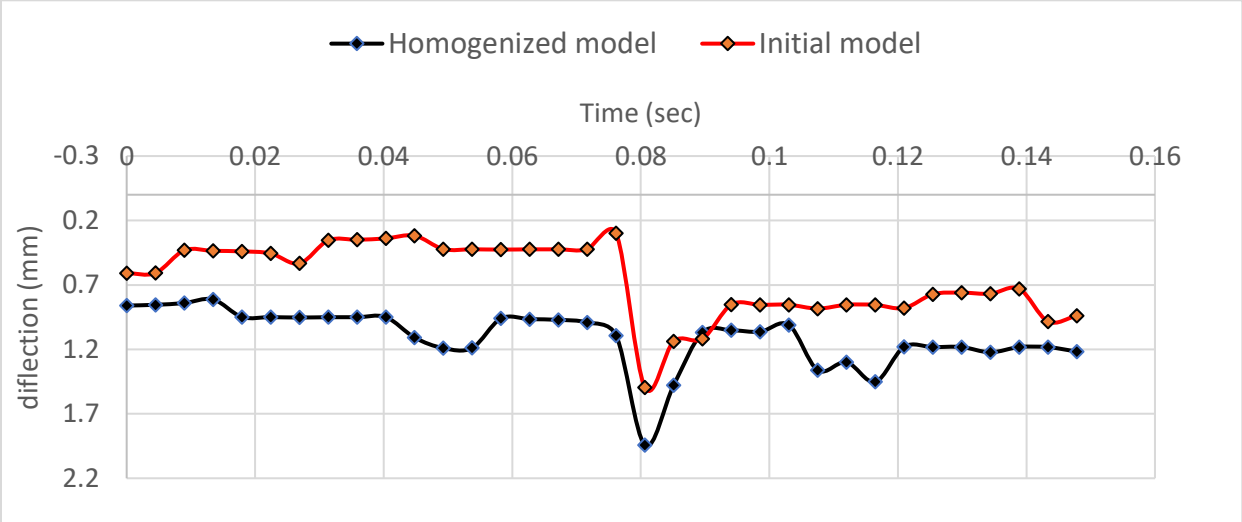

Figure 5-22: Maximum deflection - Comparison between initial and homogenized model

There is also a significant change regarding reduction in magnitude of contact forces in addition to smoothened transition between each panel as depicted in Figure 5-23.

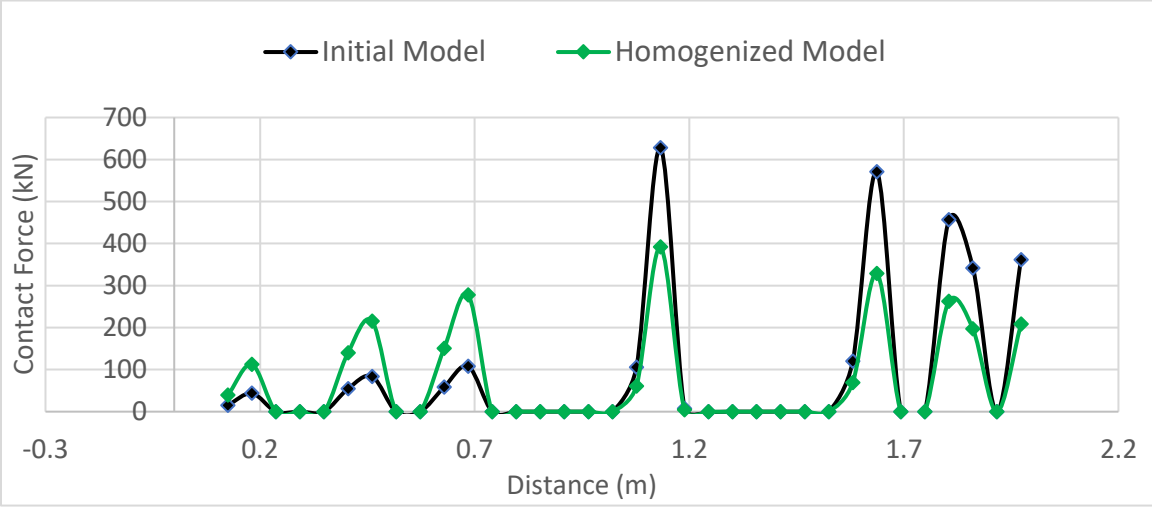

Figure 5-23: Maximum contact force - Comparison between initial and homogenized model

The overall comparison regarding stiffness variation along the small portion of the closure panel and crossing nose is presented in Figure 5-24. It is observed that introducing less-stiff pads around the closure panel and softer ones right after the crossing helps reduce contact force and smoothen stiffness transition along.

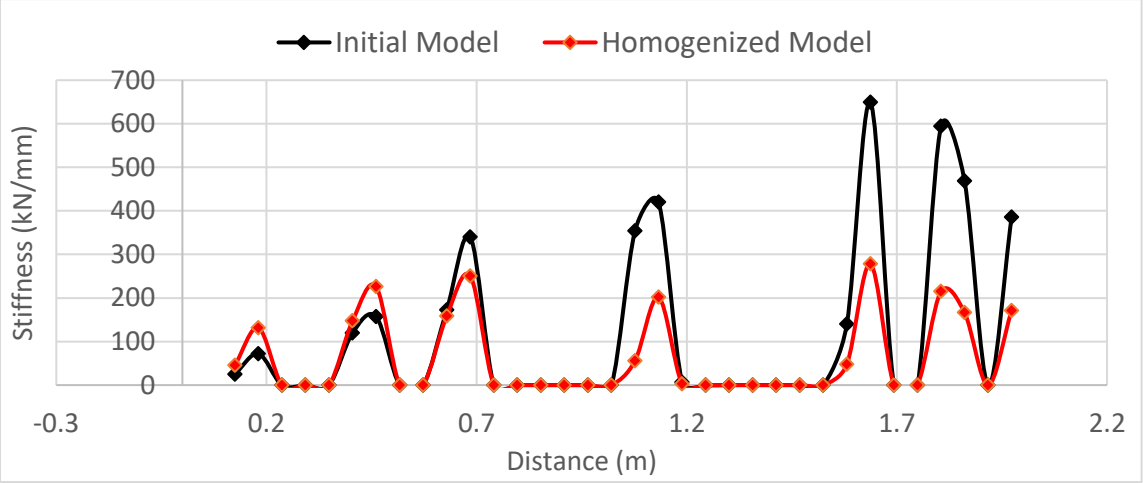

Figure 5-24: Stiffness - Comparison between initial and homogenized model

Provision of rubber pads under the rails and sleepers lowers the stiffness and this then leads to increment of the contact force and deflection. Consequently, stress comparison is done between the initial and homogenized model in order to check if the rail is subjected extra stress. As it is shown in Figure 5-25 (a) & (b), the rail is subjected to extra stress due to the softened support stiffness compared to the initial model. However, the magnitude of stress for the homogenized model is comparable with the initial model.

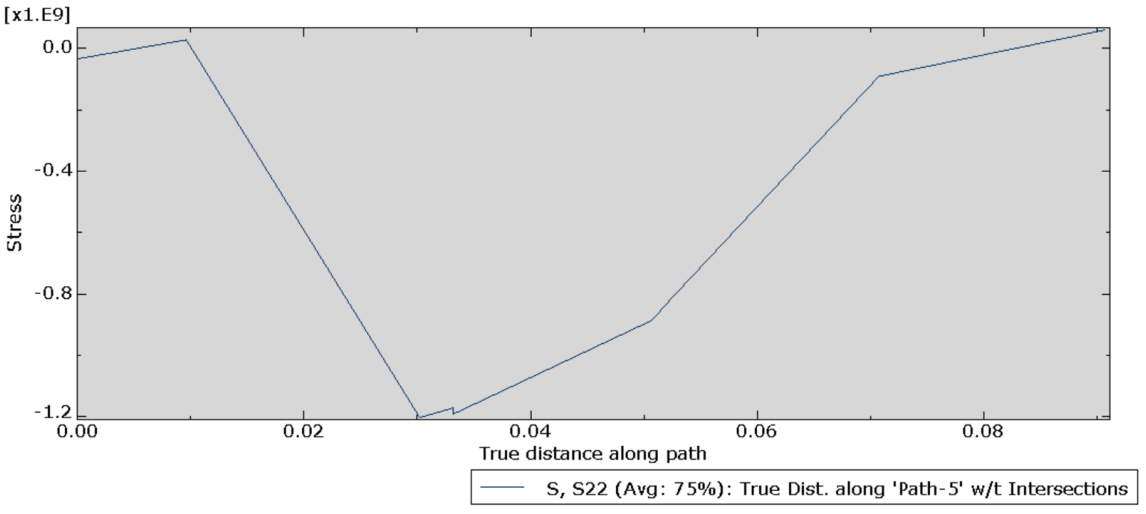

(a)

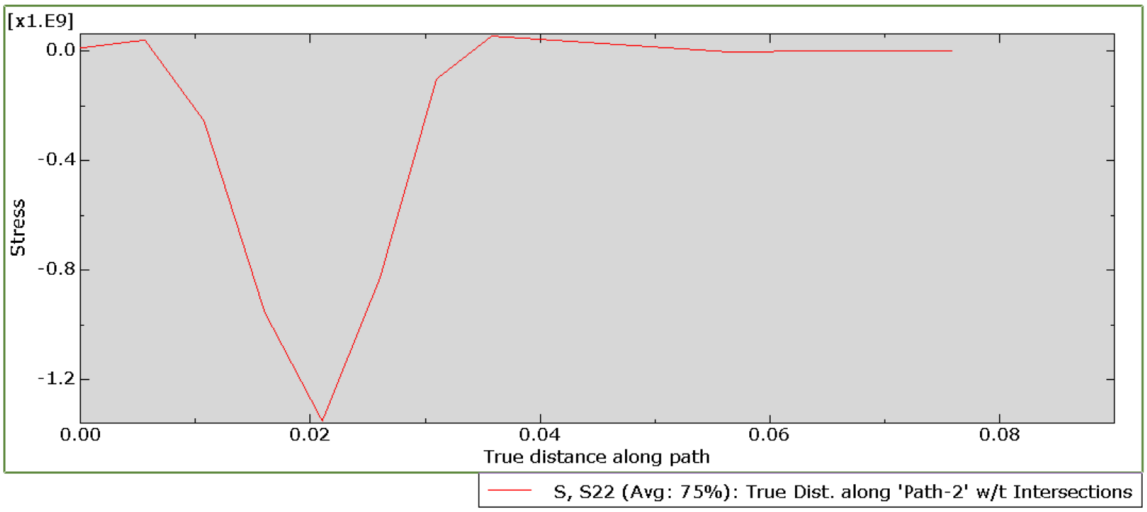

(b)

Figure 5-25: Stress, S22 comparisons initial model (a) Vs homogenized model (b)

6 CONCLUSIONS AND RECOMMENDATIONS

6.1 Conclusions

In the present study, a 3D numerical analysis of a selected turnout crossing model comprising Closure rail, crossing nose, Sleepers, Ballast, and different rubber pad components is investigated with the aim of smoothening vertical stiffness along.

Vertical Track stiffness around a selected turnout at the mixed railway line of Awash-Kombolcha-Hara Gebaya is investigated to come up with the finest stiffness of rail pads using a well-developed FE model which is verified by a simulation models that have been validated before. The maximum deflections are also then validated by comparing it with analytical approaches. The following results are drawn based on the investigations carried out:

The outputs of the initial model with uniform pads throughout shows that there is almost a 23% reduction and a 54 % increment in stiffness at the closure panel and the crossing panel compared to stiffness right at the crossing nose. Which is very expected because of the nature of the sections and the presence of that gap between the closure and the crossing panel.

For all the models analyzed, Both Contact force and maximum deflection occur right at the crossing nose while the stiffness after the crossing nose exceeds the stiffness both at the closure panel and the crossing nose. This has affected the system not only due to the presence of large forces but also due to the huge stiffness gap between consecutive points.

In the computations, rubber pads are introduced at the closure panel with a stiffness of 30% greater from the originally used pads and reducing the ones after the crossing nose by 10% and keeping the rubbers at the crossing nose the same as the initial model.

Moreover, rubber pads used in the simulation are modeled as Rubber hyper elastic materials using Yeoh's Strain Energy Potential function. The result shows a significant change regarding reduction of overall contact forces in addition to smoothened transition between each panel.

This study at least gives the overall tendency and possible ways stipulated as a solution to encounter the problem regarding stiffness variation around railway turnout crossings. The results from this numerical analysis can offer referenced results for other approaches such as theoretical or experimental.

6.2 Recommendations

This paper ultimately proposes suitable rubber pad properties using a numerical material modeling approach of hyperelastic materials by using strain energy potential function of Yeoh. It is recommended to use such hyperelastic material models when designing materials which under goes very large elastic deflection like the rubber pads in this study. In addition, Modeling of the ballast using at least simple soil models like Mohr-Coulomb Plasticity would give realistic results than assuming it as a pure elastic material.

The outputs of the initial model show that, using the line as how it is actually built would result in recurrent degradation of the turnout components leading to frequent maintenance, ride discomfort, energy dissipation and so on which ultimately affects the operational cost of the line.

Consequently, it is recommended to use either existing pads which has comparable characteristics with the ones proposed in this paper or newly produced pads fulfilling the proposed properties can be used to meet the intended objective.

It is worth noting that incorporating outputs of other optimization studies around railway turnouts regarding rail shapes, sleeper spacing etc. with the outputs of this research would give a more pleasing result.

6.3 Areas of further research

The following areas of research are proposed for investigation in order to enhance the outputs of this study.

- Energy dissipation through the rubber pads
- The effect of Rail pads and USPs on Lateral track stiffness
- The effect of altering stiffness of ballast below the crossing nose on reducing low frequency forces which are expected around the sub-structure.

REFERENCES

[1] L. Henrik and Å. Andreas, Transition zones between ballasted and ballastless tracks, Lund: Sweden Media-Tryck Library board- LTH School of Engineering at Campus Helsingborg, 2014.

[2] J. Xu, P. Wang, X. Ma, J. Xiao and R. Chen, "Comparison of calculation methods for wheel-switch rail normal and tangential," *Journal of Rail and Rapid Transit,* 2016.

[3] M. Burrow, P. Teixeira, T. Dahlberg and E. Berggren, "Railway transportation: policies, technology and perspectives," in *Track stiffness considerations for high speed railway lines*, New York, Nova Publishers, 2009, pp. 303-354.

[4] MAINLINE Consortium, "Rail Switches and Crossings. Development of new technologies for replacement," 2014.

[5] X. Jingmang, W. Ping, M. Xiaochuan, G. Yuan and R. Chen, "Stiffness Characteristics of High-Speed Railway Turnout and the Effect on the Dynamic Train-Turnout Interaction," *Shock and Vibration,* 2016.

[6] D. Nicklisch, E. Kassa, J. Nielsen, M. Ekh and S. Iwnicki, "Geometry and stiffness optimization for switches and crossings, and simulation of material degradation," Sweden, 2010.

[7] S. James, O. Mirza and S. Kaewunruen, "Nonlinear Finite Element Modelling of Railway Turnout System considering Bearer/Sleeper-Ballast Interaction," *Hindawi Publishing Corporation,* 2015.

[8] C. Wolmar, The Iron Road: The Illustrated History of Railway, Dorling Kindersley Ltd, 2014.

[9] E. Kassa, "Track stiffness optimisation to improve performance of switches & crossings," in *Digital Rail Revolution Conference*, London, 2019.

[10] E. Kassa, C. Andersson and J. Nielsen, "Simulation of dynamic interaction between train and railway turnout.," *Veh Syst Dyn,* vol. 44, pp. 247-258, 2006.

[11] Transport Asset Standards Authority, "Turnout speeds and crossing selection," Government of New South Wales, Australia, 2018.

[12] F. Zarov, Modeling fault probability in single railroad turouts in Eastern region, Sweden, with the use of logistic regression models, 2019.

[13] Robbs, "scribd-Types of Railway Turnouts and Their Components," 2018. [Online]. Available: https://www.scribd.com/document/471085581/Types-of-Railway-Turnouts-and-Their-Components.

[14] A. Alexander and B. Hanna, The Influence of Stiffness Variations in Railway Tracks, Goteborg, 2013.

[15] Åström, 2011.

[16] K. Elias, "Railway Geometry and Facilities Design course handout," Addis Ababa, 2019.

[17] E. Berggren, "Railway Track Stiffness;Dynamic Measurements and Evaluation for Efficient Maintenance," *KTH Engineering Sciences,* 2009.

[18] E. T. Selig and L. Dingqing, "Track modulus: Its Meaning and Factors Influencing It," *Transportation Research Record, No 1470,ISSN 0361-1981,* 1994.

[19] P. Wang, L. Wang, R. Chen, J. Xu and M. Gao, "Overview and outlook on railway track stiffness measurement," *Jornal of Modern Transportation,* vol. 24, pp. 89-102, 2016.

[20] K. Tzanakakis, The Railway Track and Its Long Term Behaviour, A Handbook for a Railway Track of High Quality , 2013.

[21] H. Feng, "3D-models of Railway Track for dynamic analysis," KTH architecture and the built environment, Stockholm, 2011.

[22] A. Worku, *Models for Raft Foundation Analysis,* Addis Ababa: Lecture material, 2018.

[23] J. Choi, "Qualitative Analysis for Dynamic Behavior of Railway Ballasted Track.," *PhD Dissertation, Berlin Institute of Technology, Berlin, Germany,* 2014.

[24] E. G. Berggren, A. Jahlénius and B. Bengtsson, "Continuous Track Stiffness Measurement: An Effective Method to Investigate the Structural Conditions of the Track.," in *Railway Engineering conference*, 2002.

[25] V. Milica, B. Ljiljana, L. Luka and M. Nikola, "METHODS FOR TRACK STIFFNESS MEASUREMENT - STATE OF THE ART," in *New horizons of transport and communications*, Belgrade, Serbia, 2017.

[26] T. Dahlberg, "Railway Track Stiffness Variations – Consequences and Countermeasures," *International Journal of Civil Engineerng. Vol. 8, No. 1,*, 2010.

[27] A. Mahmoud and M. Eltawil, "Beams on random elastic support," *Applied Mathematical Modelling, Vol 16(6), ,* pp. 330-334, 1992.

[28] P. Woodward, A. Elkacimi and O. Laghrouche, "Application of polyurethane geocomposites to help maintain track geometry for high-speed ballasted railway tracks," *Journal of Zhejiang University-SCIENCE A (Applied Physics & Engineering)*, 2012.

[29] J. Xiao, F. Zhang and L. Qian, "Numerical simulation of stress and deformation in a railway crossing," *Engineering Failure Analysis, Elsevier,* 2011.

[30] B. Pålsson and J. Nielsen, "Track Model Validation for Simulation of Train-Turnout Dynamics".

[31] H. Loy, "Under Sleeper Pads in Turnouts," *Railway Technical Review,*, pp. 35-38, 2009.

[32] H. Obbink and Christine, "Simuleon.com," 21 April 2020. [Online]. Available: https://info.simuleon.com/blog/hyperelastic-material-models-in-abaqus-when-to-choose-what. [Accessed 01 2021].

[33] S. Adeeb, "Introduction to Solid Mechanics and Finite Element Analysis," Wolframweb Mathematica, 2021. [Online].

[34] H. b. o. r. materials, "MIT- abaqus-docs.mit.edu," 2017. [Online]. Available: https://abaqus-docs.mit.edu/2017/English/SIMACAEMATRefMap/simamat-c-hyperelastic.htm.

[35] Finite element analysis solutions, "Yeoh hyperelastic model for non-linear finite element anaysis," WELSIM, 2020.

[36] K. Elias, "Wheel/Rail Contact Mechanics," in *Railway Track Engineering, Course lecture material*, 2018.

[37] S. Iwnicki, Simulation of wheel - rail contact forces, Manchester: Blackwell publishing ltd, 2003.

[38] C. Nkundineza, *ABAQUS training material,* February, 2020.

[39] Awash-Kombolcha-Hara Gebaya Railway Project, "AkH Railway," [Online]. Available: https://akhrailway.com/. [Accessed 23 01 2021].

[40] T. Hiran, "ANSYS for analysis and simulation," 30 December 2020. [Online]. Available: https://www.capterra.com/p/124168/ANSYS-mechanical-software-suite/reviews/#:~:text=Cons%3A%20ANSYS%20requires%20heavy%20computational,compared%20to%20other%20modeling%20tools.. [Accessed February 2021].

[41] Livermore Software Technology, "LS-DYNA," 2021. [Online]. Available: http://www.lstc.com/products/ls-dyna.

[42] G. products, "PLAXIS 3D Reviews & Product Details," 09 September 2020. [Online]. Available: https://www.g2.com/products/plaxis-3d/reviews.

[43] G. products, "Inventor Nastran Reviews & Product Details," 09 september 2020. [Online]. Available: https://www.g2.com/products/inventor-nastran/reviews.

[44] LLC FEA services, "Inspired Solutions-Impeccable Service," 2020. [Online].

[45] A. U. FEA, "Dassault systems," 2021. [Online]. Available: https://www.3ds.com/products-services/simulia/products/abaqus/.

[46] R. G. Sargent, "Verification and Validation of Simulation Models," in *Winter Simulation Conference*, NY, USA, 2011.

[47] R. Schlesinger, E. Crosbie, R. E. Gagné, G. S. Innis, C. S. Lalwani, J. Loch, R. J. Sylvester, R. D. Wright, N. Kheir and D. Bartos, "Terminology for Model Credibility," *Simulation,* vol. 3, pp. 103-104, 1979.

[48] M. Oregui, Z. Li and ". R. Dollevoet, "An investigation into the modeling of railway fastening," *International Journal of Mechanical Sciences,* vol. 92, pp. 1-11, 2015.

[49] Z. Jin-Cai and T. Chen-Xi, "Shear Strength of Railway Ballast," *Electronic Jornal of Geotechnical Engineering, EJGE,* vol. 21, p. 4766, 2016.

[50] B. Indraratna, D. Ionescu and H. D. Christie, "Shear Behavior of Railway Ballast Based on Large-Scale Triaxial Tests," *Journal of Geotechnical and Geo-Environmental Engineering,* vol. 124, pp. 439 - 449, 1998.

[51] S. Sarawade, S. Agarwal, S. A. Patil and A. R.Yeole, "Determination of Non-Linearity in Rail Pad," *IOSR Journal of Engineering (IOSR JEN)* , pp. 11-17, 2019.

[52] MIT, "Mohr-Coulomb Plasticity," Massachusetts , 2021.

[53] ABAQUS Analysis User's Manual, *Mohr-Coulomb Plasticity*, ABAQUS/Standard ABAQUS /CAE, 2014.

[54] T. Tseng, "Dynamic Responses of Wheel-Rail Systems with Block Dampers," The Acoustics, Dynamics, and Controls Commons-Mechanical (and Materials) Engineering, Lincoln, 2016.

[55] Renga Rao Krishnamoorthy et al, "The Effect of Rubber Pads on The Stress Distribution for Concrete Railway Sleepers," in *IOP Conference Series: Materials Science and Engineering*, 2018.

APPENDIX

A) Phyton code used to extract maximum deflection at each time step,


```
 # COPYRIGHT AND REUSE AUTORIZATION BY Dr. Celestin
Nkundineza
     #Import Abaqus modules
     from job import *
     from sketch import *
     from visualization import *
     from connectorBehavior import *
     import odbAccess
     import time
     def extractdata(odbfile,datarequest,filename2):
#Open the model output database by calling the Abaqus module
odbAccess and its instance openOdb; the parameters are the
path of the file and whether the file can be read or not:
          myOdb = odbAccess.openOdb(path=odbfile,
readOnly=False)
#Get the steps separately and give them variables such as
step1 and step2
          step1 = myOdb.steps['loading']
          step2 = myOdb.steps['Rolling']

#Instance to extract deflections and stresses
          myinstance=myOdb.rootAssembly.instances[datareque
st[1]]
```

```
# Also, initialize a text file name 'max_press.txt' that
will store the data and let give it a variable fmcp, and
let it open to take data
          fmcp2=open(filename2,'w')
#Write headings for each columns
          fmcp2.write('Total Time'+'\t')
          [fmcp2.write(str(datarequest[0][titledata])+'\t')
for titledata in datarequest[0].keys()]
## Go to the second line for next data writing
          fmcp2.write('\n')
#Let loop over each step
#initialize initial time to be zero
          t0=0.0

          steptime=t0
          for step in myOdb.steps.values():
               for frame in step2.frames:
#Extract step time times
          steptime=t0+frame.frameValue
          fmcp2.write(str(steptime)+'\t')
#Let extract the contact force in frame i (at time increment
i). The attribute to get the magnitude of contact force as
output fields in a frame uses a function fieldOutputs that
takes parameter variable as datav
#Extracting data components from instances
          for datav in datarequest[0].keys():
          datatypes=frame.fieldOutputs[datav]
          datatypes_region=datatypes.getSubset(region=myins
tance)
               n_data2=len(datatypes_region.values)
               all_datas=[]
```

```
                for i in range(n_data2):
                    if datav=='S':

     datavalue=datatypes_region.values[i].minPrincipal
                                    else:
#extract vertical displacement (in this case y direction:
U2)
datavalue=datatypes_region.values[i].data[1]
all_datas.append(datavalue)
all_datas=[abs(all_datas[i]) for i in
range(len(all_datas))]
                            max_d=max(all_datas)
                            fmcp2.write(str(max_d)+'\t')
#the paramter '\t' allows us to write the next value at the
next column.
                    fmcp2.write('\n')
                t0+=step.timePeriod

odbfile='C:\Users\edena\Documents\Scripting\Sample_model_Final
.odb'
     Exstract_FromInstance={'U':'Railway track vertical
displacement'}
     Instance='P54E1 -1m-1-lin-2-1'
     Datarequest=[Exstract_FromInstance,Instance]
     filename2='C:\Users\edena\Documents\Scripting\max_data
s.xls'
     extractdata(odbfile,Datarequest,filename2)
```

B) Plots of amplitudes

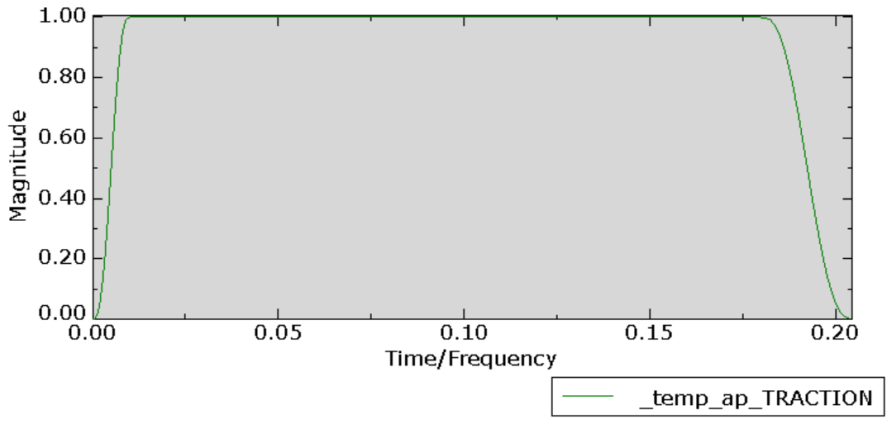

Figure 16: Amplitude for traction force

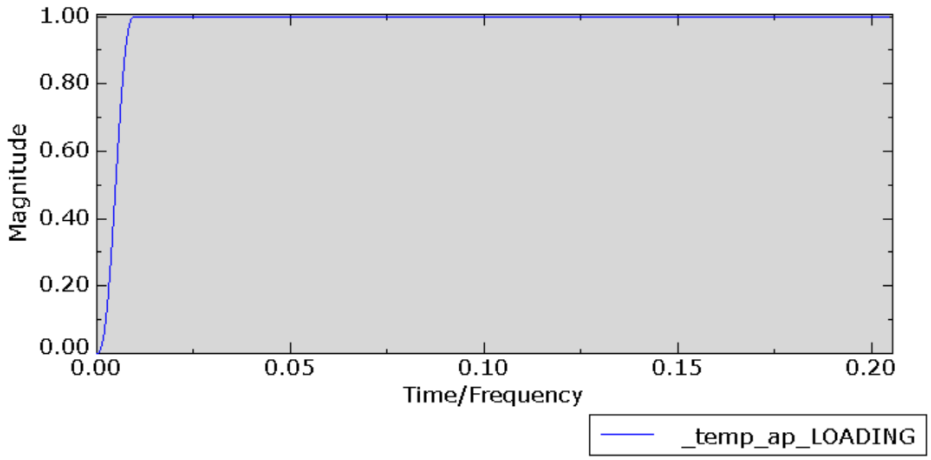

Figure 27: Amplitude for loading

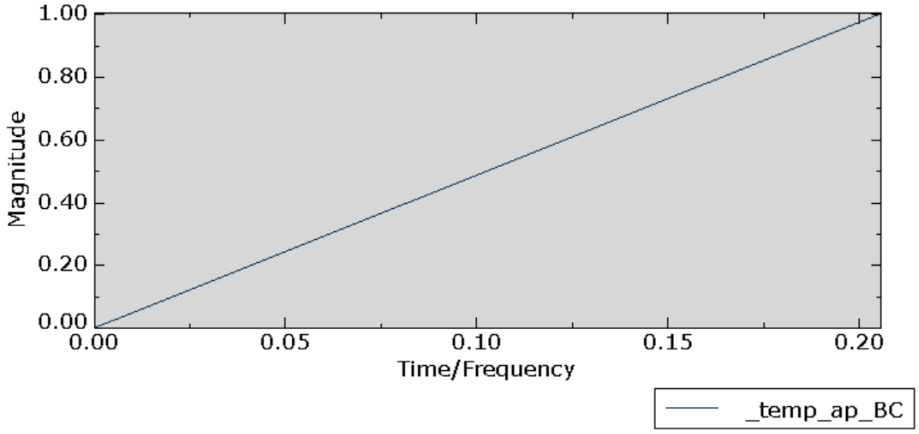

Figure 38: Amplitude for BC

C) Material characteristics of the rubber pads proposed [51]

i. For the closure panel

NOMINAL STRAIN	NOMINAL STRESS(TEST)	NOMINAL STRESS(Abaqus)
0.000	1.5200E+04	0.000
8.3333E-03	1.8100E+04	8915.
1.6667E-02	2.1400E+04	1.7563E+04
2.5000E-02	2.5300E+04	2.5852E+04
3.3333E-02	3.0000E+04	3.3740E+04
4.1667E-02	3.5600E+04	4.1251E+04
5.0000E-02	4.2100E+04	4.8485E+04
5.8333E-02	4.9900E+04	5.5638E+04
6.6667E-02	5.9100E+04	6.3011E+04
7.5000E-02	7.0100E+04	7.1019E+04
8.3333E-02	8.3000E+04	8.0204E+04
9.1667E-02	9.8300E+04	9.1240E+04
0.1000	1.1600E+05	1.0494E+05
0.1083	1.3800E+05	1.2227E+05
0.1167	1.6300E+05	1.4433E+05
0.1250	1.9400E+05	1.7240E+05
0.1333	2.2900E+05	2.0791E+05
0.1417	2.7200E+05	2.5245E+05
0.1500	3.2200E+05	3.0778E+05
0.1583	3.8100E+05	3.7585E+05
0.1667	4.5200E+05	4.5874E+05
0.1750	5.3500E+05	5.5875E+05
0.1833	6.3400E+05	6.7833E+05
0.1917	7.5100E+05	8.2011E+05
0.2000	8.9000E+05	9.8691E+05
0.2083	1.0500E+06	1.1817E+06
0.2167	1.2500E+06	1.4077E+06
0.2250	1.4800E+06	1.6682E+06
0.2333	1.7500E+06	1.9668E+06
0.2417	2.0800E+06	2.3072E+06
0.2500	2.4600E+06	2.6933E+06
0.2583	2.9100E+06	3.1291E+06
0.2667	3.4500E+06	3.6190E+06
0.2750	4.0900E+06	4.1674E+06
0.2833	4.8400E+06	4.7788E+06
0.2917	5.7400E+06	5.4582E+06
0.3000	6.7900E+06	6.2105E+06
0.3083	8.0500E+06	7.0409E+06
0.3167	9.5300E+06	7.9547E+06
0.3250	1.1300E+07	8.9575E+06
0.3333	1.3400E+07	1.0055E+07
0.3417	1.5900E+07	1.1253E+07

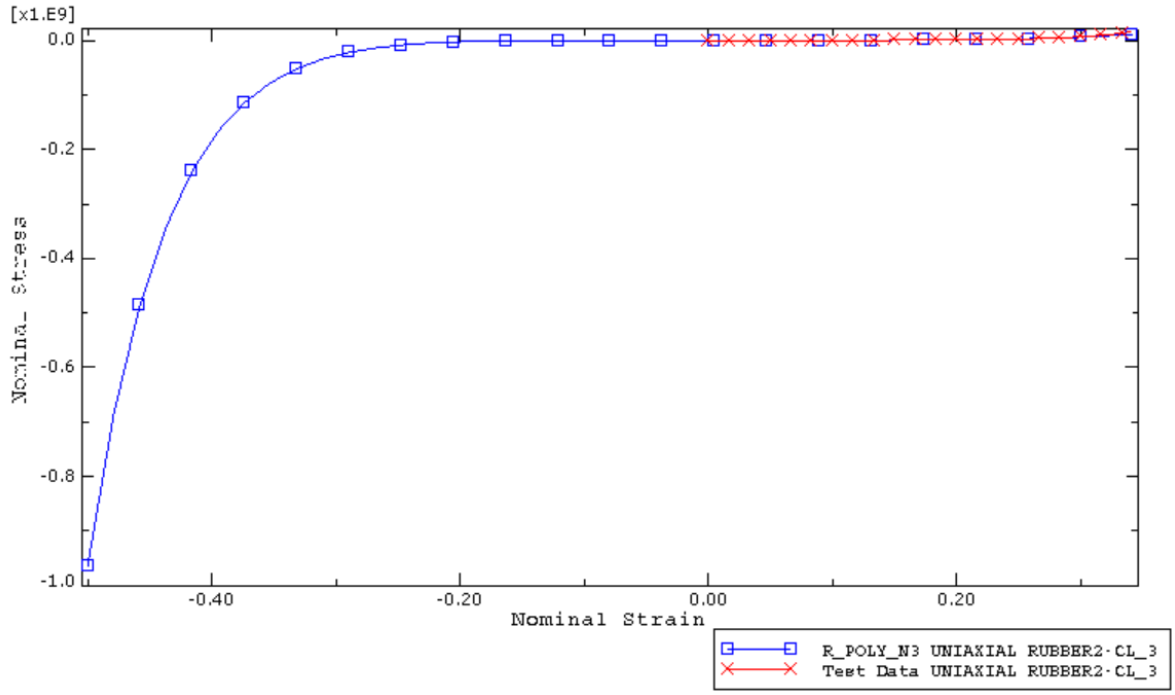
[x1.E9]
0.0
-0.2
-0.4
-0.6
-0.8
-1.0
Nominal Stress
-0.40
-0.20
0.00
0.20
Nominal Strain
R_POLY_N3 UNIAXIAL RUBBER2-CL_3
Test Data UNIAXIAL RUBBER2-CL_3

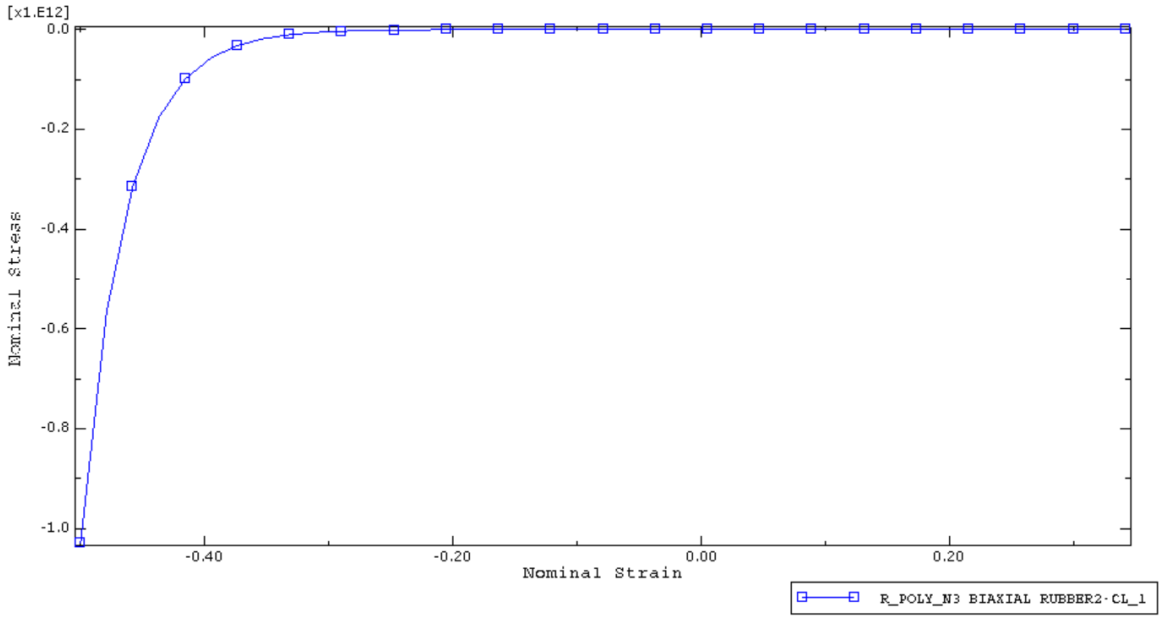
[x1.E12]
0.0
-0.2
-0.4
-0.6
-0.8
-1.0
Nominal Stress
-0.40
-0.20
0.00
0.20
Nominal Strain
R_POLY_N3 BIAXIAL RUBBER2-CL_1

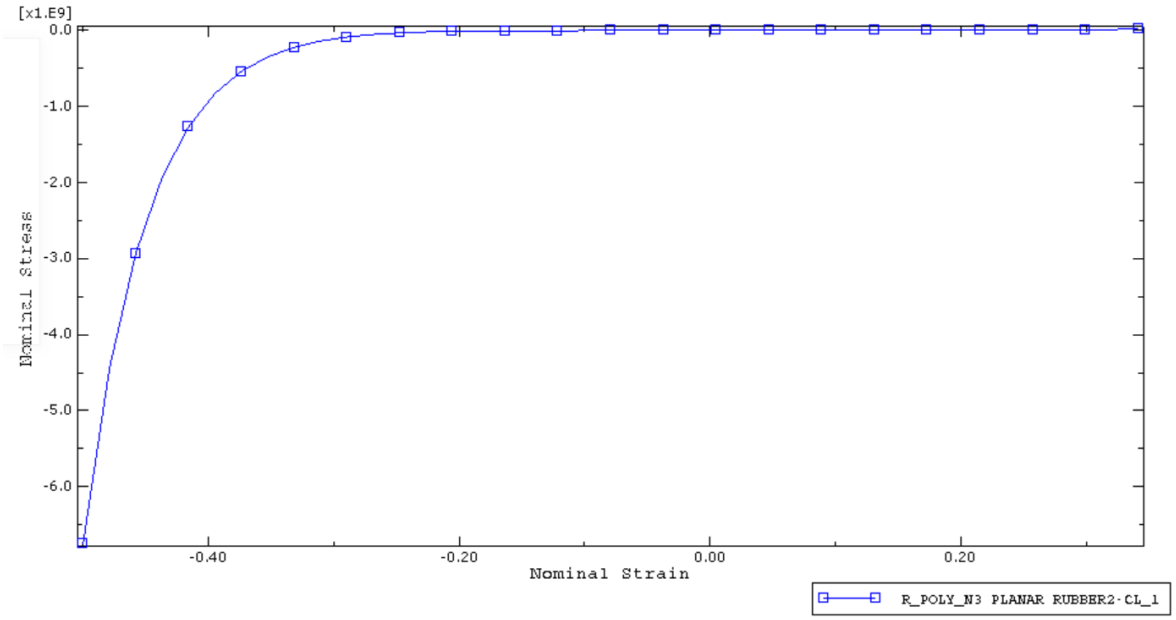
[x1.E9]
0.0
-1.0
-2.0
-3.0
-4.0
-5.0
-6.0
Nominal Stress
-0.40
-0.20
0.00
0.20
Nominal Strain
R_POLY_N3 PLANAR RUBBER2-CL_1

ii. For the Crossing panel

NOMINAL STRAIN	NOMINAL STRESS(TEST)	NOMINAL STRESS(Abaqus)
0.000	9970.	0.000
8.3333E-03	1.1811E+04	5832.
1.6667E-02	1.3991E+04	1.1489E+04
2.5000E-02	1.6574E+04	1.6911E+04
3.3333E-02	1.9634E+04	2.2072E+04
4.1667E-02	2.3259E+04	2.6986E+04
5.0000E-02	2.7554E+04	3.1719E+04
5.8333E-02	3.2641E+04	3.6400E+04
6.6667E-02	3.8667E+04	4.1224E+04
7.5000E-02	4.5806E+04	4.6464E+04
8.3333E-02	5.4263E+04	5.2473E+04
9.1667E-02	6.4281E+04	5.9692E+04
0.1000	7.6149E+04	6.8653E+04
0.1083	9.0209E+04	7.9984E+04
0.1167	1.0686E+05	9.4412E+04
0.1250	1.2659E+05	1.1277E+05
0.1333	1.4997E+05	1.3598E+05
0.1417	1.7765E+05	1.6510E+05
0.1500	2.1045E+05	2.0128E+05
0.1583	2.4931E+05	2.4578E+05
0.1667	2.9534E+05	2.9997E+05
0.1750	3.4986E+05	3.6534E+05
0.1833	4.1446E+05	4.4351E+05
0.1917	4.9097E+05	5.3620E+05
0.2000	5.8162E+05	6.4523E+05
0.2083	6.8900E+05	7.7257E+05
0.2167	8.1621E+05	9.2029E+05
0.2250	9.6690E+05	1.0906E+06
0.2333	1.1454E+06	1.2858E+06
0.2417	1.3569E+06	1.5083E+06
0.2500	1.6074E+06	1.7606E+06
0.2583	1.9042E+06	2.0455E+06
0.2667	2.2557E+06	2.3657E+06
0.2750	2.6722E+06	2.7242E+06
0.2833	3.1656E+06	3.1238E+06
0.2917	3.7500E+06	3.5679E+06
0.3000	4.4423E+06	4.0597E+06
0.3083	5.2625E+06	4.6024E+06
0.3167	6.2341E+06	5.1997E+06
0.3250	7.3851E+06	5.8552E+06
0.3333	8.7486E+06	6.5726E+06
0.3417	1.0364E+07	7.3557E+06

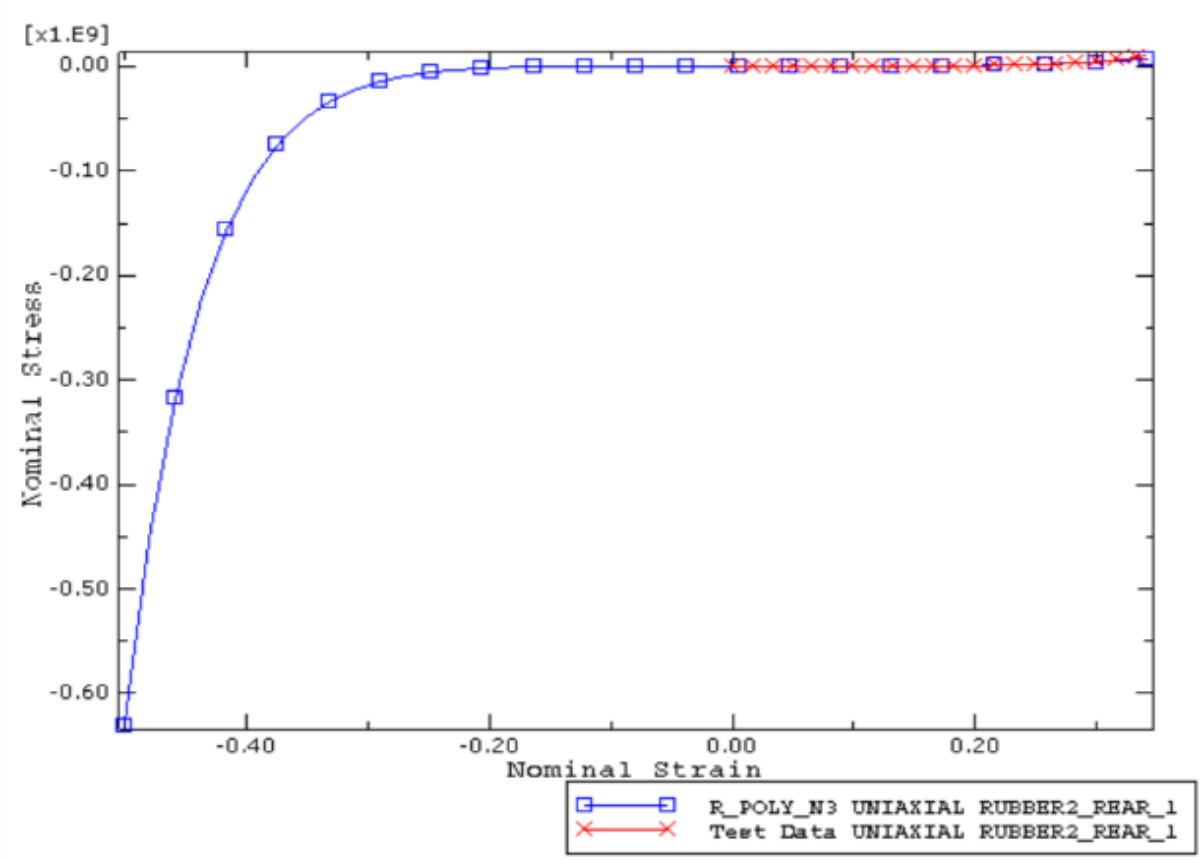
[x1.E9]
0.00
-0.10
-0.20
-0.30
-0.40
-0.50
-0.60
Nominal Stress
-0.40
-0.20
0.00
0.20
Nominal Strain
R_POLY_N3 UNIAXIAL RUBBER2_REAR_1
Test Data UNIAXIAL RUBBER2_REAR_1

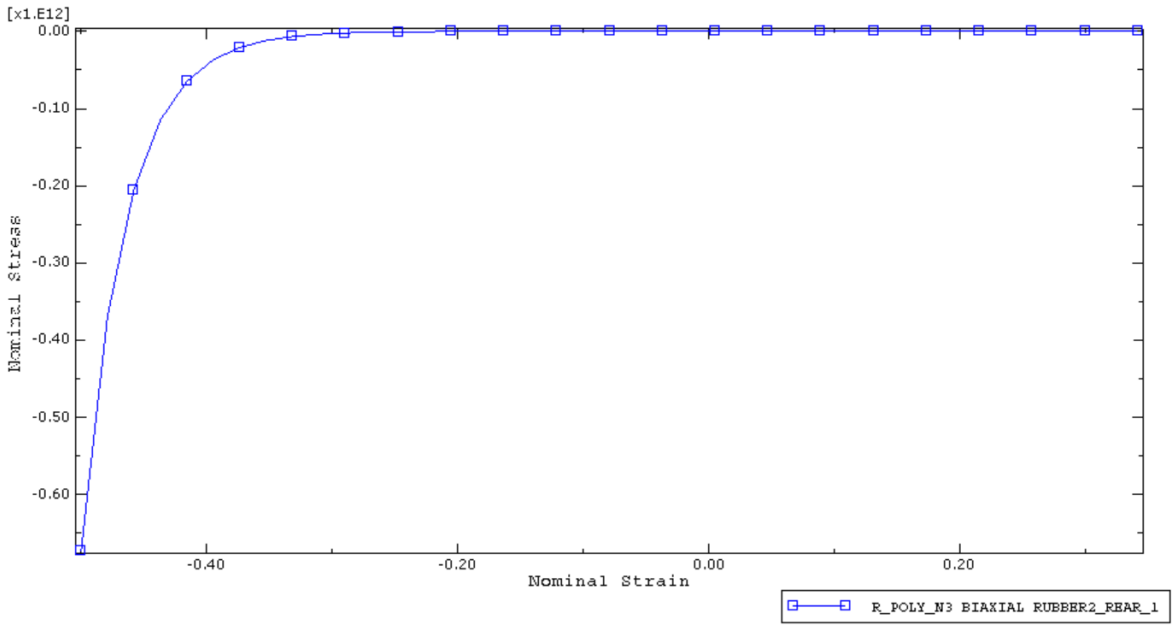
[x1.E12]
0.00
-0.10
-0.20
-0.30
-0.40
-0.50
-0.60
Nominal Stress
-0.40
-0.20
0.00
0.20
Nominal Strain
R_POLY_N3 BIAXIAL RUBBER2_REAR_1

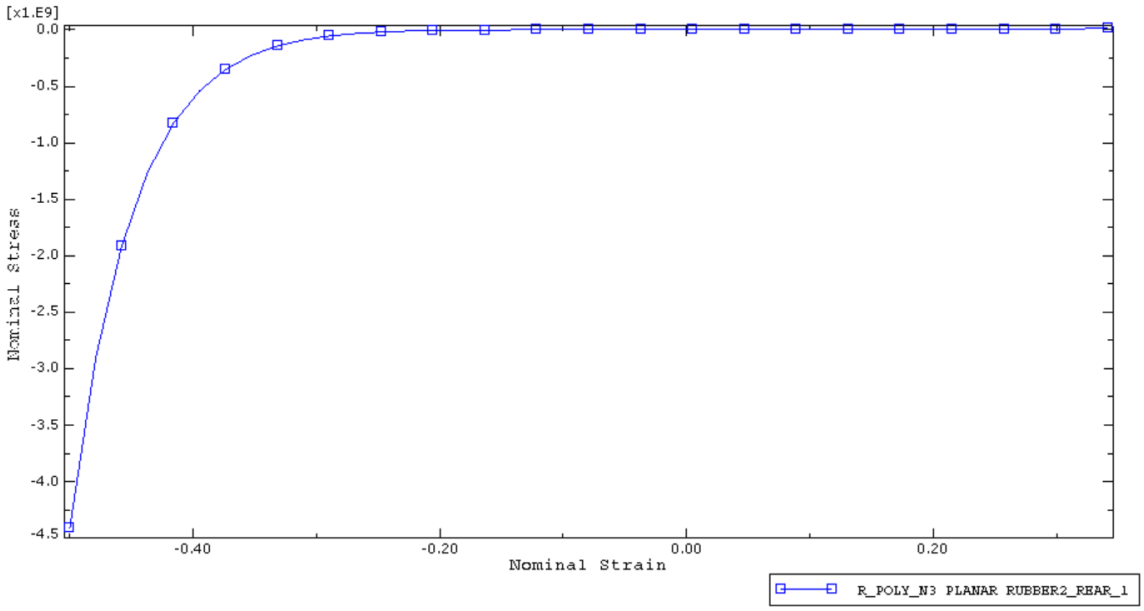
[x1.E9]
0.0
-0.5
-1.0
-1.5
-2.0
-2.5
-3.0
-3.5
-4.0
-4.5
Nominal Stress
-0.40
-0.20
0.00
0.20
Nominal Strain
R_POLY_N3 PLANAR RUBBER2_REAR_1